SECRETARIA DE RECURSOS NATURALES Y DESARROLLO SUSTENTABLE

INA

Instituto Nacional del Agua y del Ambiente

Hydraulic Studies for the Water Intake Of Central Costanera

Report LHA N° 01-155a-97

Ezeiza, May 1997

LABORATORIO DE HIDRAULICA Y DEL AMBIENTE

SECRETARIA DE ESTADO
DE RECURSOS NATURALES
Y DESARROLLO SUSTENTABLE

INSTITUTO NACIONAL
DEL AGUA
Y DEL AMBIENTE

HYDRAULIC STUDIES FOR THE WATER INTAKE OF CENTRAL COSTANERA

Report produced for

MITSUBISHI CORPORATION

Report LHA 01-155a.-97
Ezeiza, May 1997

HYDRAULIC STUDIES FOR THE WATER INTAKE OF CENTRAL COSTANERA

ABSTRACT

Two hydraulic problems, associated to the construction by Mitsubishi Corporation of a power plant for Central Costanera, are studied.They are the possible influence of the discharged heated water on the temperature of the intake water and the sedimentation rate in the dredged region around the water intake. The studies are undertaken with numerical techniques. Three nested 2D hydrodynamic models are implemented. They feed a heat transfer model and a sediment transport model. It is shown that the overtemperature at the water intakes manifests itself as more or less definite pulses, with durations of a few hours and with peak values in the range from 2 to 5°C, and that the feedback effect is quite small. On the other hand, a maintenance dredging between 10 and 30 m^3/month is estimated for the dredged zone, with null values of siltation close to the intake itself, up to distances of about 15 m, and with an increment of siltation volume between 0.5 and 1.5 m^3/month for each additional meter of dredging zone length.

INA AUTHORITIES

PRESIDENT:

Dr. Mario R. DE MARCO NAON

MANAGER OF PROGRAMS AND PROJECTS:

Dr. Raúl A. LOPARDO

DIRECTOR OF HYDRAULIC AND ENVIRONMENTAL LABORATORY:

Ing. Julio C. DE LIO

WORK TEAM

HEAD OF COMPUTATIONAL HYDRAULICS PROGRAM:

Dr. Angel N. MENENDEZ

RESEARCHERS:

Ing. Fabián A. BOMBARDELLI
Lic. Pablo A. TARELA
Lic. Carla P.X. VILELA

REPORT PRODUCED BY:

Dr. Angel N. MENENDEZ

HYDRAULIC STUDIES FOR THE WATER INTAKE OF CENTRAL COSTANERA

INDEX

1 INTRODUCTION

Mitsubishi Corporation is in charge of the construction of a power plant for Central Costanera. (Figure 1.1). The plant will take water for refrigeration from the Riachuelo and will discharge it into the Río de la Plata.

In view of the necessity of performing some hydraulic studies, Mitsubishi commissioned INA, through its Hydraulic and Environmental Laboratory (LHA), to undertake them.

Two hydraulic problems were studied:

i) The possible influence of the discharged heated water on the temperature of the intake water had to be established in order to guarantee an adequate performance of the refrigeration system.

ii) As dredging will be performed around the water intake (in order to establish a sufficiently low intake level that guarantees the refrigeration system functioning even during extreme ebb events), the sedimentation rate in the dredged region had to be evaluated in order to estimate the maintenance dredging.

The studies were undertaken with numerical techniques:

a) Based on the shallow water character of the study zone, a horizontal 2D hydrodynamic model was implemented to describe the water currents. Details of this technique have been published in Reference [1].

b) The results of the hydrodynamic model feeded a heat transfer model of the plume. This is also based on a horizontal 2D analysis. Details of this technique have been published in Reference [2].

c) The results of the hydrodynamic model were also an input for a sediment transport model. Siltation rates were calculated based on the computed velocity fields and sedimentation formulas.

The models needed a variety of field data:

A) Bathymetric information was obtained from available nautical charts and navigation channel surveys and from localized bathymetric surveys specially performed for Mitsubishi.

B) Historical records of the Río de la Plata water levels were used to characterize the flow regime.

C) From disperse information, including measurements specially made for Mitsubishi, a characterization of the water currents in the study zone was achieved.

D) From available information and additional data specially measured for Mitsubishi, a quantification of the sediment properties was obtained.

E) The intake and dredging conditions were specified by Mitsubishi.

This report is organized as follows. In chapter 2 the data acquisition and processing for the study is described in detail. The thermal and the sedimentologic studies are presented in chapters 3 and 4, respectively. Finally, in chapter 5 the final conclusions of both studies are summarized.

2 DATA ACQUISITION AND PROCESSING

2.1 Hydrodynamic regime

The hydrodynamics of the study region is essentially controlled by the tidal-eolical regime of the Río de la Plata. Under normal conditions, the influence of the Riachuelo discharge is negligible. Only during big floods of the Matanza-Riachuelo basin some effects can be expected.

The hydrodynamic regime of the Río de la Plata is the result of the combined action of the following factors:

i) The oceanic tidal wave.
ii) The local wind action.
iii) The water discharge from the tributaries.

The oceanic tidal wave has itself astronomical components (with a mean amplitude of about 0.60 m and with the M2 component as dominant) and metheorological effects. This wave generates water currents between, approximately, 0.20 and 0.70 m/s. Of particular significance are the storm surges linked to the storm events known as "sudestadas" (associated to strong and persistent winds from the southeast), that can generate large increments of the mean river level.

Local winds can produce strong setups or setdowns at the river head, i.e., the Paraná Delta front. During the "sudestadas" the water level increment at the Delta front may be higher than 1 meter. In fact, the water level variations due to wind action is much more significant that astronomical changes due to stationality.

The significant tributaries of the Río de la Plata are the Paraná and Uruguay rivers, with a total average discharge of about 22,000 m^3/s. They produce a net drift current towards the Ocean of the order of 0.10 m/s.

2.2 Water levels

A characterization of the flow regime of the Río de la Plata in the neighbourhood of Buenos Aires city (including the study zone) can be achieved by analyzing the available water level records.

As an illustration, Figure 2.1 shows the time series of the water level, referred to the plane of reference (zero "MOP" or zero "Riachuelo") corresponding to a particular period of 30 days at Palermo station, in Buenos Aires city. Note that the disturbances caused by the wind action are as significant as the astronomical tide.

The distribution function (or rather, the histogram for a 0.25 m class interval) for the hourly water level at Palermo, over the period 1989-91, is presented in Figure 2.2. The mean water level is 0.88 m MOP. However, along the whole historical record (starting at 1905) the mean value is lower: 0.79 m MOP. This difference could be associated to the observed relatively wet hydrological cycle of the tributaries along the last two decades.

In Figure 2.3 the cummulative frequency of hourly levels, expressed as a frequency of exceedence, is shown. Note that 90% of the time the water level exceeds 0.25 m MOP, while only 10% of the time is over 1.6 m MOP. This means that 80% of the time the level is within a band of 1.35 m.

A similar analysis can be made for the peaks, i.e., flood (local maximum) or ebb (local minimum) conditions. Figures 2.4 and 2.5 present the histogram (for the same class interval as before, i.e., 0.25 m) and the frequency of exceedence for flood conditions at Palermo. The average value is 1.21 m MOP. During 80% of the time the flood level varies in a band of 1.3 m that goes from 0.6 to 1.9 m MOP.

Analogously, the histogram and frequency of exceedence for the ebb conditions are shown in figures 2.6 and 2.7. The mean value is 0.51 m MOP, and it moves within a band of 1.1 m, from 0.0 to 1.1 m MOP, during 80% of the time.

The relatively large width of the variation band of the flood and ebb levels put in evidence the strong influence of the local winds on the water levels.

In order to investigate the existence of a pattern in the time variation of the water level, a correlation analysis between ebb levels and the subsequent tidal wave height was performed. Figure 2.8 shows the correlogram for these two quantities. It is observed that the correlation is rather poor, indicating a quite random pattern. However, a weak trend can be distinguished, associating larger heights to lower ebb levels, as expected.

As a characterization of extreme events, annual maximum and minimum water levels at Palermo station were analyzed. Figure 2.9 presents the recurrence period for the annual maximum levels. It is observed that a peak level of about 3.0 m MOP can be expected each 2 years. A 10 years recurrence period is associated with a level of about 3.6 m MOP.

Analogously, the recurrence period for the annual minima are shown in Figure 2.10. Once each 2 years a minimum of about -1.1 m MOP can be expected, while the level -2.4 m MOP has a recurrence period of 10 years.

2.3 Water currents

The wind-perturbed tidal wave that travels upstream the Río de la Plata is, essentially, a long gravity wave. Hence, the relation between its height H and its velocity amplitude V_a is, within the linear approximation, given by [3,4]:

$$\frac{V_a}{H} = \frac{1}{2}\sqrt{\frac{g}{h}} \qquad (2.1)$$

where g is the acceleration of gravity and h is the mean depth.

Figure 2.11 shows current velocity records (for the period 04 to 07/Apr/87) corresponding to a point located about 30 km downstream the Riachuelo mouth and 9 km off the coast [5], which can be considered as "open waters", in the sense that the hydrodynamics there is only poorly influenced by the coast. The motion is essentially one-directional, i.e., the current only inverts its direction. In Figure 2.12 the corresponding peak velocities with the associated (recorded) flood and ebb levels are presented.

An analysis of these data was performed in order to verify equation 2.1. The best correlation between peak velocity and tidal wave height was obtained when the peak velocity was associated with the previous wave height. Taking h = 9 m (representative of a mean depth along the wave trajectory from the ocean), the coefficient $2V_a/H\sqrt{(h/g)}$ is plotted in Figure 2.13 for various values of the drift current (subtracted, with the corresponding sign, from the peak values). It is observed that it fluctuates around the theoretical value 1. The "best fit", i.e., the one with the lowest mean square error, corresponds to the drift current of 0.10 m/s.

2.4 Riachuelo discharge

As explained above, under normal conditions the flow regime in the Riachuelo mouth is controlled by the Río de la Plata. Hence, a pulsatile flow prevails, with ebb and tide conditions in phase with the ones corresponding to the Río de la Plata.

Available results of simulations made with a hydrodynamic mathematical model of the Matanza-Riachuelo River [6] include discharge time series about 15 km upstream of its mouth for normal conditions. The peak values are about 10 m^3/s both for ebb and flood conditions (with associated peak velocities of about 0.10 m/s for both conditions).

2.5 Definition of scenarios

Based on the previous information, particular scenarios can be defined, i.e., sets of statistically significant hydrodynamic conditions in open waters, that can later be used for model runs (see next chapters).

The establishment of scenarios was started with the selection of an ebb level. According to Figure 2.2, the most frequent ebb level (with a class interval of 0.25 m) is about 0.38 m MOP, with a frequency of 26.1%. The associated distribution of tidal wave height (taken from Figure 2.8) is illustrated in Figure 2.14. The value 0.60 m was taken as representative of (the center of gravity of) the water level excursion. This means that the subsequent flood level is 0.98 m MOP.

Now, the peak velocities associated with this tidal excursion can be calculated assuming that equation 2.1 holds (for h = 9 m). Considering that the drift current towards the ocean is 0.10 m/s, in agreement with the analysis developed in section 2.2, the obtainedd ebb and flood velocities are 0.50 and 0.30 m/s, respectively.

To complete the needed hydrodynamic conditions for a model operation (see chapter 3), a discharge of ± 10 m^3/s out from the Riachuelo mouth was associated to ebb and flood conditions, respectively. A complete set of hydrodynamic conditions characterizing this scenario, named Scenario A, is presented in Table 2.1.

With the explained methodology, one more scenario was build, correponding to a relatively high ebb level of 1.13 m MOP, with a frequency of 6.5% (Scenario B). The complete set of hydrodynamic conditions associated to this scenario is also shown in Table 2.1.

The results for scenario B will show the sensitivity of the results to variations in the hydrodynamic conditions.

2.6 Water discharge and intake from and for the power plant

Presently there exits refrigeration circuits for seven units, named U1 to U7. The intakes for all of them are concentrated in the same zone, within the Riachuelo mouth. The discharges, instead, are located at two different points along the Río de la Plata coast (Figure 2.15):

i) For units U1 to U5 there is a total discharge of 75,000 m^3/h (20.8 m^3/s) with an overtemperature of 8°C.

ii) Units U6 and U7 have associated discharges of 46,000 m^3/h (12.8 m^3/s) each, but with different overtemperatures: 7 and 8°C, respectively.

The total intake/discharge for the refrigeration circuits is then of 167,000 m^3/h (46.4 m^3/s).

The intake for the new power plant will lie closer to the Río de la Plata, while the discharge will be implemented at one of the present locations (Figure 2.15). The intake/discharge will be of 60,000 m^3/h (16.7 m^3/s), which will be added to the present value.

2.7 Bathymetry and chartography

The bathymetry of the study region was built compossing data from different sources:

a) For the Río de la Plata fringe adjacent to the coast, bathymetric charts from the Hydrografic Service of the Navy (SIHN) were used. In particular, the most updated chart (H155A) was taken.

b) For the navigation channel (Canal Sur), giving access to Dock Sud, surveys made by the National Direction of Harbour Works (DNCPyVN) during August 1996 were obtained.

c) A bathymetric survey of the Riachuelo mouth was specially made for Mitsubishi during January 1997.

In Figure 2.16 bathymetric contour lines of the compossed bottom topography are shown. This representation is considered to be completely adequate to modelling purposes.

A detailed chartography of the study zone was obtained through digitalization of aerial photographs (approximate scale 1:7000) purchased at Base Aeronaval Punta Indio.

2.8 Sedimentation

Bathymetric surveys identified as (b) and (c) in the previous section superpose in most of the Riachuelo mouth. As a measurable sedimentation ocurred in the dredged zones (navigation channel and access channel to the power plant dock) during the five months period between them, a data processing was performed in order to quantify it.

The superposition zone was divided in cells, according to Figure 2.17. Note that one set of cells aligns with the navigation channel, following the contour line -8 m MOP (according to the August survey), while the remaining ones lie on the access channel to the power plant dock region.

The sedimentation for each cell was evaluated by simply calculating the volume between the two topographic surfaces. Figure 2.18 shows the monthly sedimentation rate for the navigation channel. The mean value is 0.13 m/month. The general trend seems to be a smooth increase in the sedimentation rate when moving into the Riachuelo mouth.

The sedimentation rate in the dock access channel is presented in Figure 2.19. The mean value is now somewhat higher, 0.17 m/month. No general trend is observed. Hence the variations may be associated to estimation errors.

2.9 Suspended sediment

During the campaign made specially for Mitsubishi, water samples at three locations were taken in order to make granulometric analyses of the suspended sediment.

The three locations are shown in Figure 2.20. One corresponds to the discharge area, while the other two are associated to the actual and future intake areas. For each location three water samples were taken: one at the bottom, one at the middle of the water column and the third one at the water surface.

Figure 2.21 shows the measured suspended sediment concentrations for each point. Note that all of them are between 25 and 35 mg/l for the intake regions. They are larger for the discharge zone: nearly doubled for the middle and surface positions and a peak of about 270 mg/l at the bottom.

The granulometry of the taken samples for the three locations are presented in figures 2.22 to 2.24. As expected, they are essentially constituted of silt and clay (diameters lower than about 60 μm). Note that, in all cases, the material is finer towards the surface, as expected. For the intake regions the mean diameter is between 3 and 7 μm. That is also the case for the middle and surface positions at the discharge location. However, at this location the mean diameter is about 13 μm at the bottom.

Taking as a reference a concentration between 60 and 100 mg/l and a mean diameter of around 10 μm in open waters [7], the observed suspended sediment characteristics can be explained as follows:

i) The lower concentrations and granulometry for the intake regions are consistent with the fact that only the finer material makes its way through the Riachuelo mouth, due to the decreasing water currents.

ii) The suspended sediment characteristics at the middle and surface positions of the dicharge location are similar to the open water values, which is consistent with a more exposed zone.

iii) The peak concentration and mean diameter at the bottom of the discharge zone shows that the discharge itself is exerting some influence on the suspended sediment, probably putting in suspension part of the bottom sediment.

2.10 Dispersion coefficients

Heat transfer within the fluid will be subjected to turbulent diffusion. In addition, due to the vertically integrated analysis, differential advection due to the vertical gradient of the horizontal current velocity must also be considered. The combined effect is represented through the

dispersion coefficients, relating the diffusivity to the product of the local shear velocity and water depth.

Values of the dispersion coefficients close to the coast of the Río de la Plata are available from previous studies made at INA [8]: 20.0 for the longitudinal coefficient and 0.23 for the transversal one. They were used as valid for the dispersion of heat in the present study.

3 THERMAL STUDIES

3.1 Physical description of the problem

The heated water discharged to the Río de la Plata by the refrigeration system will merge with the river waters. After a short distance, where the initial dilution takes place, a jet amenable to a horizontal 2D analysis will develop.

Both the jet momentum and the plume overtemperature will gradually attenuate while they develop into the river. This attenuation is mainly due to the combined action of two physical mechanisms: the water currents and the turbulent diffusion (the heat radiation towards the atmosphere is practically negligible over the short distances of interest).

The development of the thermal plume will be subjected to the tidal action, which will transport it back and forth during the tidal cycle. Hence, it is expected that, at least during part of this cycle, the plume makes its way towards the water intakes, which exert significant "calls" to the river waters.

3.2 Hydrodynamic modelling

The water current is the driving mechanism of heat transfer from the discharge zone to open waters or, eventually, towards the intake locations. Hence, it has to be represented with enough accuracy.

A nesting modelling procedure was undertaken. Two hydrodynamic models were implemented (Figure 3.0):

i) A "regional" model: It includes the mouth of the Riachuelo and a coastal strip of the Río de la Plata. Its extension is 3,000 m in the longitudinal direction (parallel to the coast) and 2,000 m in the transversal direction. It must fulfill known conditions in the open waters of the Río de la Plata.

ii) A "local" model: It includes the zone of development of the thermal plume. Its extension is 2,000 m in the longitudinal direction and 1,825 m in the transversal direction. Its boundary conditions are provided by the regional model.

Due to the small spatial scale of the study zone, relative to the tidal wave, dynamics effects within the model domains are negligible. Hence, instantaneous states can be simulated by imposing the appropriate (fixed) boundary conditions (water levels and velocities).

The northeast open boundary of the regional model was considered to be completely aligned with the water particles trajectories (coincident with the streamlines due to the neglection of dynamic effects). Hence it was treated as an impervious border.

Once a scenario is chosen and a particular condition (associated to a particular instant of the tydal cycle) selected, the boundary conditions at the two remaining open borders of the regional model were taken as follows:

a) Southeast boundary: The water level corresponding to the selected condition was imposed all along.

b) Northwest boundary: The water discharge was imposed so as the velocity at the open waters extreme of the boundary was equal to the value corresponding to the selected condition.

The northeast open boundary of the local model is located in a zone where the influence of the discharges from the water plant has already died out. Hence, the runs made with the regional model can be used for both conditions: actual and future.

The local model was run for each one of the defined stages of the two scenarios and for the two discharge/intake conditions. Each simulated instantaneous hydrodynamic stage of each scenario was associated to a particular instant of the tidal cycle, according to Table 3.1. The origin of time is taken as coincident with the peak ebb flow. This cycle is repeated succesively. Figures 3.1 to 3.6 show the calculated velocity fields for scenario A.

The system evolves smoothly from one stage to the other. It was supposed that the intermediate stages can be obtained by linear interpolation between them.

In order to understand the water movement, a follow up of the positions of water particles emerging from one of the discharges location was done. The results for the actual conditions are shown in figures 3.7 to 3.17, while figures 3.18 to 3.29 present the ones corresponding to the future conditions. The call from the actual water intake is clearly observed. The second call, from the new water intake, is also noticed for the future situation. It is observed that, for both situations, only some of these particles are able to penetrate into the Riachuelo mouth and reach the intake locations. Hence, the effect of the overtemperature on the water intakes is felt only during a time window.

3.3 Heat transfer modelling

The modelling technique used to represent the unsteady thermal plume consists in the discretization of the heat discharge into short pulses, each of which gives small (gaussian) clouds of overtemperature. The model follows the position, shape and orientation parameters of each cloud. The overtemperature at a particular point in space and at a particular instant of time is calculated through the superposition of the effects of all clouds. This methodology is quite efficient in treating this complicated heat transfer problems.

According to the results of the foregoing section, the heat clouds, and hence the thermal plume, will be able to penetrate into the Riachuelo mouth only during a time window. The remaining time "fresh water", coming directly from the Río de la Plata, hits the water intakes. As a consequence, the intake water will be subjected to pulses of overtemperature, which values have to be determined by the thermal model.

Figures 3.30 to 3.37 present instantaneous thermal plumes corresponding to scenario A for the actual conditions, while the corresponding results for the future conditions are shown in figures 3.38 to 3.45. As expected, the plumes for the future situation are "thicker" than for the actual situation, due to the enhanced heat discharge. Note that there appear some overtemperature local maxima, with peak values sometimes greater than the overtemperature at the discharges

themselves. This is a typical unsteadiness effect, which occurs due to the local reduction of the current velocity along the fluid particles trajectories, leading to heat accumulation.

Figure 3.46 shows the overtemperature for the actual conditions at the actual and future intake locations for the whole tidal cycle of scenario A. It must be mentioned that some minor quantitative corrections were made to these results in order to disregard a spurious effect emerging from the accumulation of heat clouds in a quasi-stagnant region close to the future intake location. The heat clouds accumulation led to the appearance of a relatively small, but measurable, overtemperature threshold. This accumulation could only be avoided by increasing the spatial resolution or diminishing the temporal resolution, an impractical solution due to the short time available for the study. Hence, and ad-hoc correction of the model results was made by estimating this overtemperature threshold (0.45°C for the future intake location and 0.35°C for the actual intake location) and substracting it from the results.

From Figure 3.46 it is observed that two overtemperature pulses of about 2 to 3 hours duration are observed at the actual intake location, with peak values of 1.2 and 2.7°. At the future intake location only the main pulse is observed. It leads the one at the actual location by about three hours and attains practically the same peak value (2.6°C).

The results for the future situation are shown in Figure 3.47. Now the two pulses are significant at both intake locations and they occur sooner within the tidal cycle. At the actual intake location the peak values are similar for both pulses and lie in between the values for the previous case (they reach about 1.9°C). Both pulses are mounted on a base overtemperature of the order of 0.5°C and about 10 hours duration. This change of behaviour must be due to the "calling effect" of the new water intake, that produces an approximation of the thermal plume to the coast.

At the future intake location the overtemperature peak values of the two pulses are about 2.3 and 3.2°C.

Figures 3.48 and 3.49 present the results corresponding to scenario B for the actual and future conditions, respectively. They are qualitatively and quantitatively similar to the ones for scenario A, though significant phase differences occur in association with the different pattern of velocity variation during the tidal cycle. The most significant difference is the increase of the peak overtemperature at the future water intake to a value close to 5°C. This gives a measure of the expected overtemperature variation due to changes in the hydrodynamic regime.

3.4 Overtemperature feedback

The fact that there appears a measurable overtemperture at the water intake produces an increment of the heated water overtemperture at the discharge, due to the fact that the refrigeration system imposes a (practically) fixed temperature increase to the flowing water, which in turn generates an increment of the overtempertaure at the water intake, thus leading to a positive feedback mechanism. In order to quantify it, the following calculation procedure was implemented:

i) The calculated overtemperatures at the water intakes (figures 3.46 or 3.47 for scenario A) were added to the overtemperature at the discharge, but introducing a time lag due to the time it takes to the water to travel all along the refrigeration circuit. This is conservative in the sense that no temperature decay is assumed.

ii) Assuming that the relative overtemperature calculated by the model at the water intake locations, with respect to the overtemperature at the water discharge, remains the same irrespective of the absolute value of the latter, the absolute overtemperature at the water intakes was calculated using the augmented overtemperature at the discharge, but introducing a time lag representative of the time of travel of the water particles from the discharge to the intake.

iii) The procedure was repeated succesively in time until convergence was achieved.

The estimated times of travel were the following:

From actual water intake to main water discharge:	1 hour
From new water intake to main water discharge:	0.5 hour
From main water discharge to actual water intake:	5 hours
From main water discharge to future water intake:	2 hours

The former two time values were estimated based on the available planes of the power plant, from which a representative length and a transversal section of the conducting pipe were obtained. The last two time values, instead, were obtained from the the hydrodynamic model.

An initial mean temperature of 7.5°C at the main water discharge was assumed.

The obtained results were not too sensitive to variations in the values of the foregoing parameters.

Figure 3.50 shows the overtemperature at the main water discharge for the actual conditions. The observed peaks are a direct consequence of the overtemperture at the actual water intake.

The calculated change of the overtemperature at the actual water intake location, due to this temperature increase at the water discharge, was practically negligible, due to the fact that the time lag of about 5 hours (for pulses durations of the order of 2 to 3 hours) makes it impossible for the augmented overtemperature to reach this location. Hence, the results of figure 3.46 are representative of the final situation.

For the future conditions, the existence of two water intakes produces a superposition of effects arising from them. The effective overtemperature of the water emerging from the main water discharge was estimated as a weighted average between the two of them. Figure 3.51 shows the obtained results for this overtemperature. The corresponding overtemperture at the water intakes are presented in figure 3.52. Comparing with figure 3.47, it is observed that the increments due to the feedback mechanism are very small.

4 SEDIMENTOLOGIC STUDIES

4.1 Physical description of the problem

The upper Río de la Plata constitutes a siltation basin for the fine-grained suspended sediment carried as wash load by the Paraná River. As a matter of fact, the sudden expansion of the flow at the Delta front produces a continuous advancement of the Delta frontline. However, most of the sediment injected by the Paraná River is maintained into suspension by the tidal currents and transported downstream by the drift current, while loosing a fraction by deposition. Siltation is, then, a continuous process modulated by the hydrodynamic cycle.

This siltation mechanism means that at any place where quasi-stagnant conditions are attained the siltation rate may be significant, producing a natural filling. This must be taken into account when undertaking coastal engineering works.

4.2 Detailed hydrodynamic model

To estimate the siltation rate, and hence the maintenance dredging of the excavation around the future water intake, mathematical modelling techniques were used.

In the first place, a 2D "detailed" hydrodynamic model, centered around the new intake location, was implemented. Figure 4.1 shows the model domain. Its extension is 560 m in the longitudinal direction and 650 in the transversal direction. The spatial discretization step was taken as 6.25 m.

The boundary conditions were provided by the local hydrodynamic model. Figures 4.2 to 4.7 present velocity fields corresponding to different instants of the tidal cycle for scenario A and actual conditions, while figures 4.8 to 4.13 show the correponding ones for future conditions.

4.3 Sedimentologic model

The sedimentation model is based on the following siltation formula for suspended fine sediment [9]:

$$S = \frac{c\, w_s}{1 - p} F\left(\frac{u_*}{u_c}\right)$$

where S is the siltation rate, c the suspended sediment concentration, w_s the settling velocity of the representative (mean) sediment diameter, p the porosity of the deposits, u_* the shear velocity, u_c the critical value for deposition of the shear velocity and F the following function:

$$F(x) = \begin{cases} 0 & \text{if} \quad u_* > u_c \\ 1 - \left(\frac{u_*}{u_c}\right)^2 & \text{if} \quad u_* > u_c \end{cases}$$

4.4 Model calibration

The values of the sediment parameters (c, w_s, , p and u_c) were considered as uniform throughout the study region. Hence, siltation changes across the domain are controlled by the shear velocity, a hydrodynamic parameter which is obtained from the results of the detailed hydrodynamic model.

A value of 35 mg/l was taken as representative of the concentration c, according to the measurements presented in chapter 2. The value of the critical bottom shear stress u_c was chosen as 8.4 mm/s, in agreement with the literature [10] and past experience in the Río de la Plata. The porosity p of the bottom deposits was estimated as 0.8 from analysis performed at INA on this region [11].

The remaining parameter, namely the settling velocity w_s, associated to a representative sediment diameter, is the controlling parameter of the absolute value of the siltation rate for very fine sediments like the present ones, according to the data presented in chapter 2. This is, then, the actual calibration parameter. The selection of its value can be made based on the estimated siltation rates of the study zone, also presented in chapter 2.

The net siltation rate associated to a tidal cycle was obtained through a weighting average of the values corresponding to each one of the six hydrodynamic stages simulated by the hydrodynamic model. The weights were proportional to the assigned time interval, according to a step-like representation of the cycle. The contour lines of annual siltation rates associated to mean diameters of 15 and 30 μm are presented in figures 4.14 and 4.15. It is observed that the second one is in better agreement with the observed values (0.13 m/month on the navigation channel and 0.17 m/month on the dock access, according to the analysis of chapter 2). However, as this diameter is relatively high in relation with the measured granulometric curves, calculations of siltation will be performed for both diameters, as a way of obtaining a measure of the uncertainty associated to the estimations.

4.5 Maintenance dredging

A dredged zone at -4 m IGM with a rectangular form was consider, as shown in Figure 4.16. The minor side of the rectangle is paralell to the water intake mouth and has a length of 12.5 m. The major side is 44 m long, and reaches the access channel to the power plant dock.

Figure 4.17 and 4.18 present the siltation rate contour lines around the dredged zone, corresponding to the two diameter values. It is observed that a non-siltation zone occurs around the intake mouth due to the relatively high water velocities, which produce a shear velocity above the critical value. Its extension is about 15 m and its width 5 m.

Figure 4.19 shows the siltation rate along the dredged zone for the two diameter values. It is observed that they grow relatively fast when moving away from the intake mouth. It is also noted that the difference between the siltation rates associated to the two diameters is high, which illustrates the above mentioned sensitivity to this parameter.

By integration of the siltation curves, total siltation volumes of about 7.5 and 26 m^3/month are obtained for the 15 and 30 μm diameters, respectivley. Hence, it can be concluded that the maintenance dredging is in the order of 10 to 30 m^3/month, expressed in terms of in-situ volumes.

The increment of siltation volume due to a deeper excavation level is primarily related to the increment of length of the dredging zone. As a rough estimation, the increase of siltation volume, for each additional meter of dredging zone length, is between 0.5 and 1.5 m^3/month.

5 CONCLUSIONS

The following are the main conclusions of the studies.

Thermal study:

The overtemperature at the water intakes manifest itself as more or less definite pulses, with durations of a few hours and with peak values in the range from 2 to 5°C, which automatically superpose on the overtemperature at the water discharge after a time of the order of 1 hour. However, the feedback effect is quite small due to the fact that the time of travel of the overheated water is of the order of half the tidal cycle, making impossible its reaching to the intake locations.

Sedimentation study:

The estimated maintenance dredging, for a dredged zone about 45 m long at - 4 m IGM around the future water intake, ranges between 10 and 30 m^3/month, with null values of siltation close to the intake itself, up to distances of about 15 m. The increment of siltation volume, for each additional meter of dredging zone length, is between 0.5 and 1.5 m^3/month.

REFERENCES

1 Menéndez, A.N., *Sistema Hidrobid II para simular corrientes en cuencos*, Revista Internacional de Métodos Numéricos para Cálculo y Diseño en Ingeniería, Vol. 6, 1, 25-36, 1990

2 Carreras, P.E., Menéndez, A.N., *Mathematical simulation of pollutant dispersion*, Ecological Modelling, 52, 29-40, 1990.

3 Menéndez, A. N., Norscini, R., *Spectrum of Shallow Water Waves: An Analysis*, Journal of the Hydraulics Division, ASCE, Vol. 108, No. HY1, January, 1982.

4 Menéndez, A. N., Norscini, R., "Wave Attenuation in Open Channel Flow". Encyclopedia of Fluid Mechanics, N. P. Cheremisinoff, editor, Gulf Publishing Co., Vol. 2, 1986.

5 Carreras, P.E., Menéndez, A.N., *Proyecto de tratamiento y disposición de efluentes cloacales del Gran Buenos Aires. Modelo Matemático hidrodinámico*, Report LHA-INCYTH 070-002-87, December 1987.

6 UTE Engevix, Cowi, Inconas, *Plan de Gestión Ambiental y de Manejo de la Cuenca Hídrica Matanza-Riachuelo. Anexo Técnico-A. Modelo Matemático*, SRNyAH de la Nación, Argentina, marzo 1995.

7 Hopwood, H.J., Menéndez, A.N., Chividini, M.F., Cavaliere, M.A., Brea, D., *Informe de diagnóstico sobre navegación en la ruta Rosario-Océano*, Informe LHA-INCYTH 114-01-91, Comitente: Cámara de Propietarios de Puertos Privados Comerciales, mayo de 1991).

8 Carreras, P.E., Menéndez, A.N., *Proyecto de tratamiento y disposición de efluentes cloacales del Gran Buenos Aires. Modelos Matemáticos de dispersión de contaminantes*, Report LHA-INCYTH 070-003-88, April 1988.

9 Partheniades, E., *Estuarine Sediment Dynamics and Shoaling Processes*, Handbook of Coastal and Ocean Engineering, vol. 3, John B. Herbich (editor), Gulf Publishing Company, 1992.

10 Kirk Ziegler, C., Nisbet B.S., *Lont-Term Simulation of Fine-Grained Sediment Transport in Large Reservoir*, Journal of Hydraulic Engineering, ASCE, vol. 121, No. 11, November, 1995.

11 Lobos, J., *Personal communication*, INA, 1997.

TABLE 2.1
Hydrodynamic conditions for different scenarios

Scenario A

ID	Water level (m MOP)	Velocity (m/s)	Riachuelo discharge (m3/s)
AN1	0.38	0.50	10.00
AN2	0.50	0.34	6.00
AN3	0.60	0.21	2.67
AN4	0.70	0.07	-0.67
AN5	0.80	-0.06	-4.00
AN6	0.98	-0.30	-10.00

Scenario B

ID	Water level (m MOP)	Velocity (m/s)	Riachuelo discharge (m3/s)
BN1	1.13	0.43	10.00
BN2	1.30	0.21	3.20
BN3	1.45	0.01	-2.80
BN4	1.63	-0.23	-10.00

File: C:\COSTANER\INFO\VEL_INT.WQ2

TABLE 3.1
Hydrodynamic cycle for different scenarios

Scenario A

ID	Time (hours)
AN1	0.00
AN2	1.70
AN3	2.30
AN4	2.70
AN5	3.32
AN6	5.00
AN5	6.98
AN4	7.71
AN3	8.19
AN2	8.89
AN1	12.00

Scenario B

ID	Time (hours)
BN1	0.00
BN2	2.50
BN3	3.00
BN4	5.00
BN3	7.36
BN2	7.95
BN1	12.00

File: C:\COSTANER\INFO\VEL_INT.WQ2

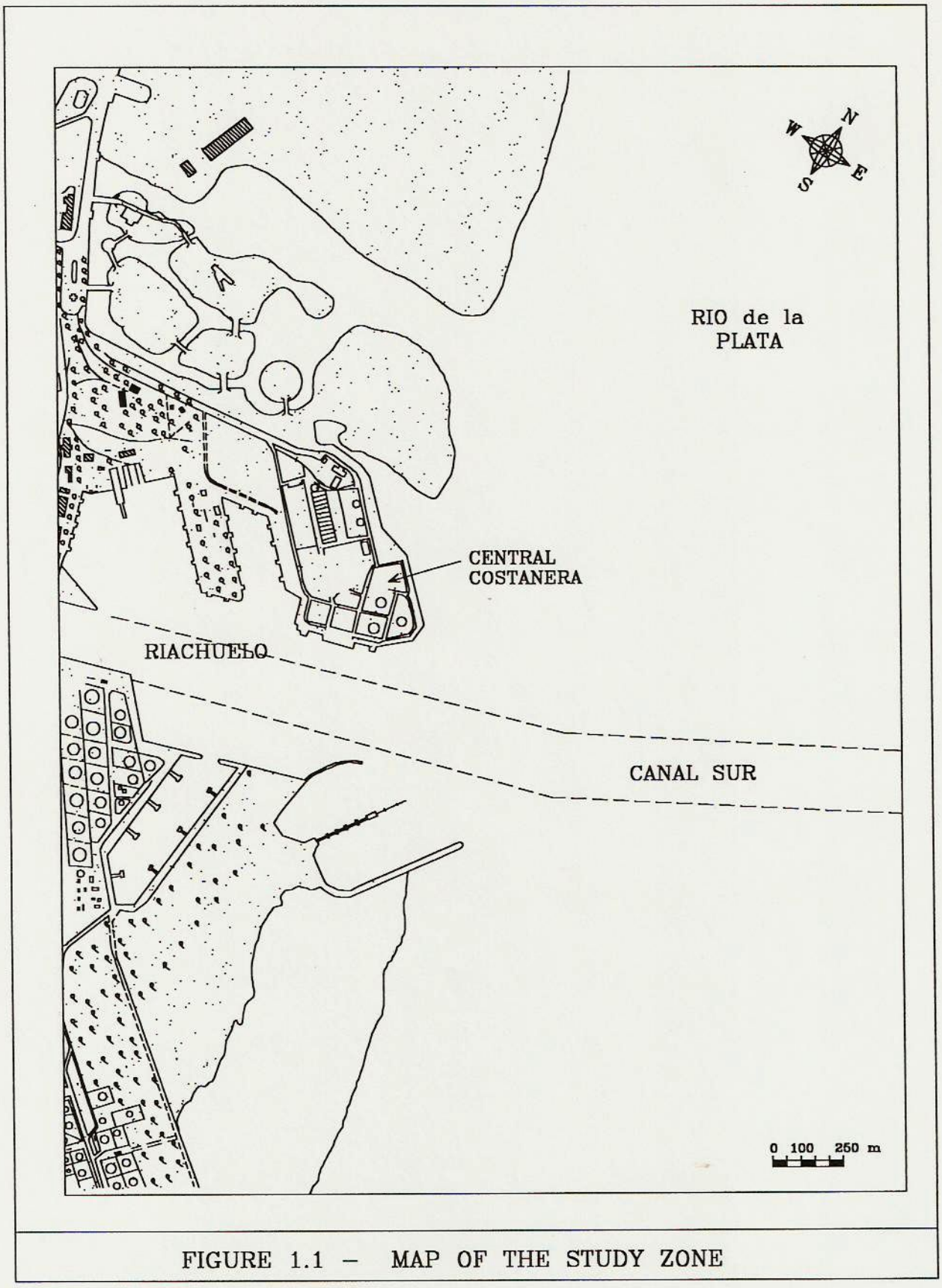

FIGURE 1.1 – MAP OF THE STUDY ZONE

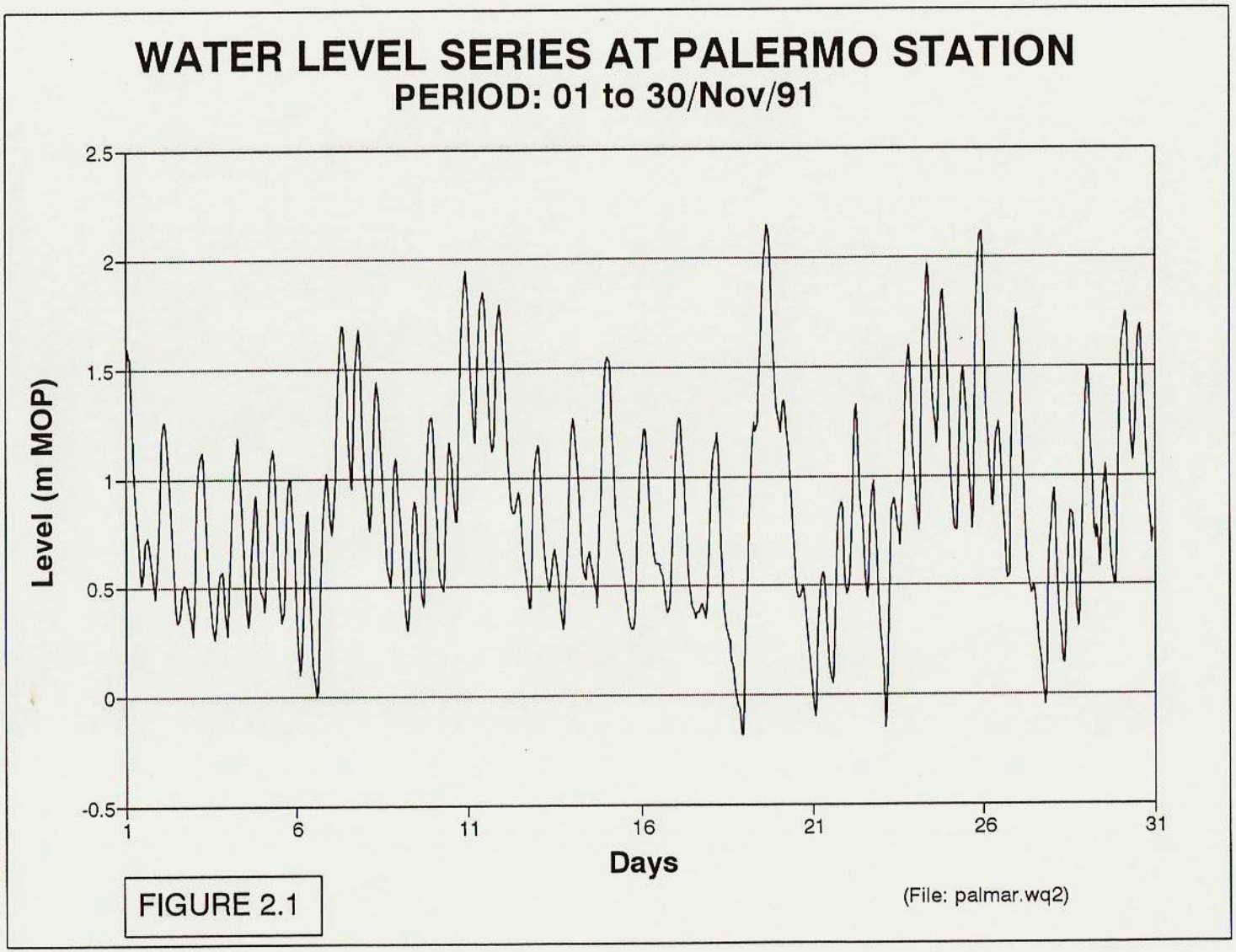
WATER LEVEL SERIES AT PALERMO STATION
PERIOD: 01 to 30/Nov/91
Level (m MOP)
2.5
2
1.5
1
0.5
0
-0.5
1
6
11
16
21
26
31
Days
(File: palmar.wq2)

FIGURE 2.1

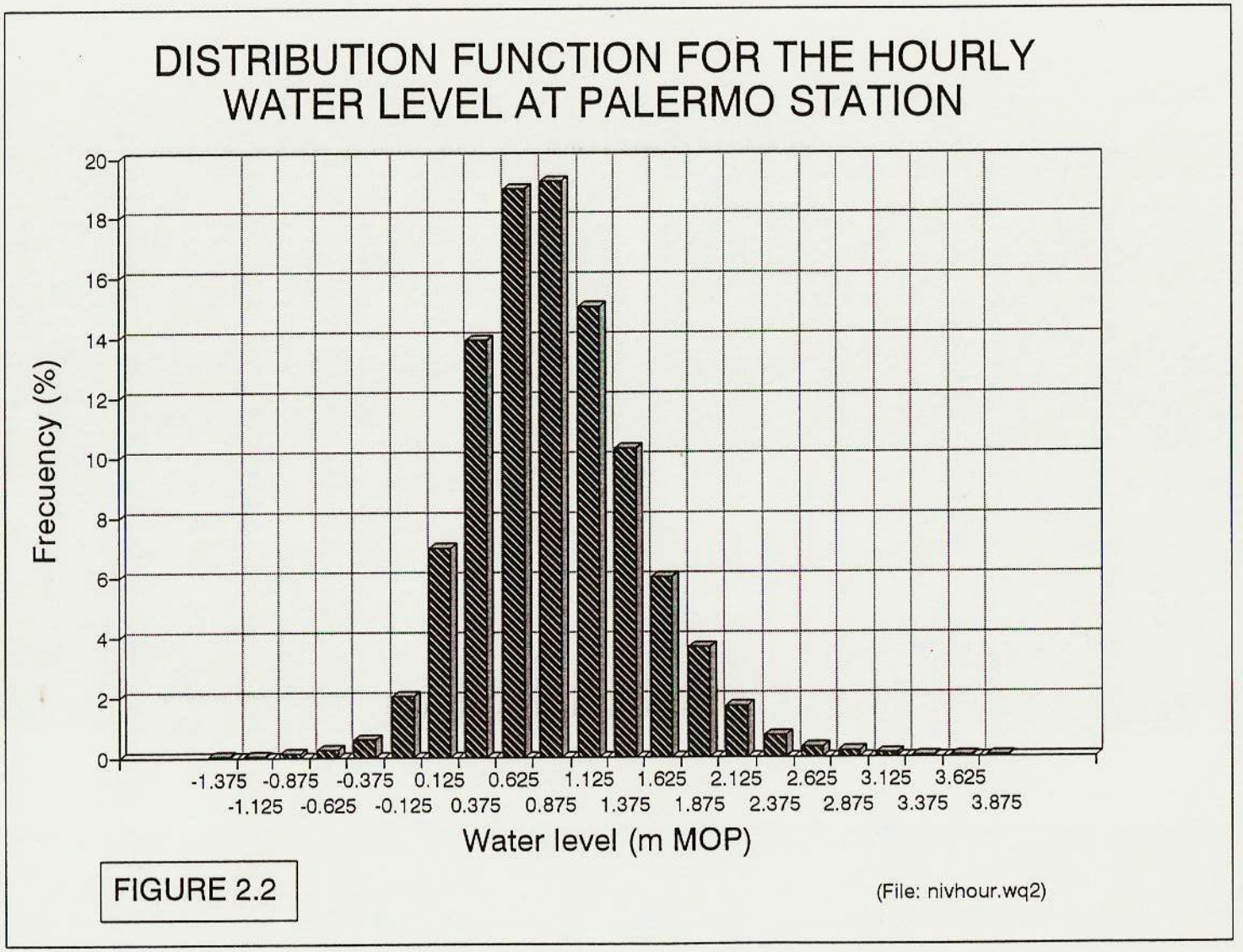

FIGURE 2.2

(File: nivhour.wq2)

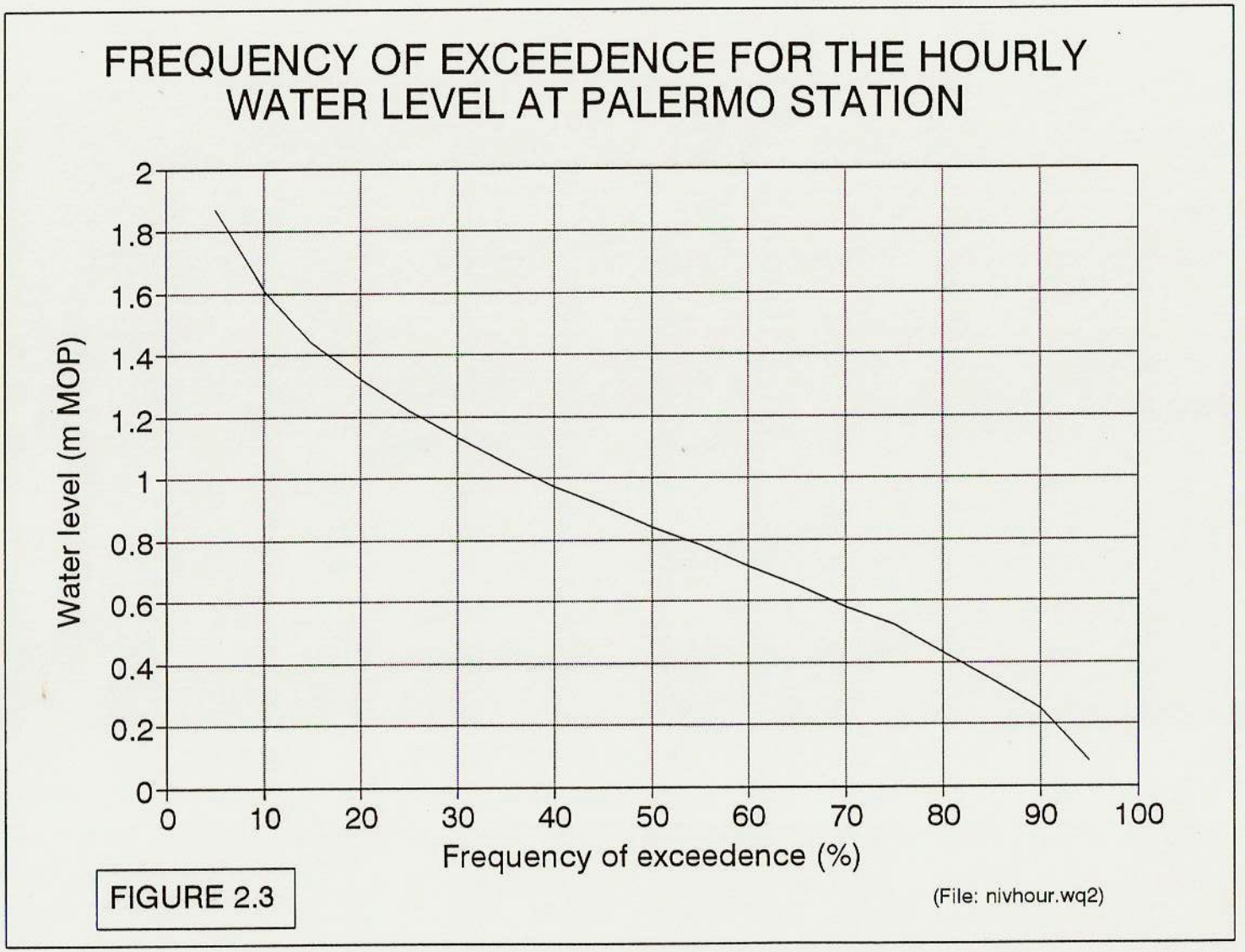
FREQUENCY OF EXCEEDENCE FOR THE HOURLY WATER LEVEL AT PALERMO STATION
Water level (m MOP)
2
1.8
1.6
1.4
1.2
1
0.8
0.6
0.4
0.2
0
0
10
20
30
40
50
60
70
80
90
100
Frequency of exceedence (%)
FIGURE 2.3
(File: nivhour.wq2)

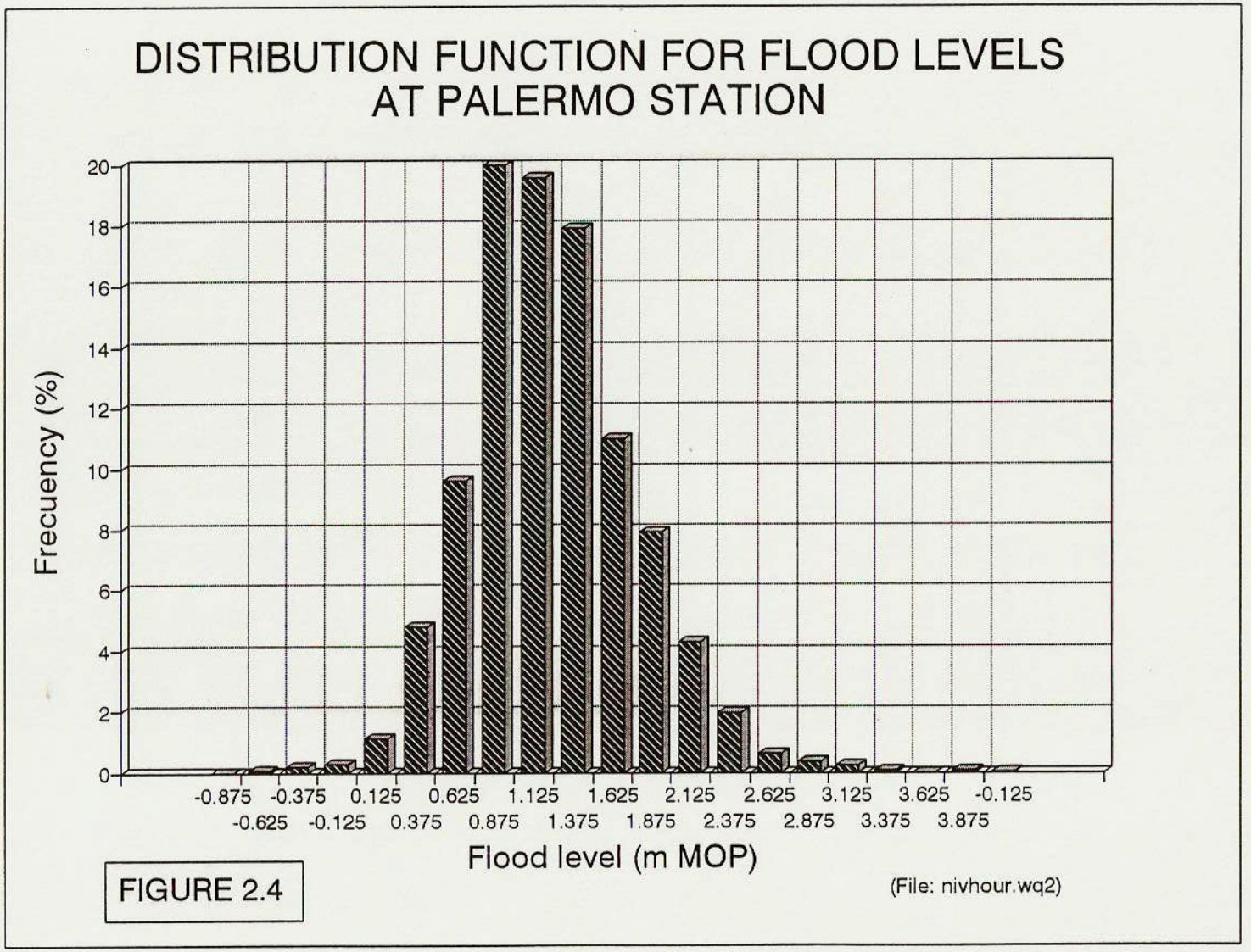
DISTRIBUTION FUNCTION FOR FLOOD LEVELS
AT PALERMO STATION
Frecuency (%)
20
18
16
14
12
10
8
6
4
2
0
-0.875
-0.625
-0.375
-0.125
0.125
0.375
0.625
0.875
1.125
1.375
1.625
1.875
2.125
2.375
2.625
2.875
3.125
3.375
3.625
3.875
-0.125
Flood level (m MOP)
FIGURE 2.4
(File: nivhour.wq2)

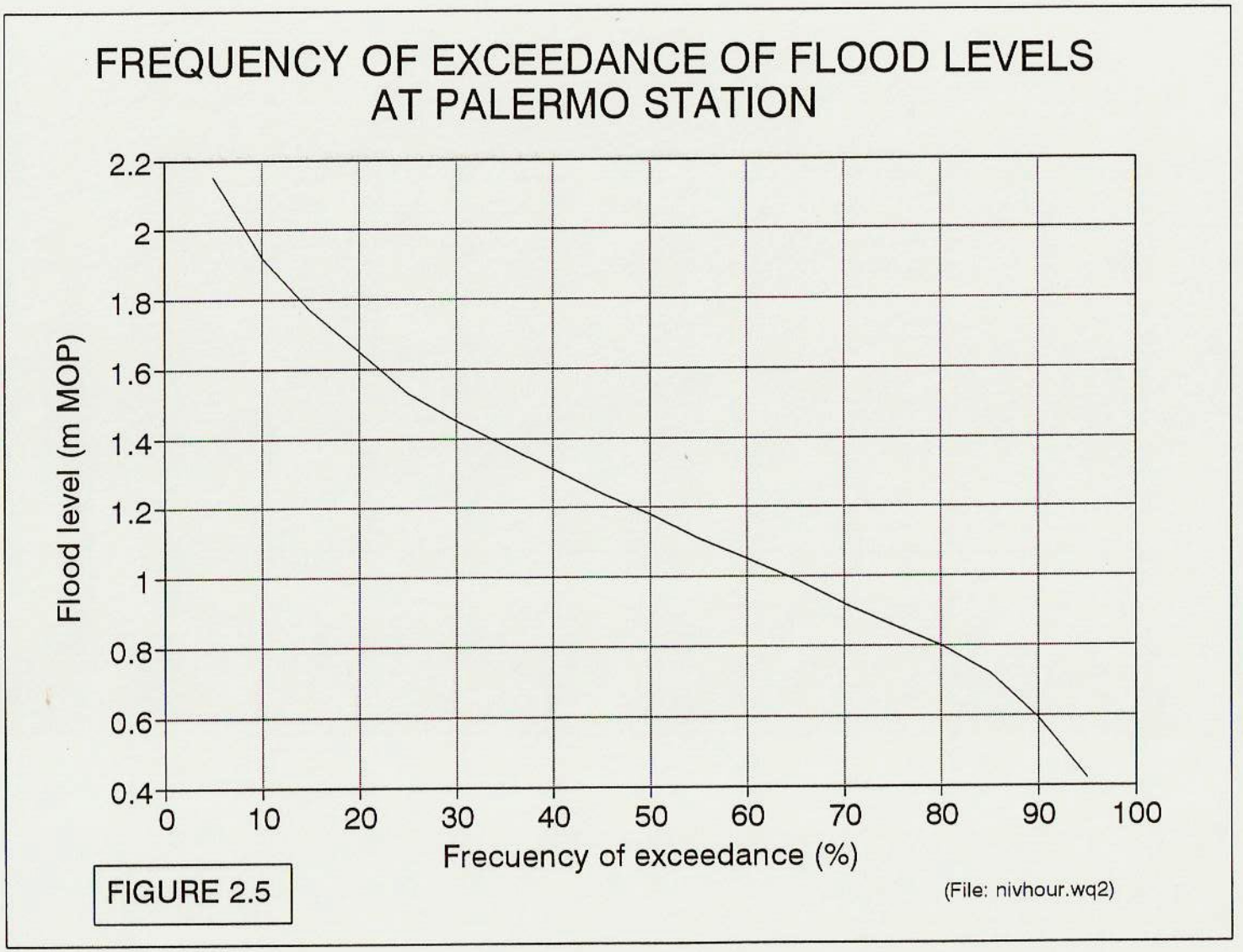
FREQUENCY OF EXCEEDANCE OF FLOOD LEVELS
AT PALERMO STATION
Flood level (m MOP)
2.2
2
1.8
1.6
1.4
1.2
1
0.8
0.6
0.4
0
10
20
30
40
50
60
70
80
90
100
Frecuency of exceedance (%)
FIGURE 2.5
(File: nivhour.wq2)

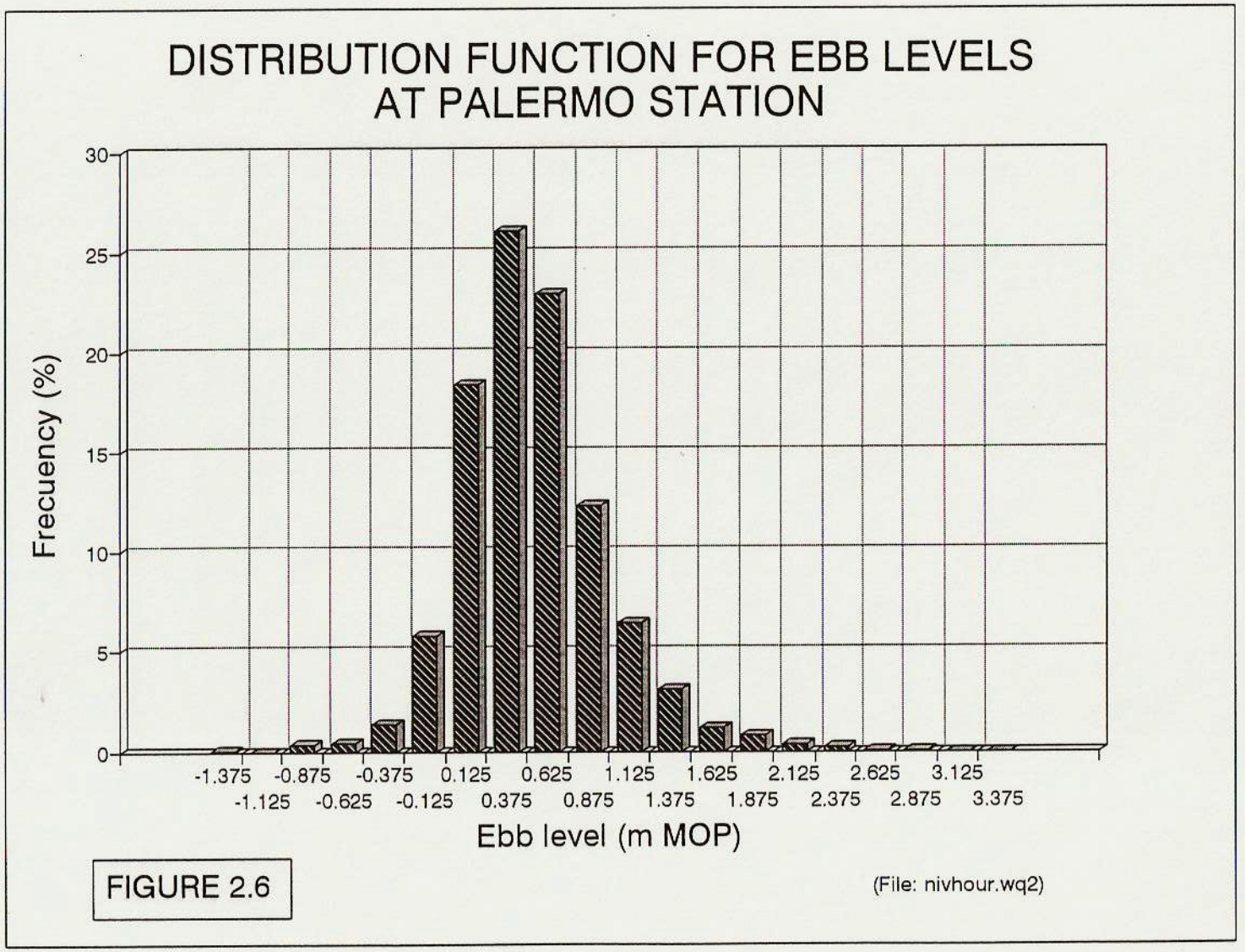

FIGURE 2.6

(File: nivhour.wq2)

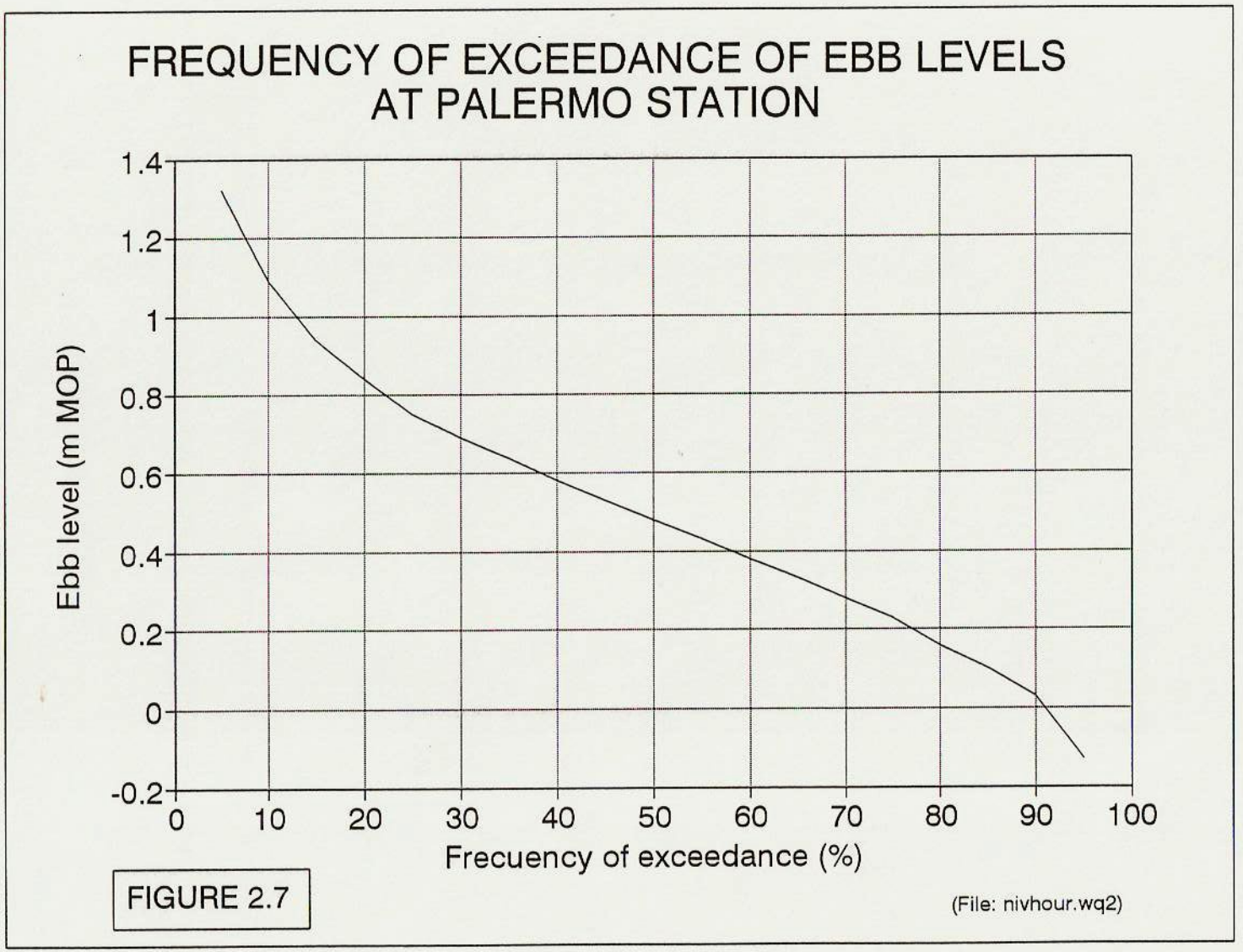
FREQUENCY OF EXCEEDANCE OF EBB LEVELS
AT PALERMO STATION
Ebb level (m MOP)
1.4
1.2
1
0.8
0.6
0.4
0.2
0
-0.2
0
10
20
30
40
50
60
70
80
90
100
Frecuency of exceedance (%)
FIGURE 2.7
(File: nivhour.wq2)

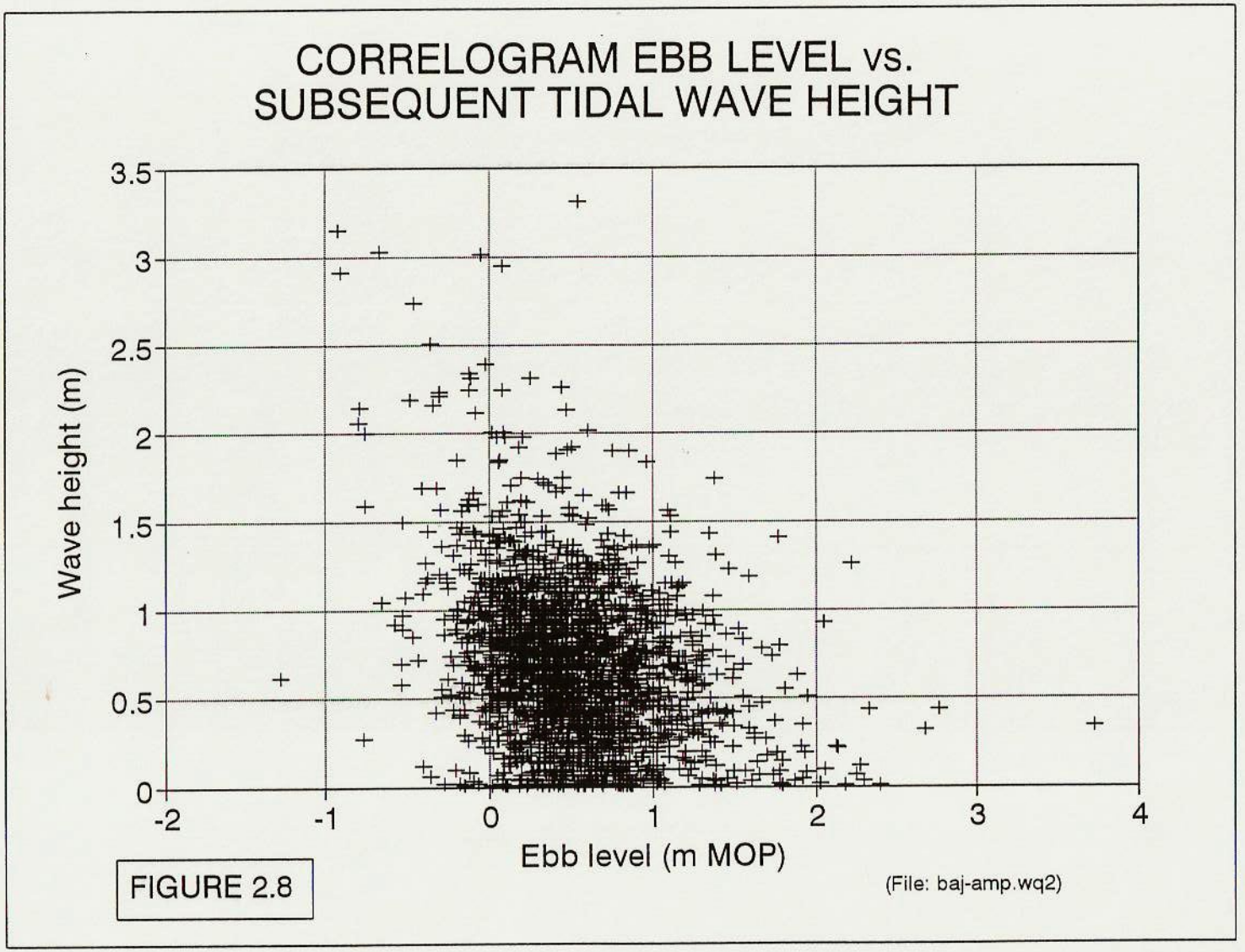
CORRELOGRAM EBB LEVEL vs.
SUBSEQUENT TIDAL WAVE HEIGHT
Wave height (m)
3.5
3
2.5
2
1.5
1
0.5
0
-2
-1
0
1
2
3
4
Ebb level (m MOP)
(File: baj-amp.wq2)

FIGURE 2.8

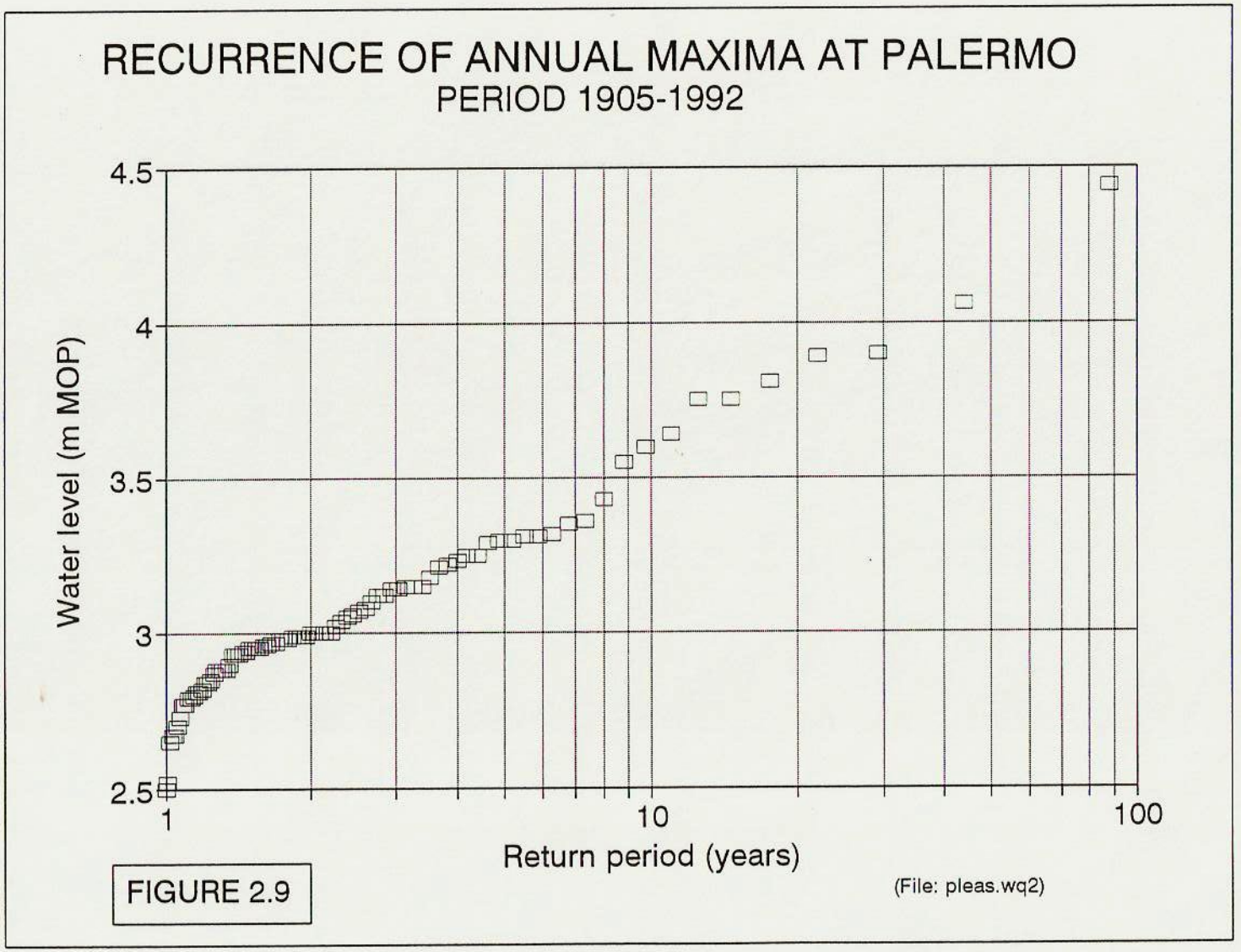
RECURRENCE OF ANNUAL MAXIMA AT PALERMO
PERIOD 1905-1992
Water level (m MOP)
4.5
4
3.5
3
2.5
1
10
100
Return period (years)
(File: pleas.wq2)

FIGURE 2.9

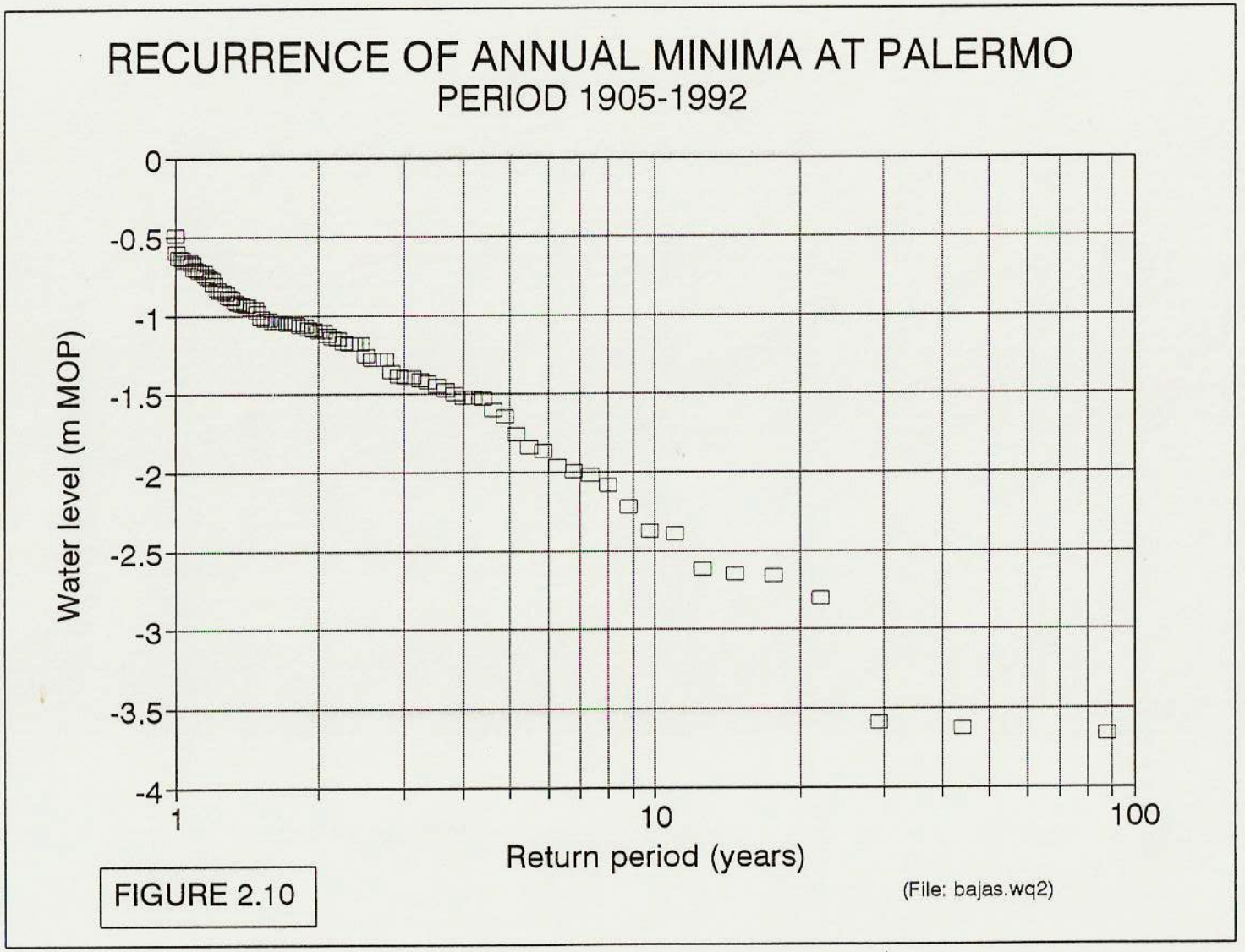
RECURRENCE OF ANNUAL MINIMA AT PALERMO
PERIOD 1905-1992
Water level (m MOP)
0
-0.5
-1
-1.5
-2
-2.5
-3
-3.5
-4
1
10
100
Return period (years)
(File: bajas.wq2)

FIGURE 2.10

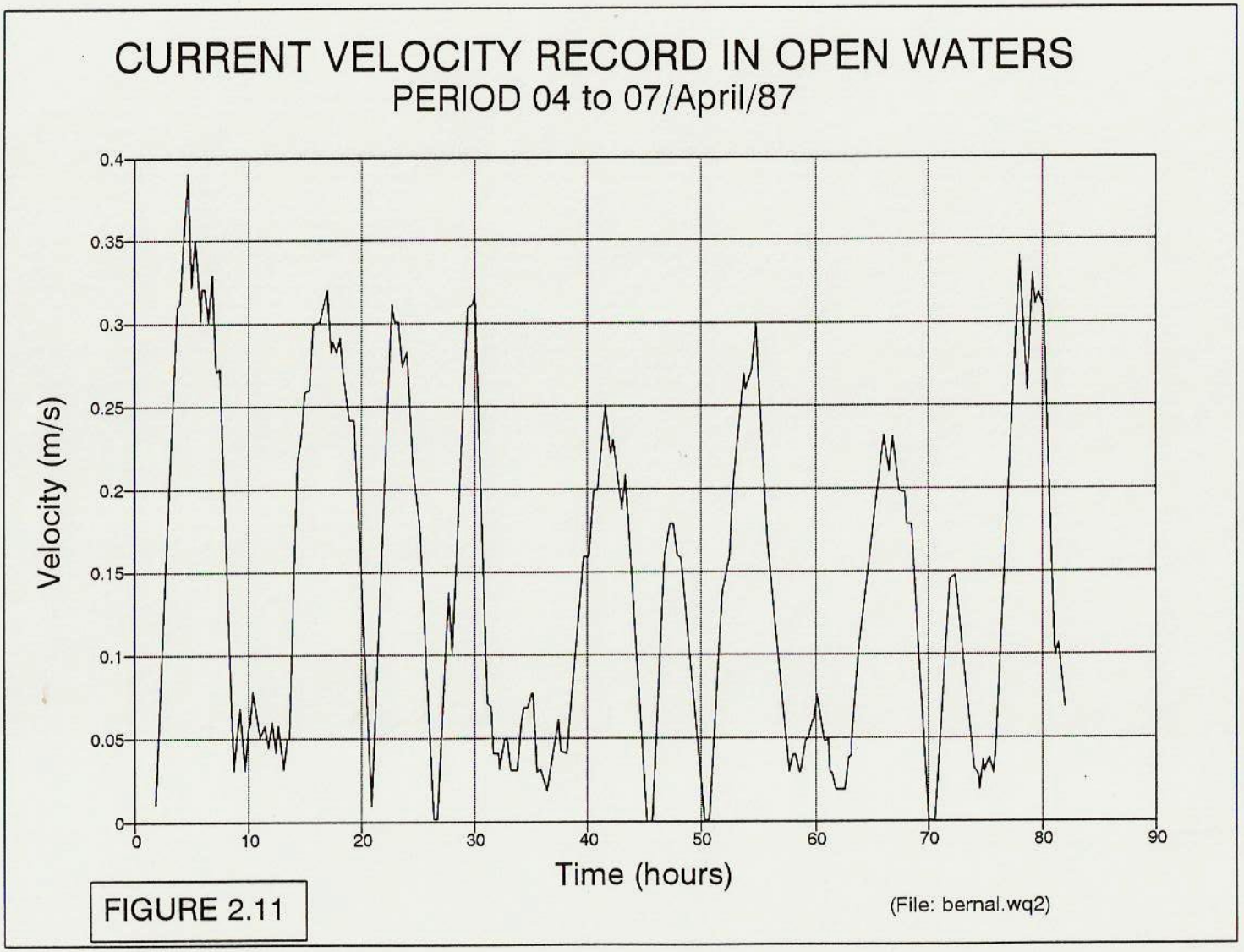
CURRENT VELOCITY RECORD IN OPEN WATERS
PERIOD 04 to 07/April/87
Velocity (m/s)
0.4
0.35
0.3
0.25
0.2
0.15
0.1
0.05
0
0
10
20
30
40
50
60
70
80
90
Time (hours)
(File: bernal.wq2)

FIGURE 2.11

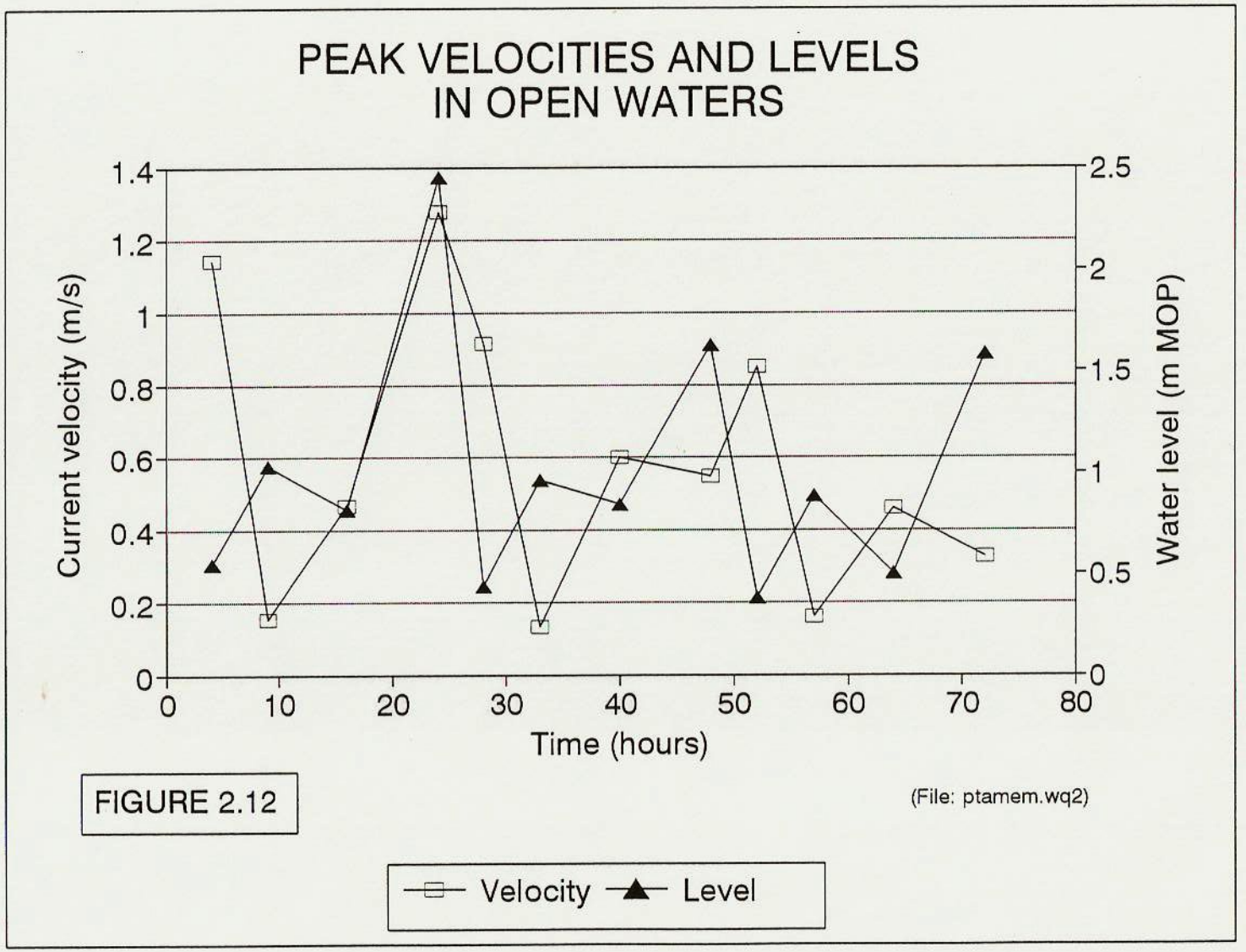

FIGURE 2.12

(File: ptamem.wq2)

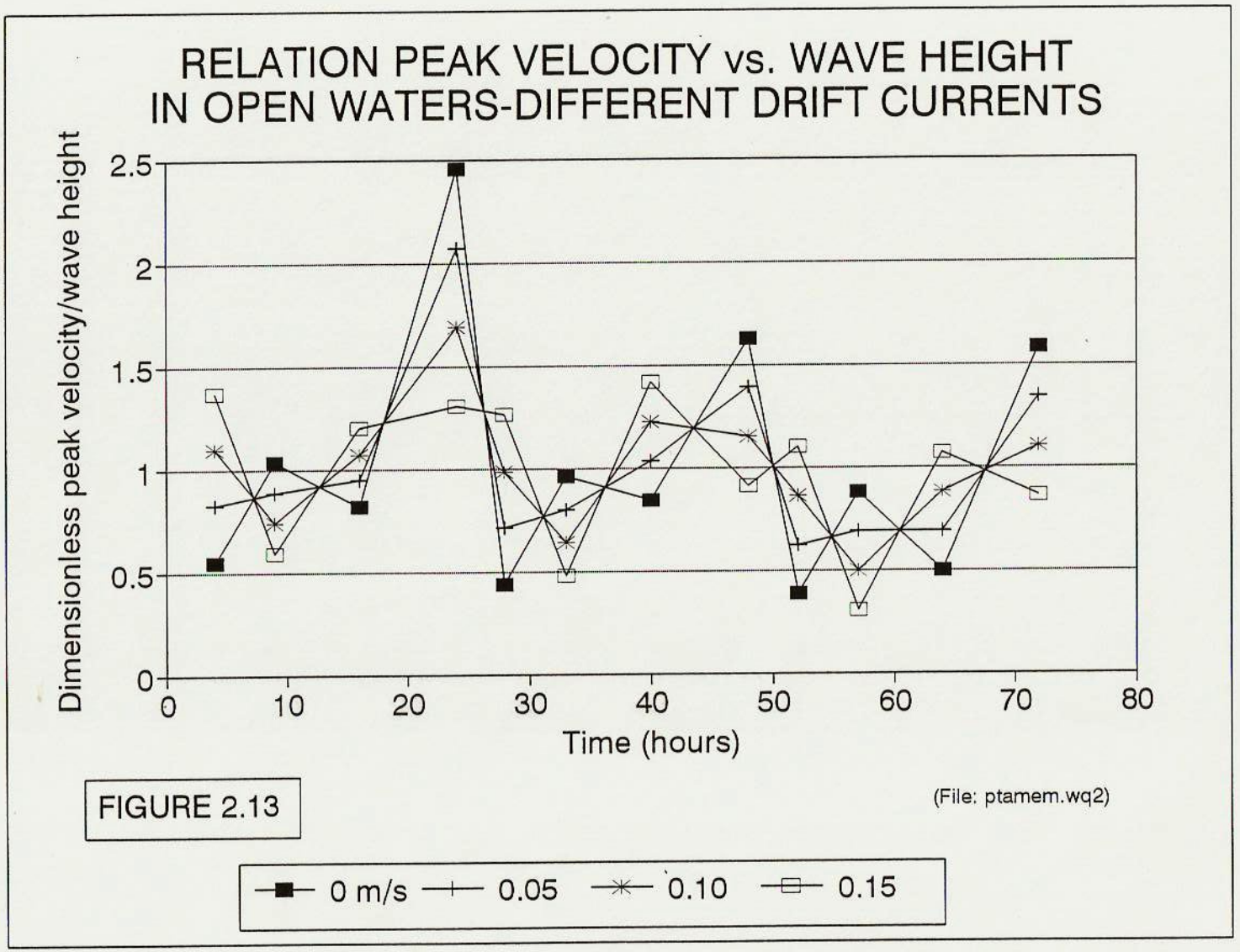

FIGURE 2.13

(File: ptamem.wq2)

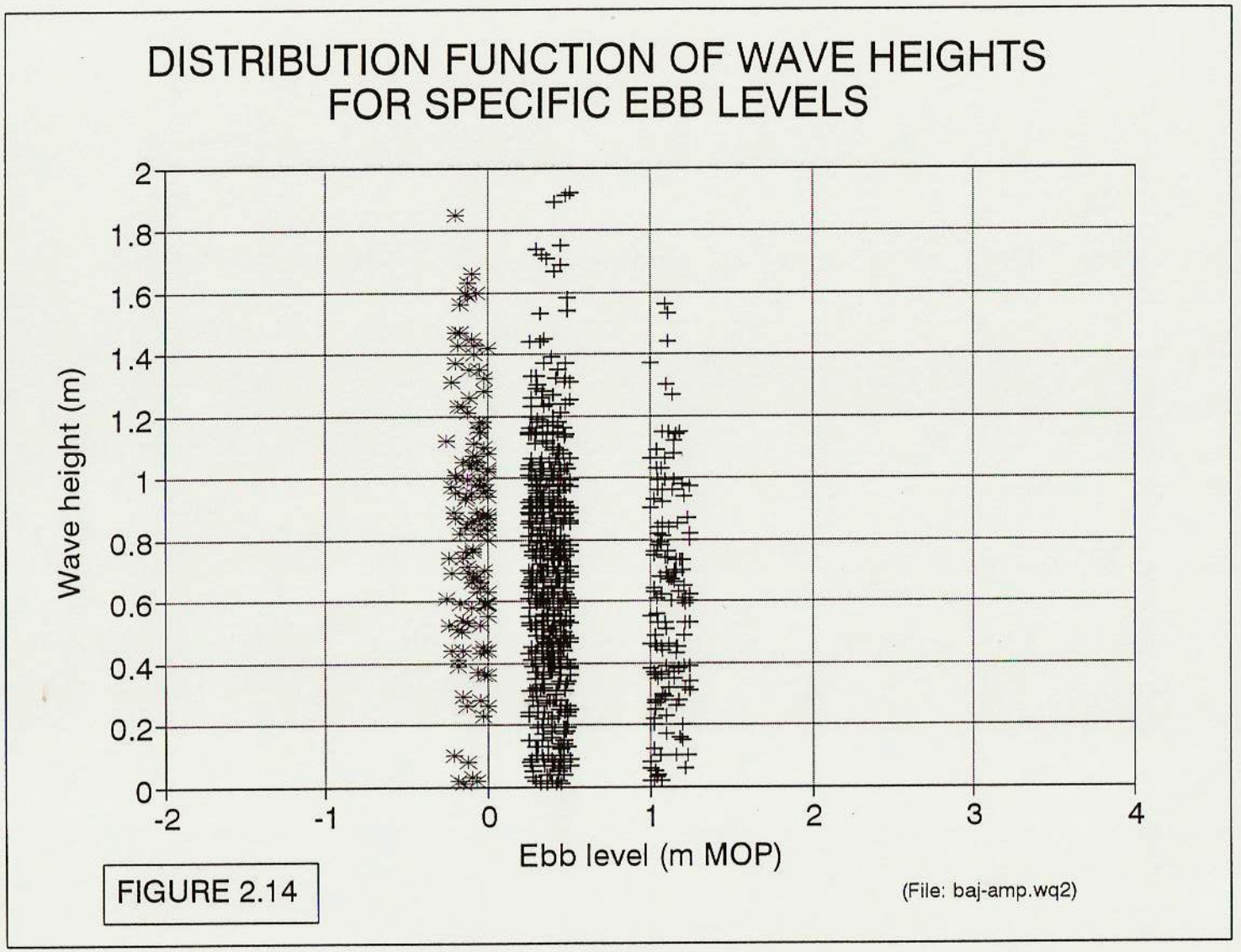
DISTRIBUTION FUNCTION OF WAVE HEIGHTS
FOR SPECIFIC EBB LEVELS
Wave height (m)
2
1.8
1.6
1.4
1.2
1
0.8
0.6
0.4
0.2
0
-2
-1
0
1
2
3
4
Ebb level (m MOP)
FIGURE 2.14
(File: baj-amp.wq2)

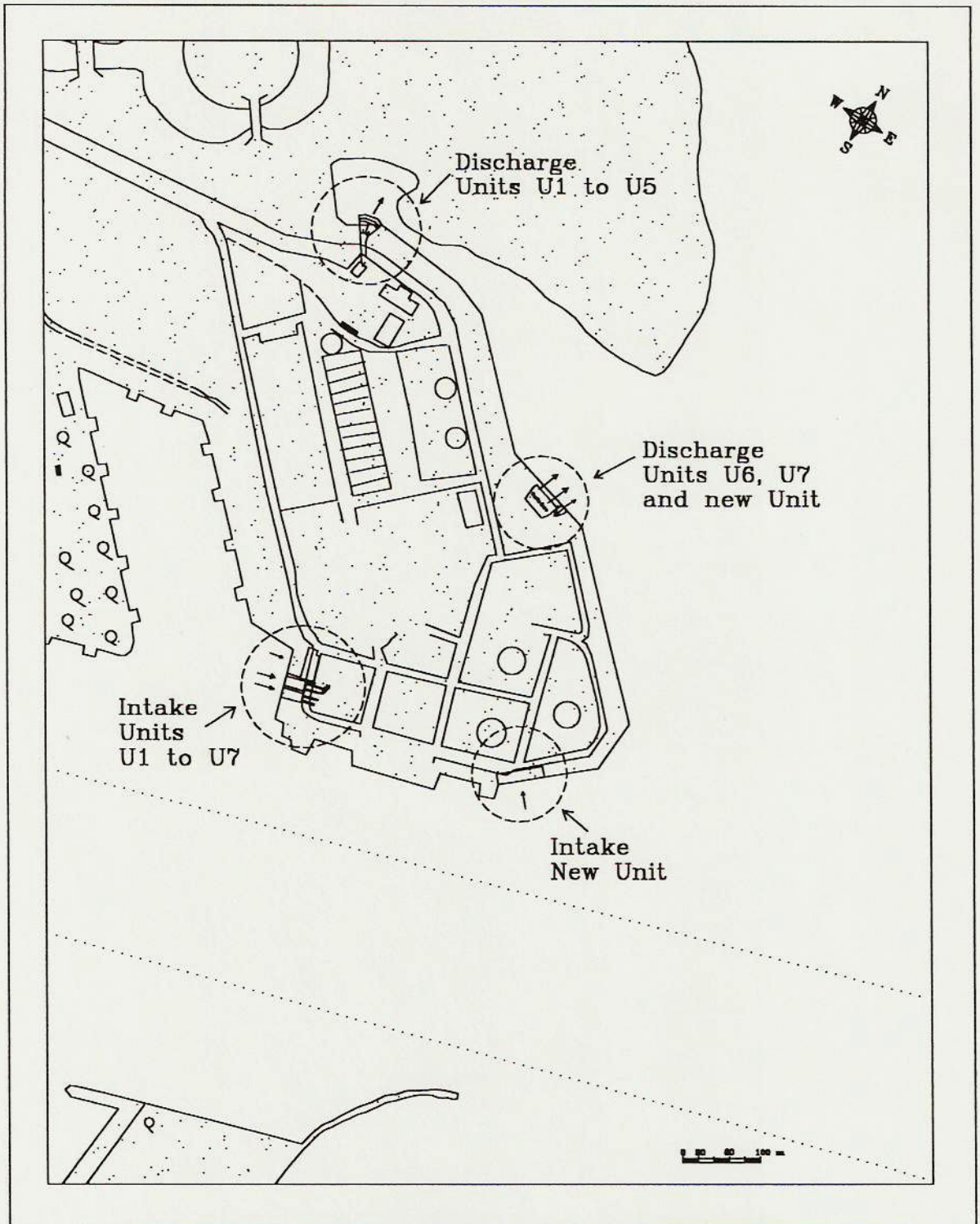

FIGURE 2.15 – INTAKE AND DISCHARGE LOCATIONS

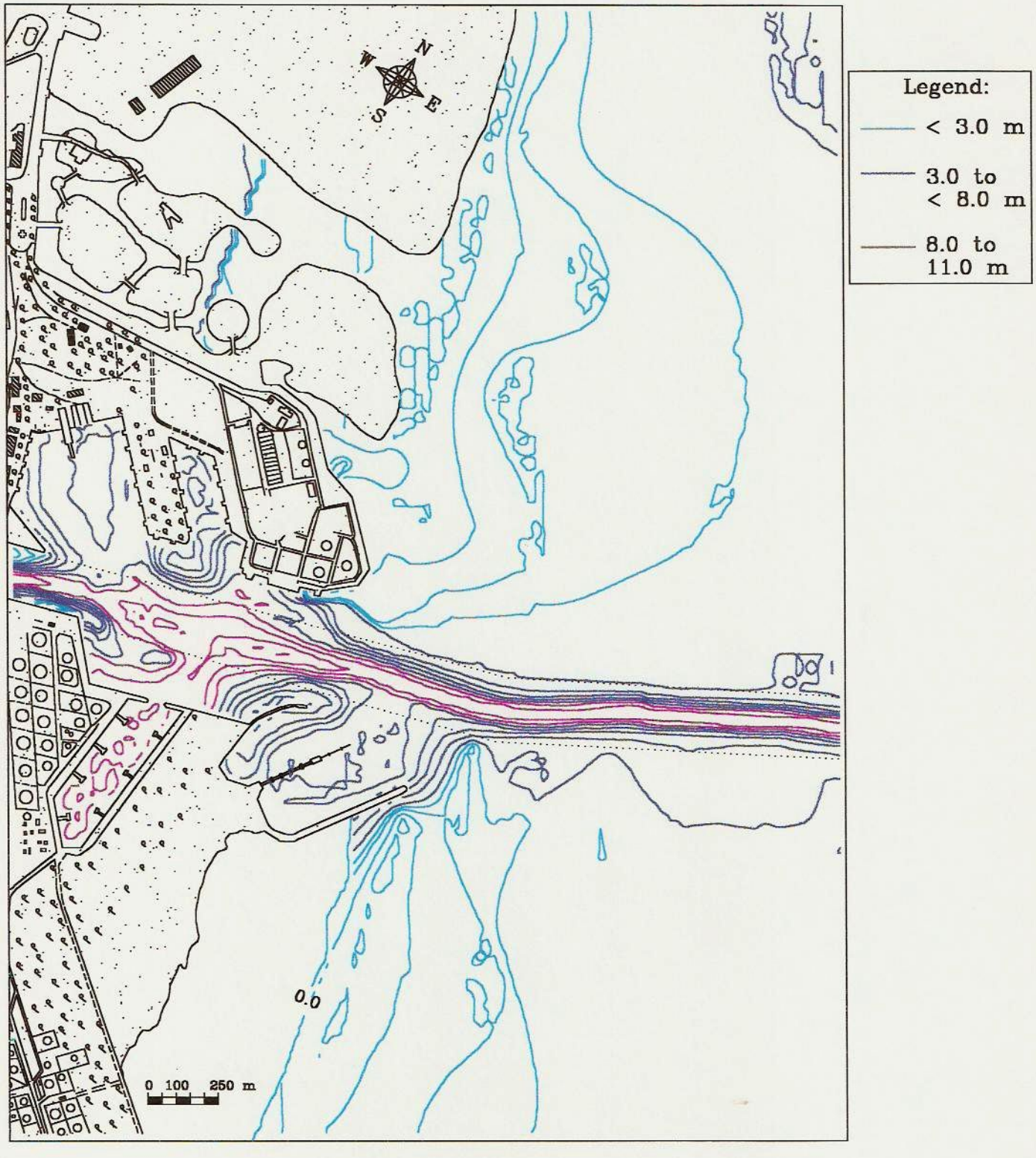

FIGURE 2.16 – BATHYMETRY OF THE STUDY ZONE

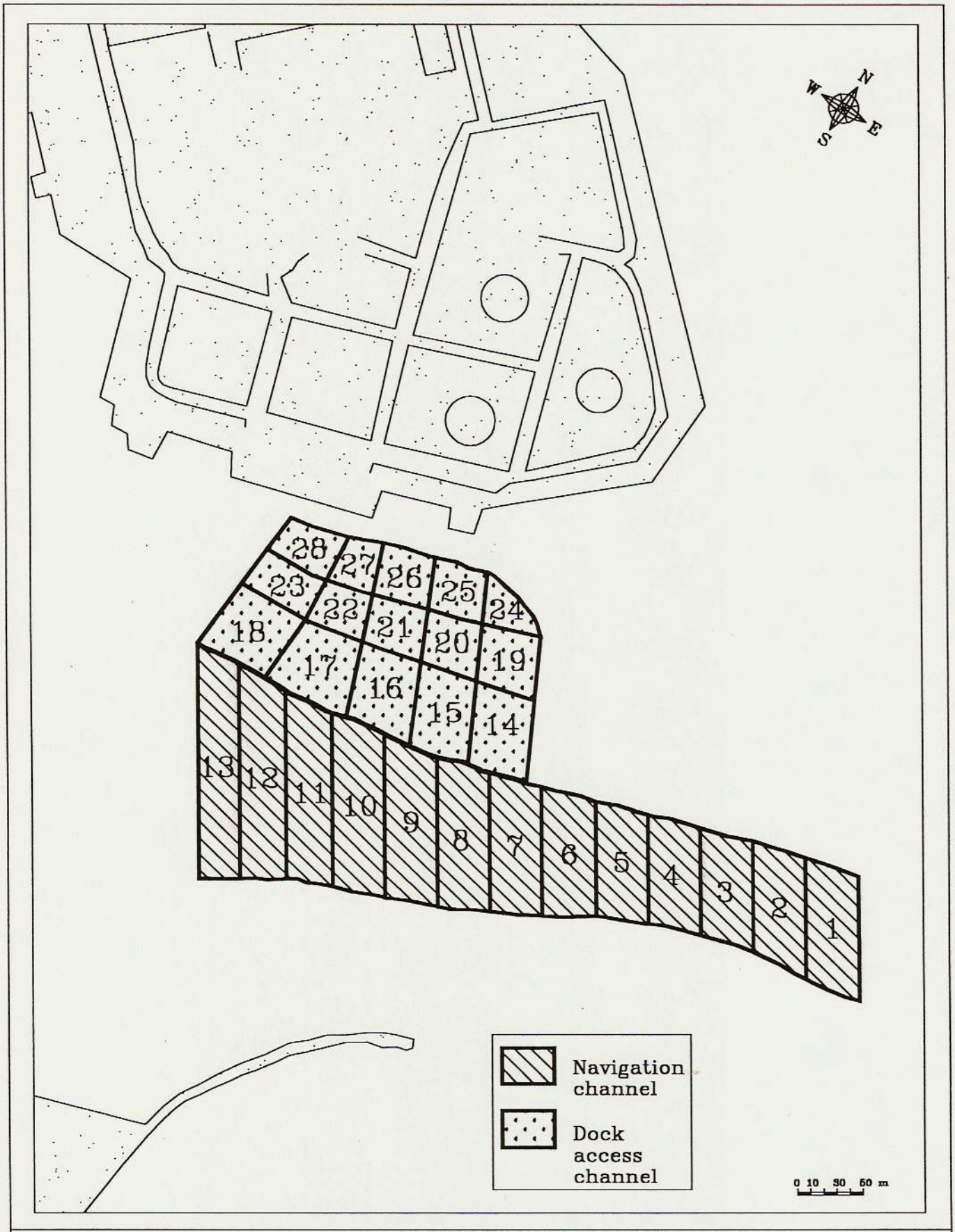

FIGURE 2.17 – CELLS FOR SEDIMENTATION ANALYSIS

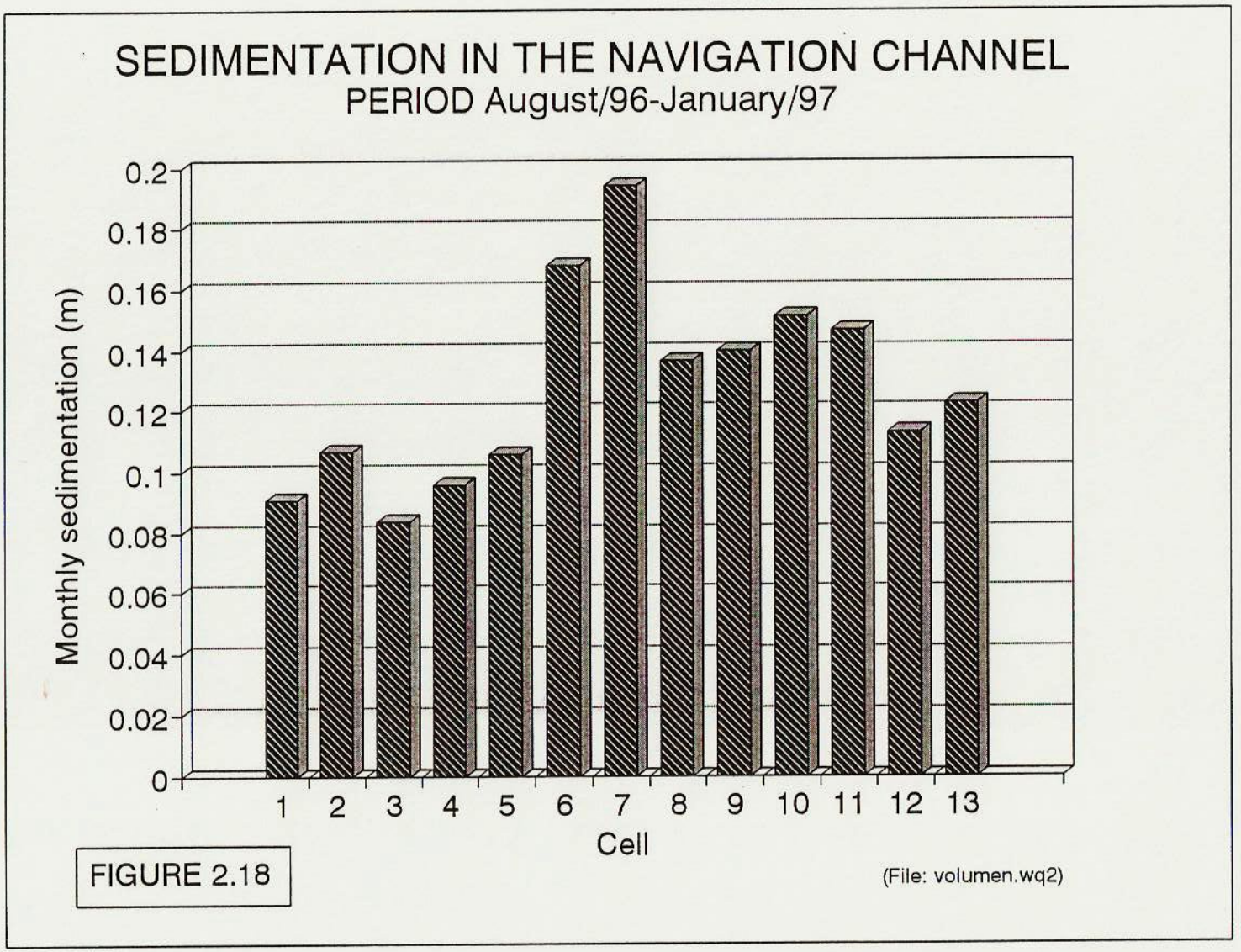
SEDIMENTATION IN THE NAVIGATION CHANNEL
PERIOD August/96-January/97
Monthly sedimentation (m)
0.2
0.18
0.16
0.14
0.12
0.1
0.08
0.06
0.04
0.02
0
1 2 3 4 5 6 7 8 9 10 11 12 13
Cell
(File: volumen.wq2)

FIGURE 2.18

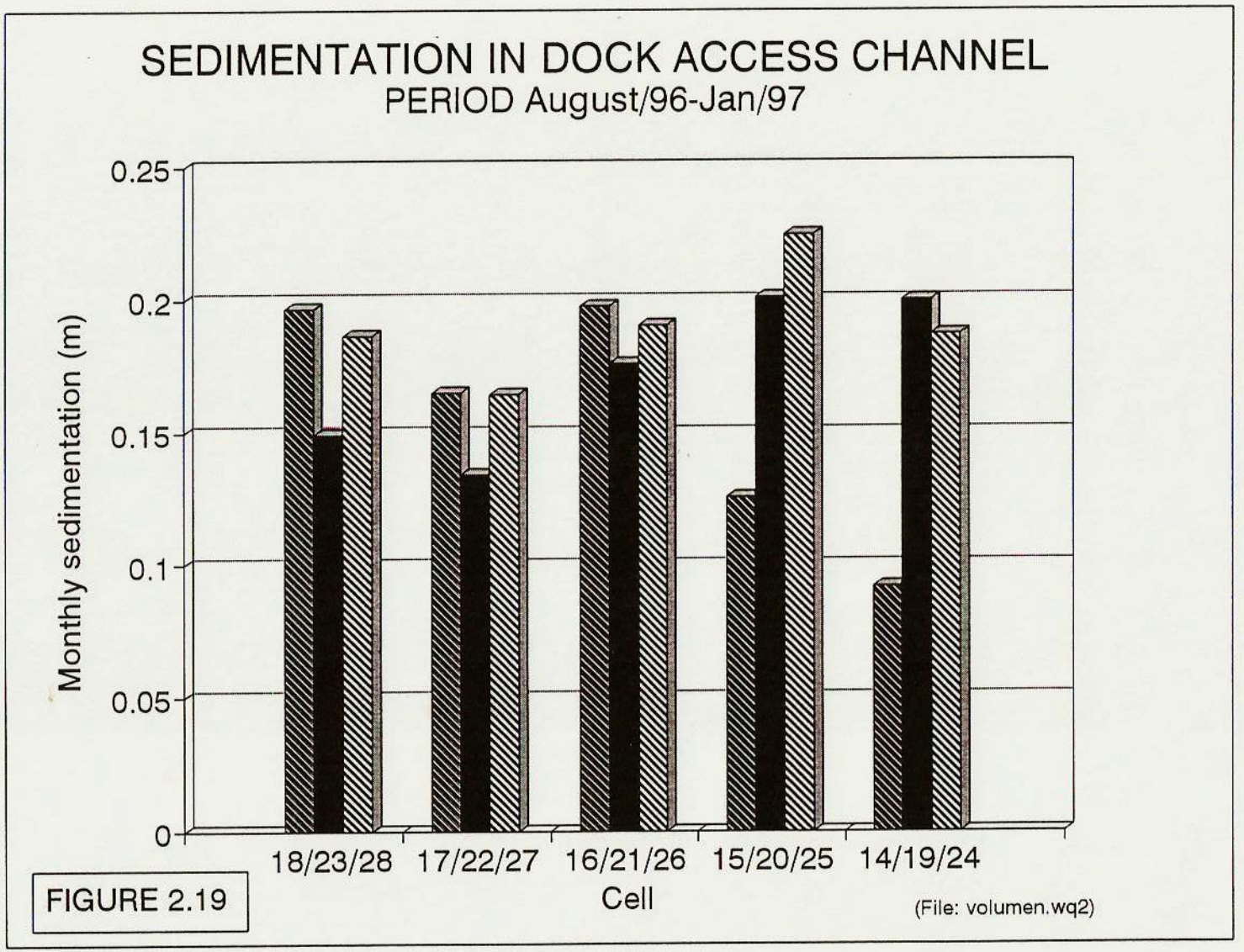
SEDIMENTATION IN DOCK ACCESS CHANNEL
PERIOD August/96-Jan/97
Monthly sedimentation (m)
0.25
0.2
0.15
0.1
0.05
0
18/23/28
17/22/27
16/21/26
15/20/25
14/19/24
Cell
(File: volumen.wq2)

FIGURE 2.19

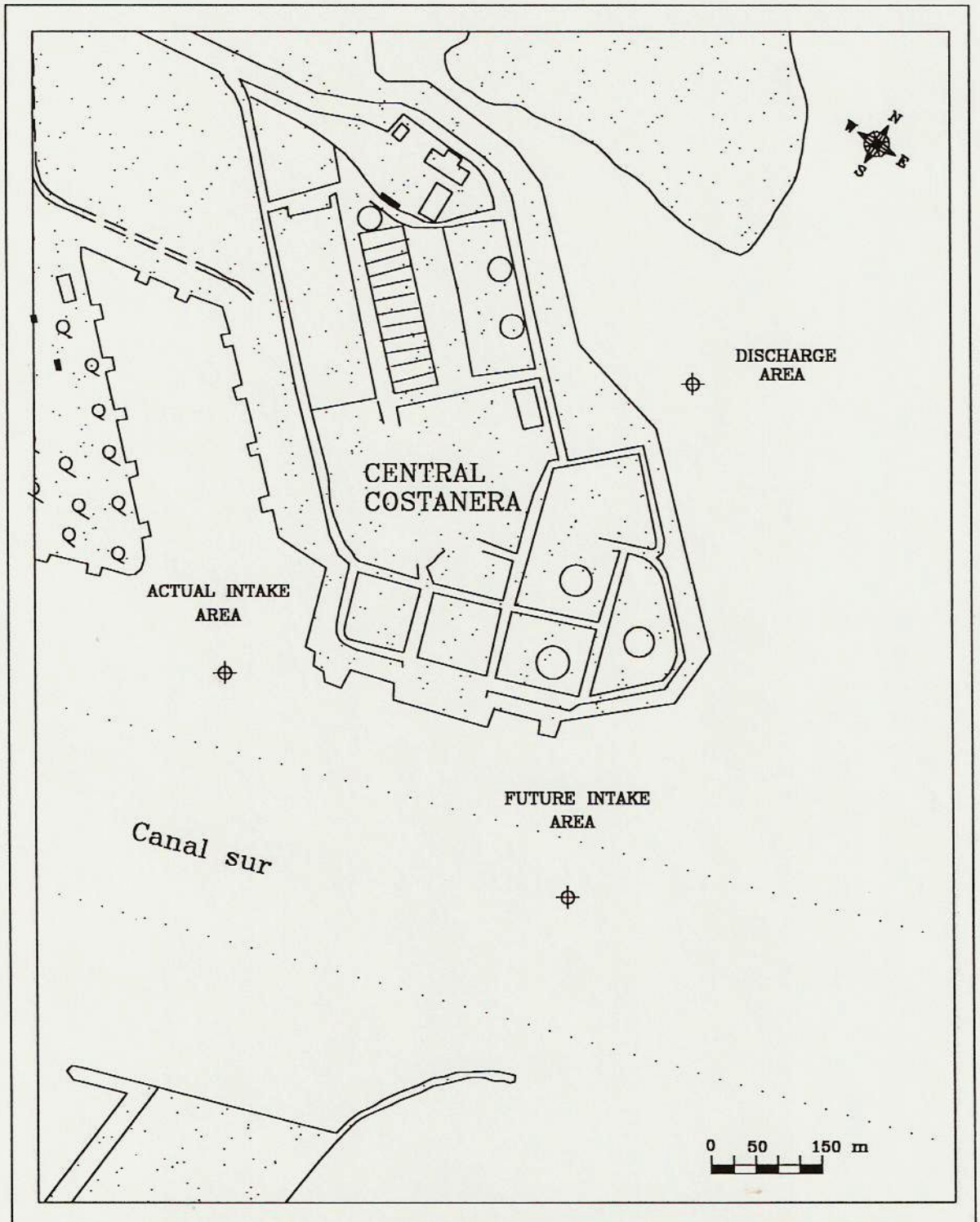

FIGURE 2.20 – LOCATION OF WATER SAMPLES

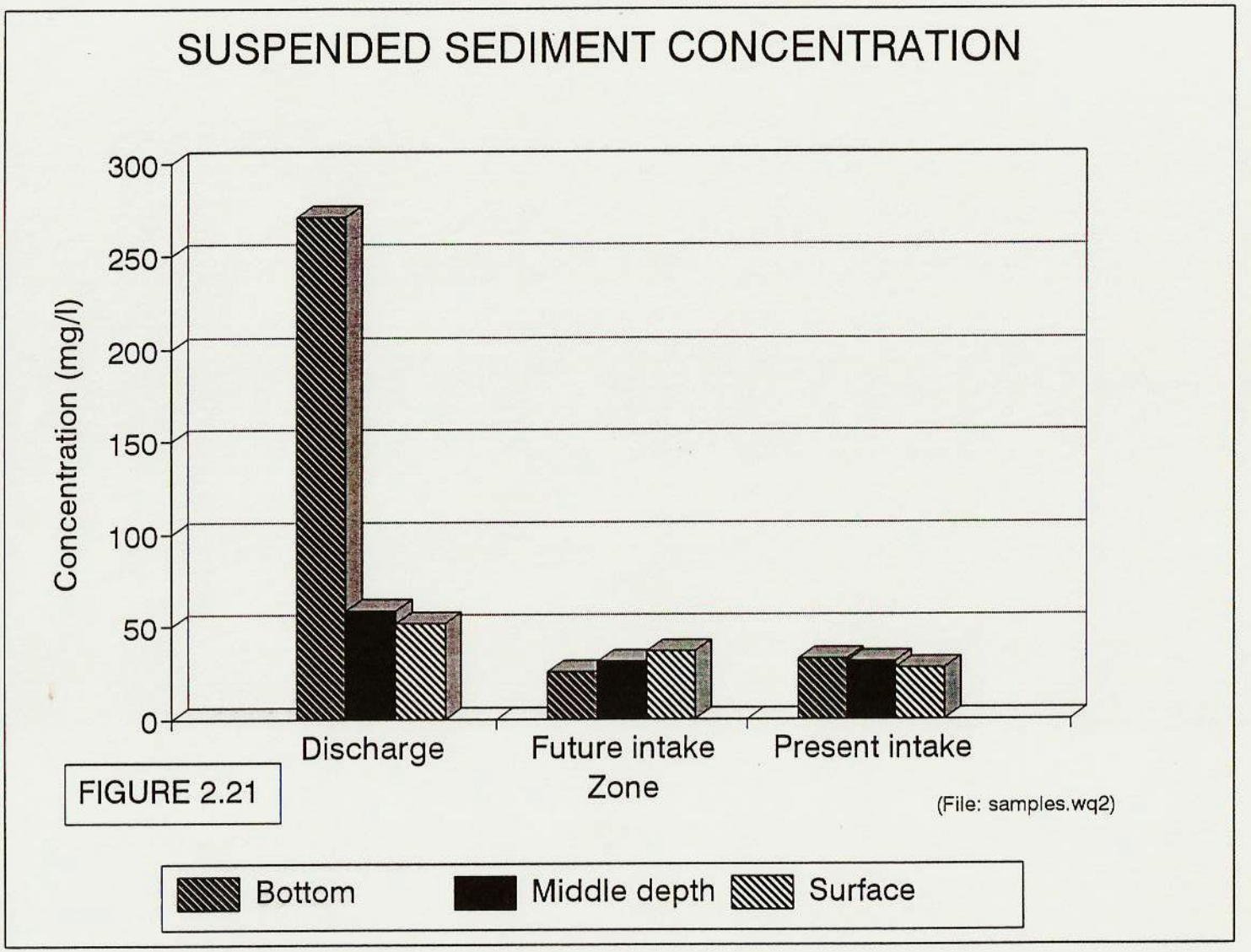
SUSPENDED SEDIMENT CONCENTRATION
Concentration (mg/l)
300
250
200
150
100
50
0
Discharge
Future intake Zone
Present intake
(File: samples.wq2)
Bottom
Middle depth
Surface

FIGURE 2.21

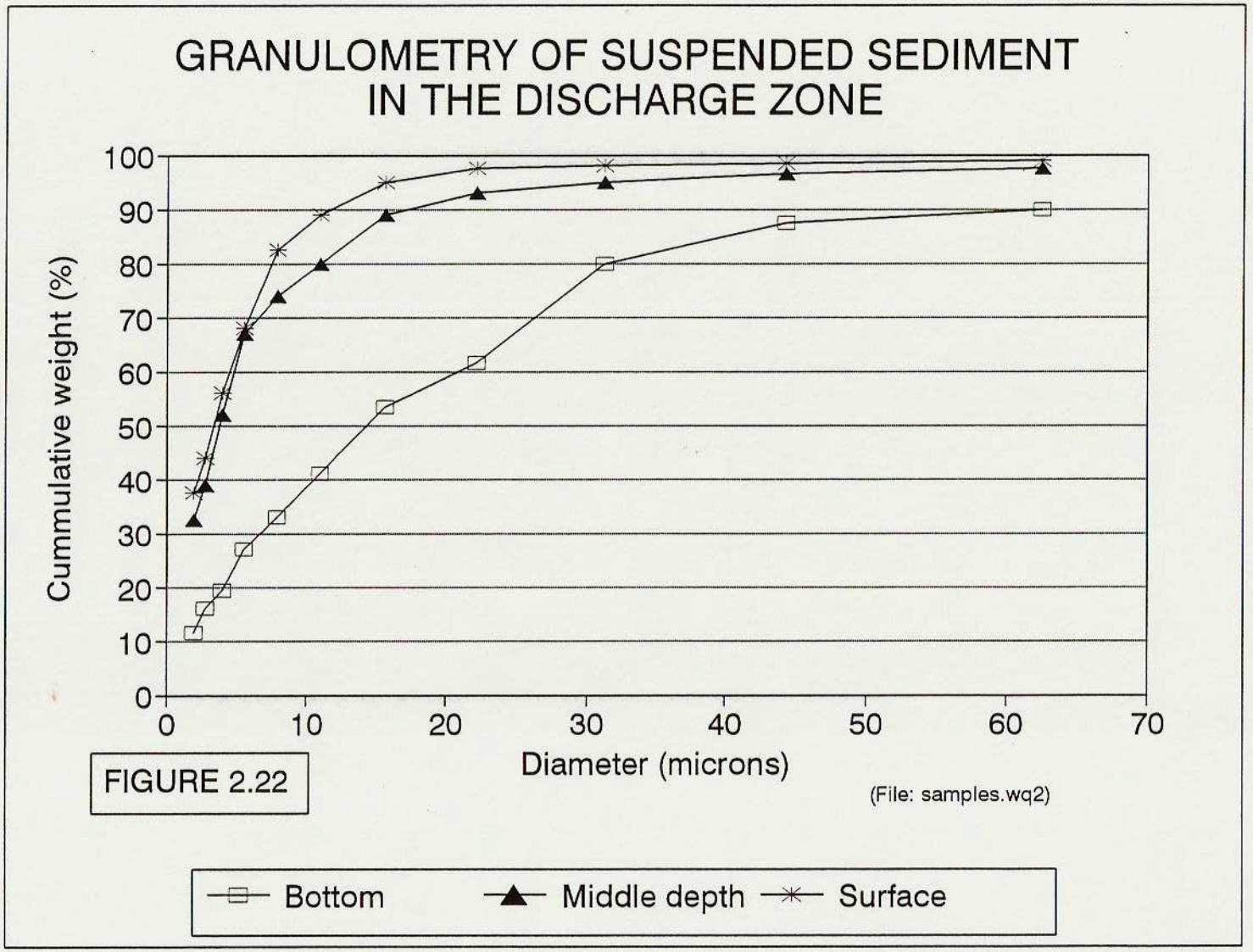
GRANULOMETRY OF SUSPENDED SEDIMENT
IN THE DISCHARGE ZONE
Cummulative weight (%)
100
90
80
70
60
50
40
30
20
10
0
0
10
20
30
40
50
60
70
Diameter (microns)
(File: samples.wq2)
Bottom
Middle depth
Surface

FIGURE 2.22

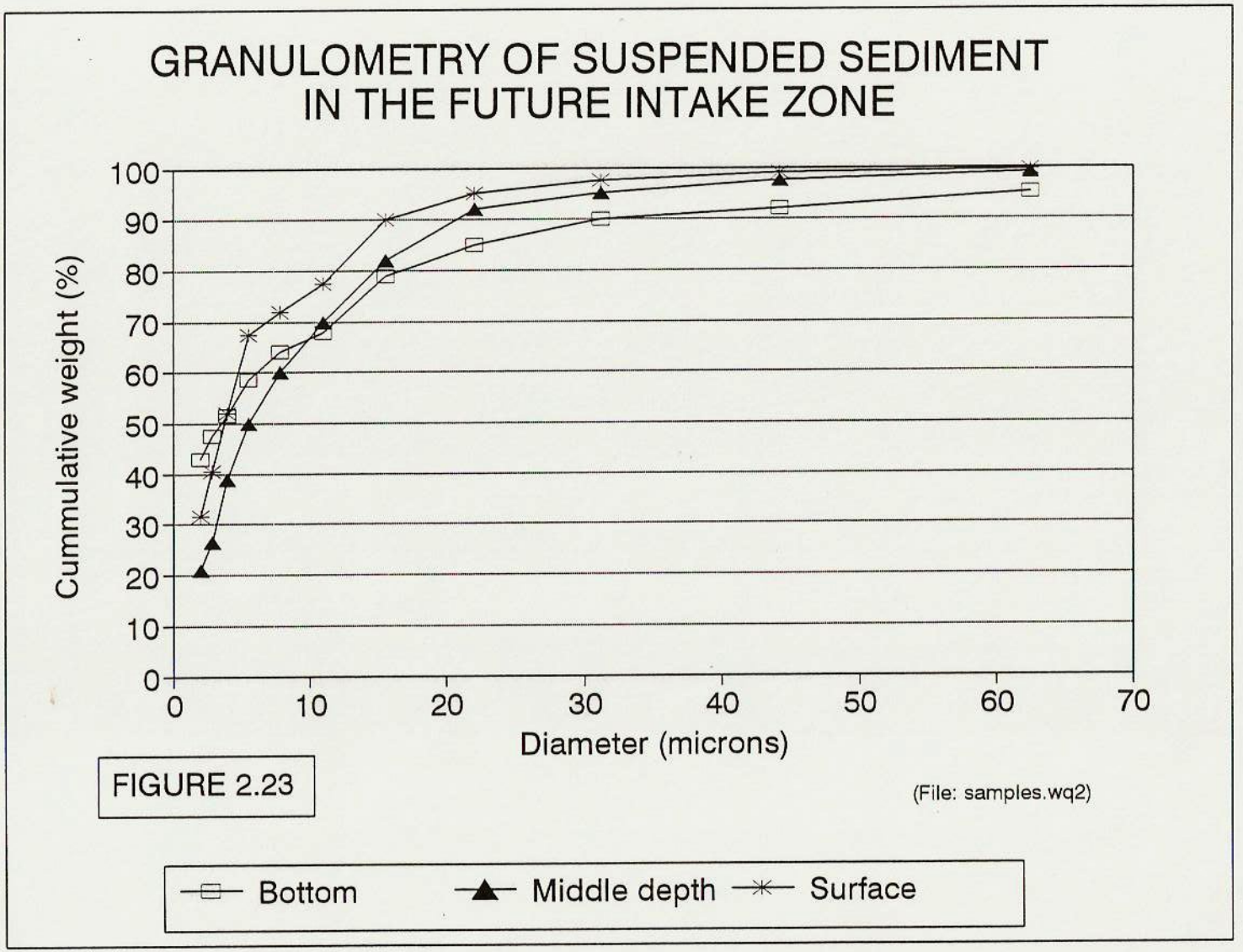
GRANULOMETRY OF SUSPENDED SEDIMENT
IN THE FUTURE INTAKE ZONE
Cummulative weight (%)
100
90
80
70
60
50
40
30
20
10
0
0
10
20
30
40
50
60
70
Diameter (microns)
FIGURE 2.23
(File: samples.wq2)
Bottom
Middle depth
Surface

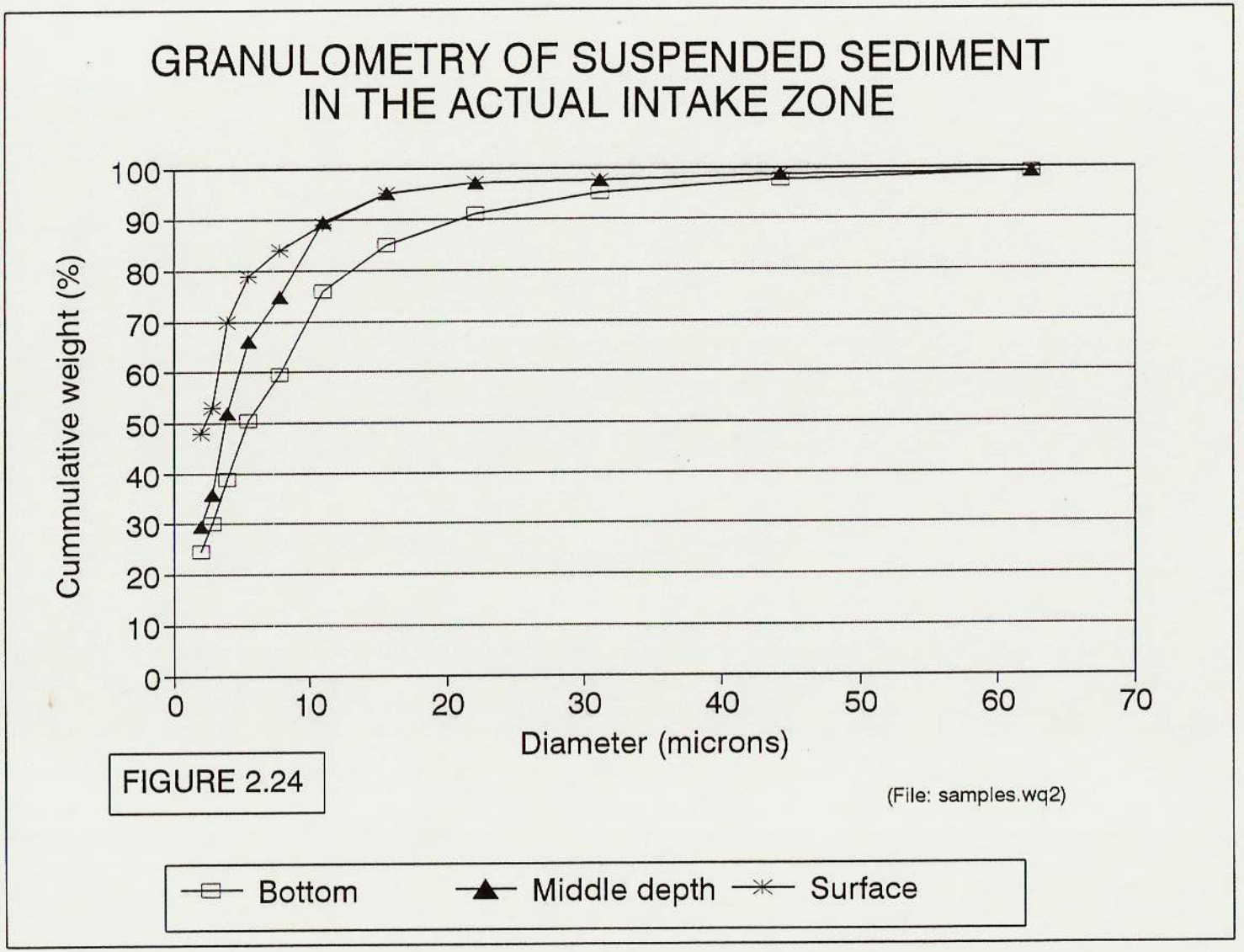

FIGURE 2.24

(File: samples.wq2)

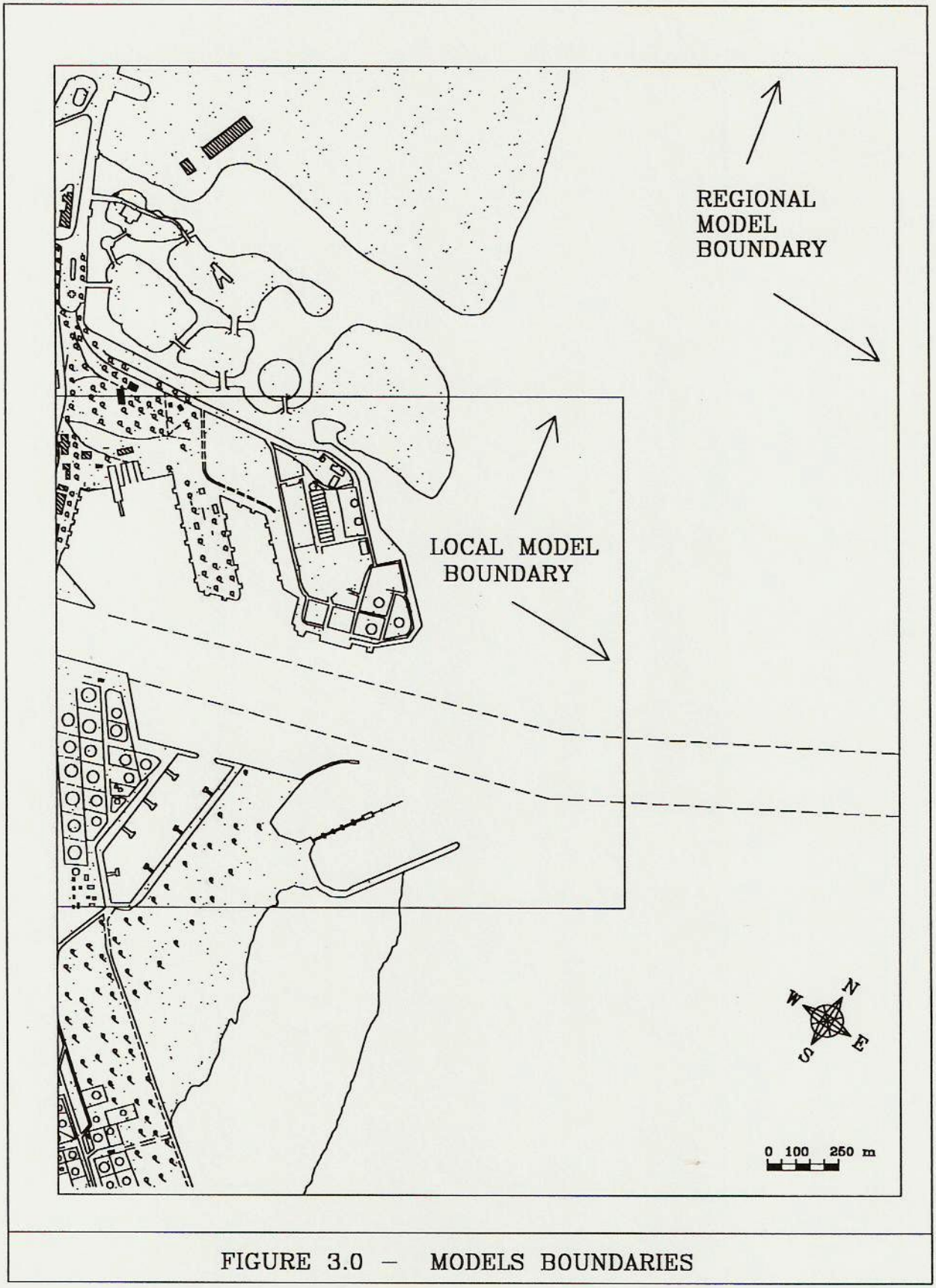

FIGURE 3.0 – MODELS BOUNDARIES

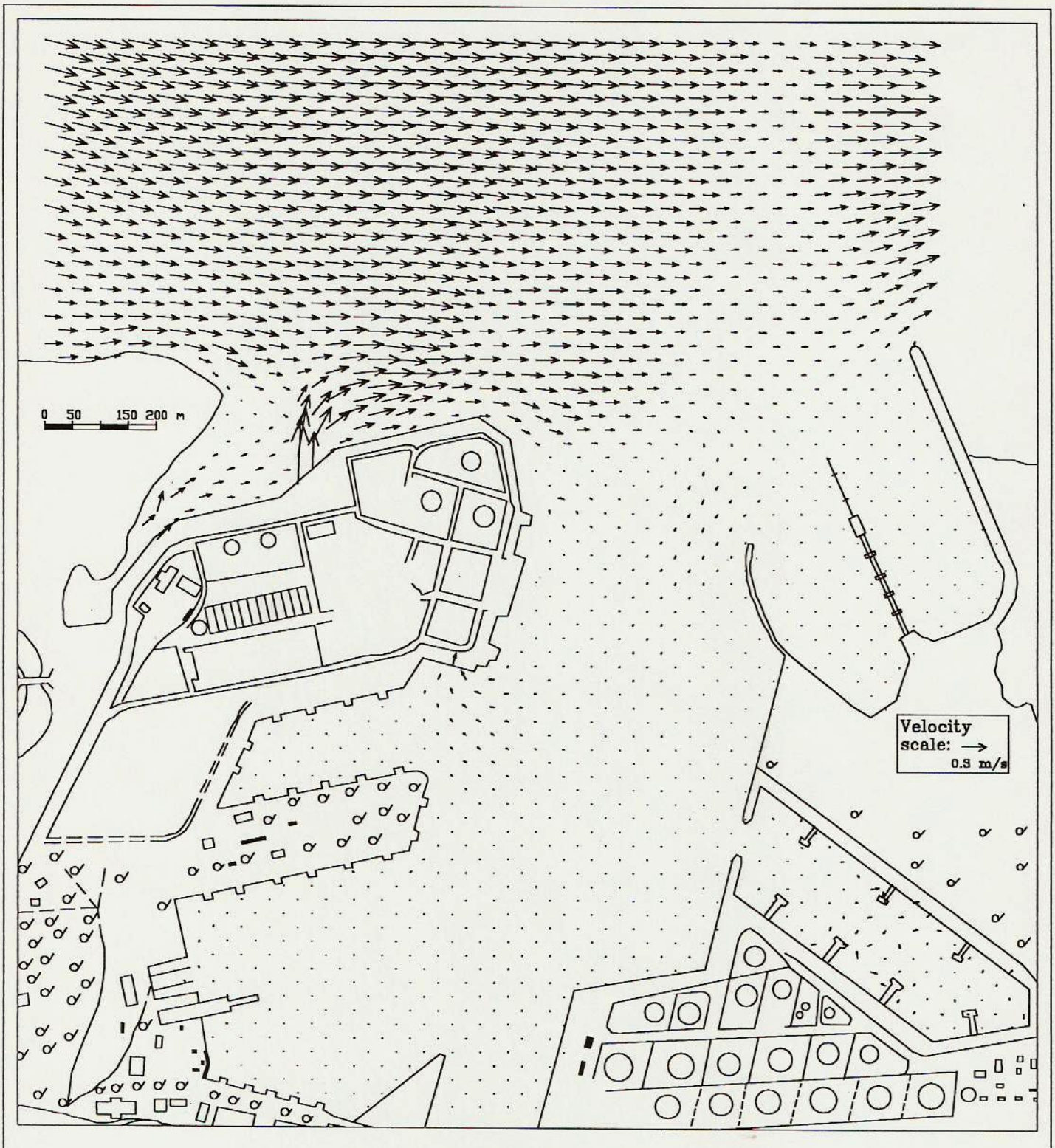

VELOCITY FIELD FOR T=0 AND T=12 HOURS.
SCENARIO A. FUTURE CONDITIONS.

FIGURE 3.1

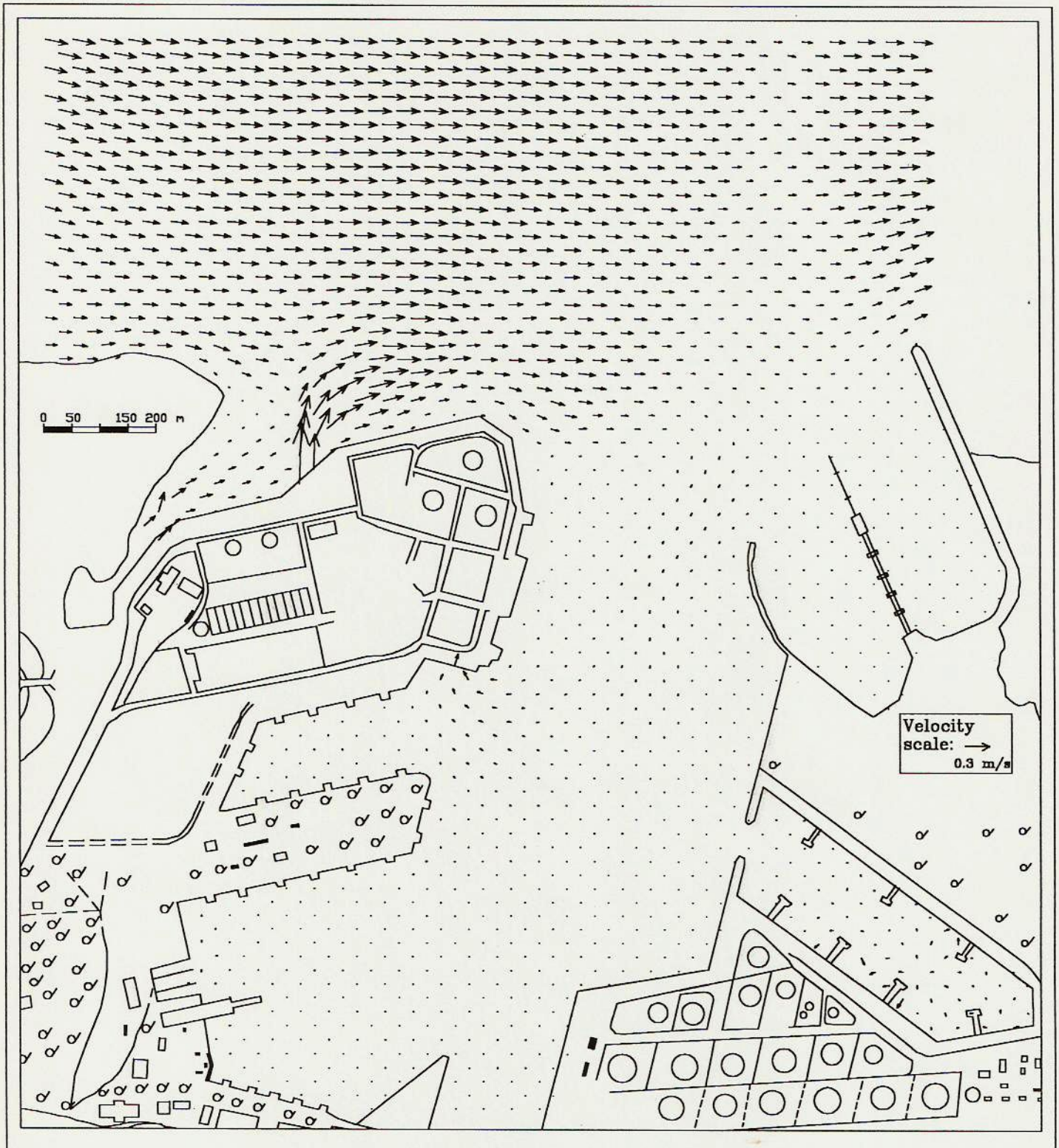

VELOCITY FIELD FOR T=1.7 AND T=8.9 HOURS.
SCENARIO A. FUTURE CONDITIONS.

FIGURE 3.2

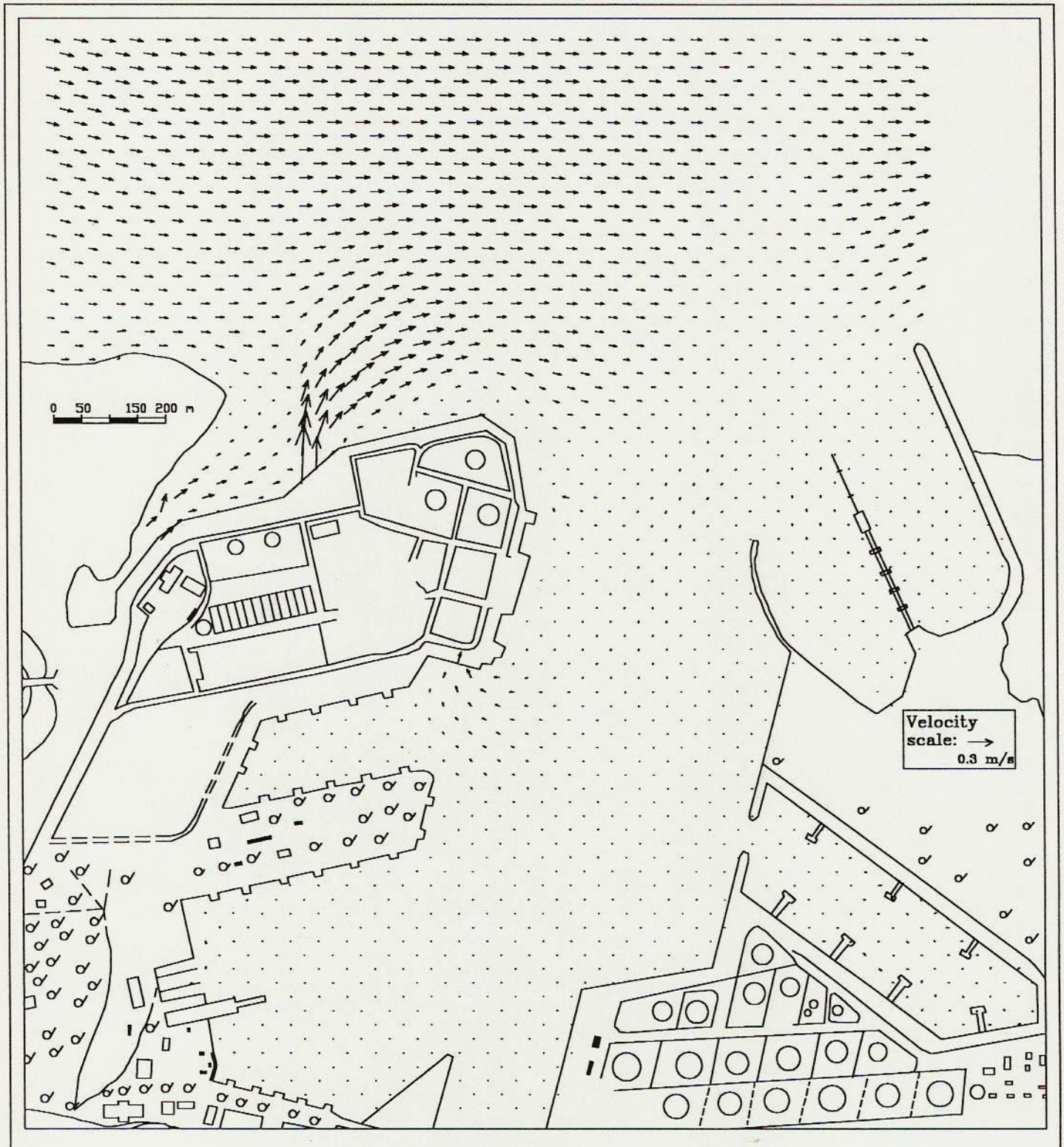

VELOCITY FIELD FOR T=2.3 AND T=8.2 HOURS.
SCENARIO A. FUTURE CONDITIONS.

FIGURE 3.3

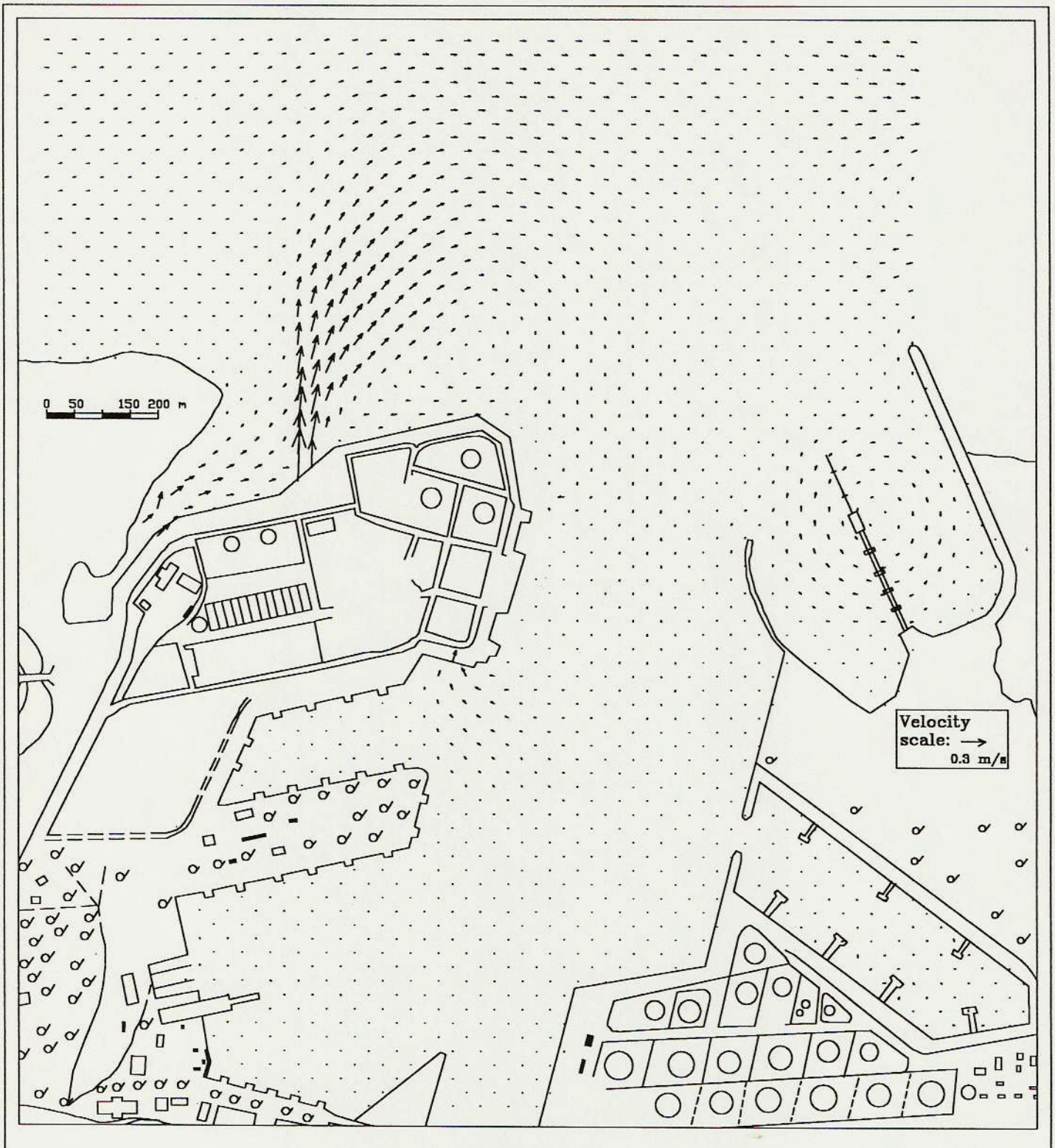

VELOCITY FIELD FOR T=2.7 AND T=7.7 HOURS.
SCENARIO A. FUTURE CONDITIONS.

FIGURE 3.4

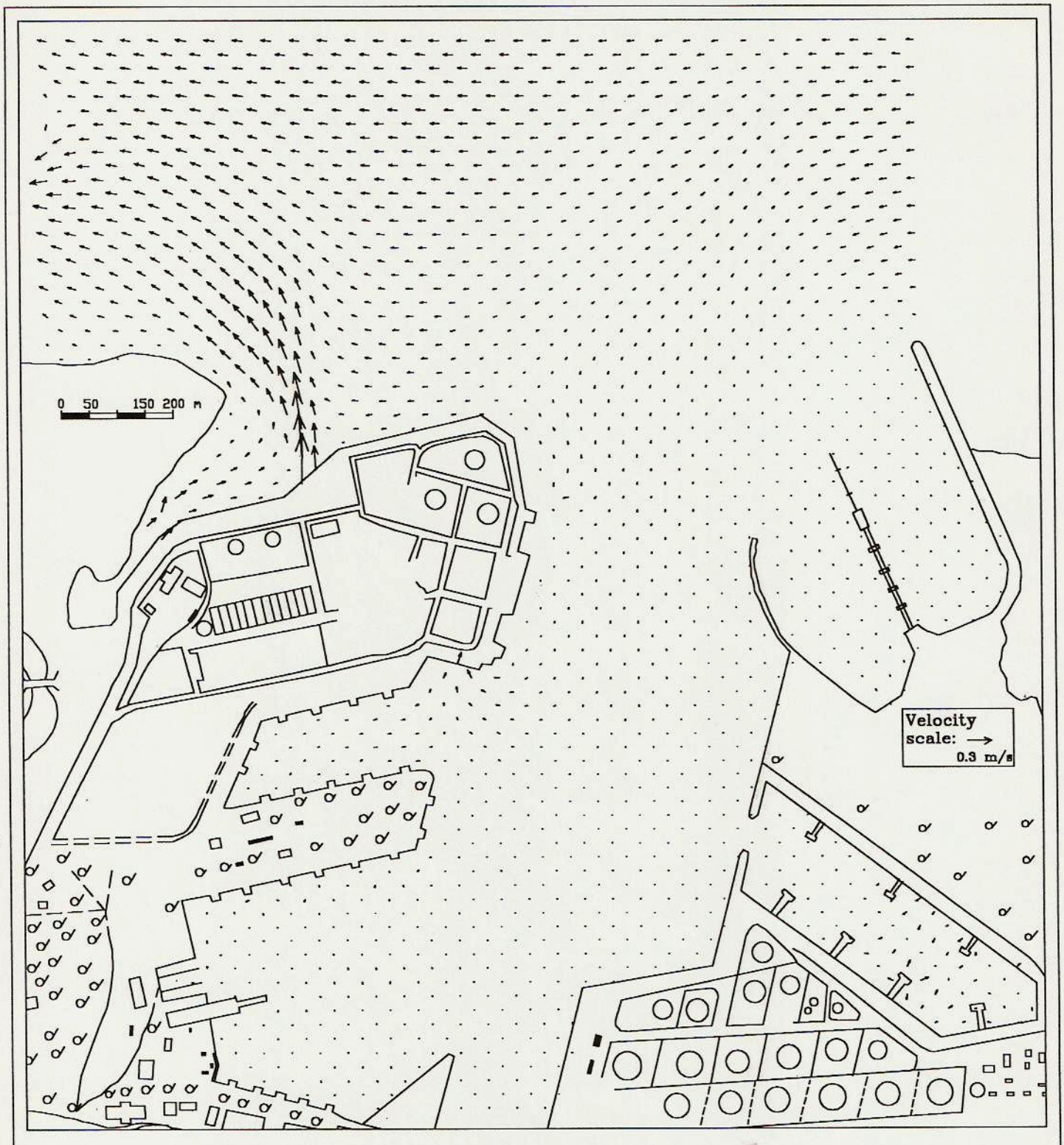

VELOCITY FIELD FOR T=3.3 AND T=7 HOURS.
SCENARIO A. FUTURE CONDITIONS.

FIGURE 3.5

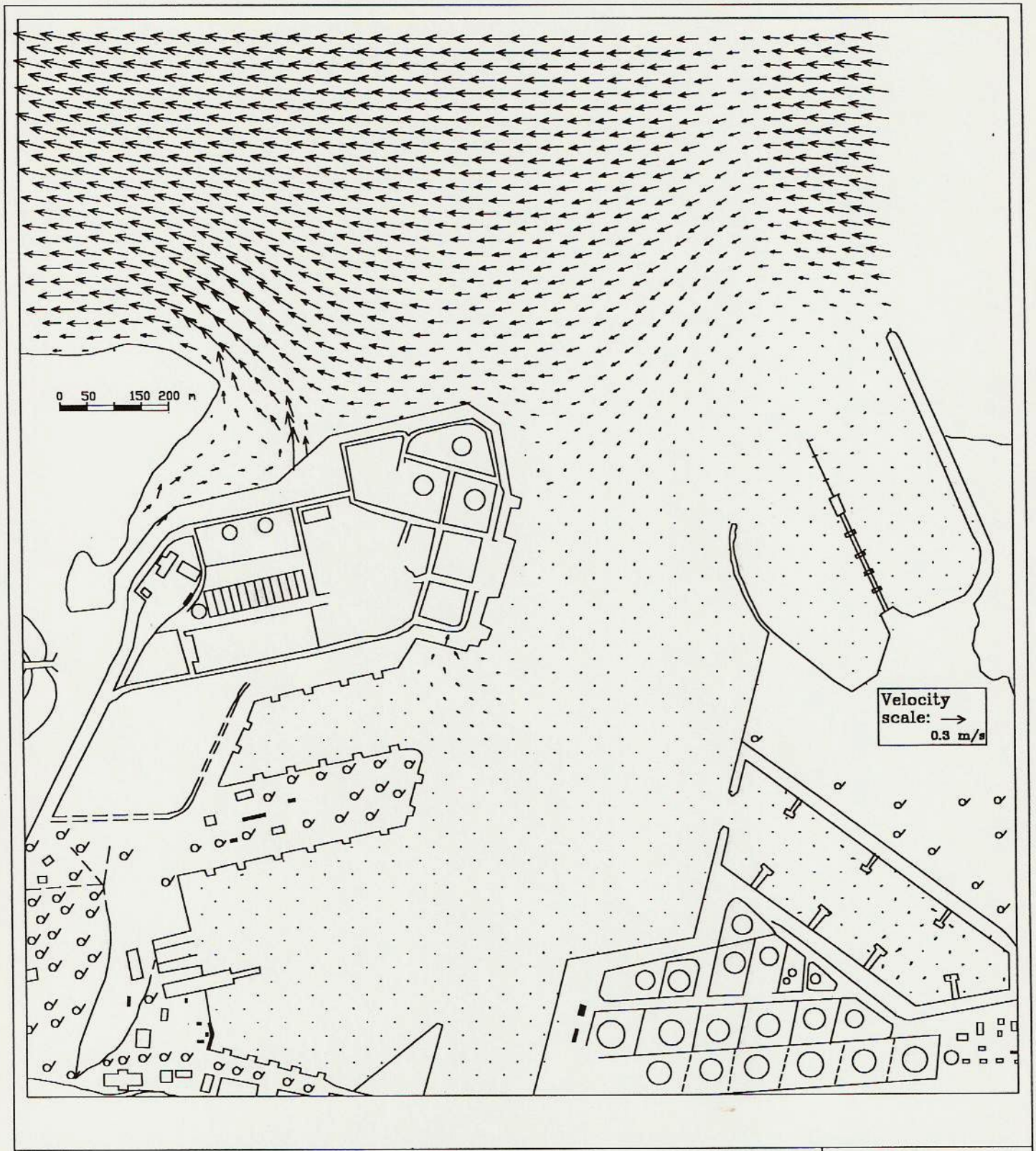

VELOCITY FIELD FOR T=5 HOURS.
SCENARIO A. FUTURE CONDITIONS.

FIGURE 3.6

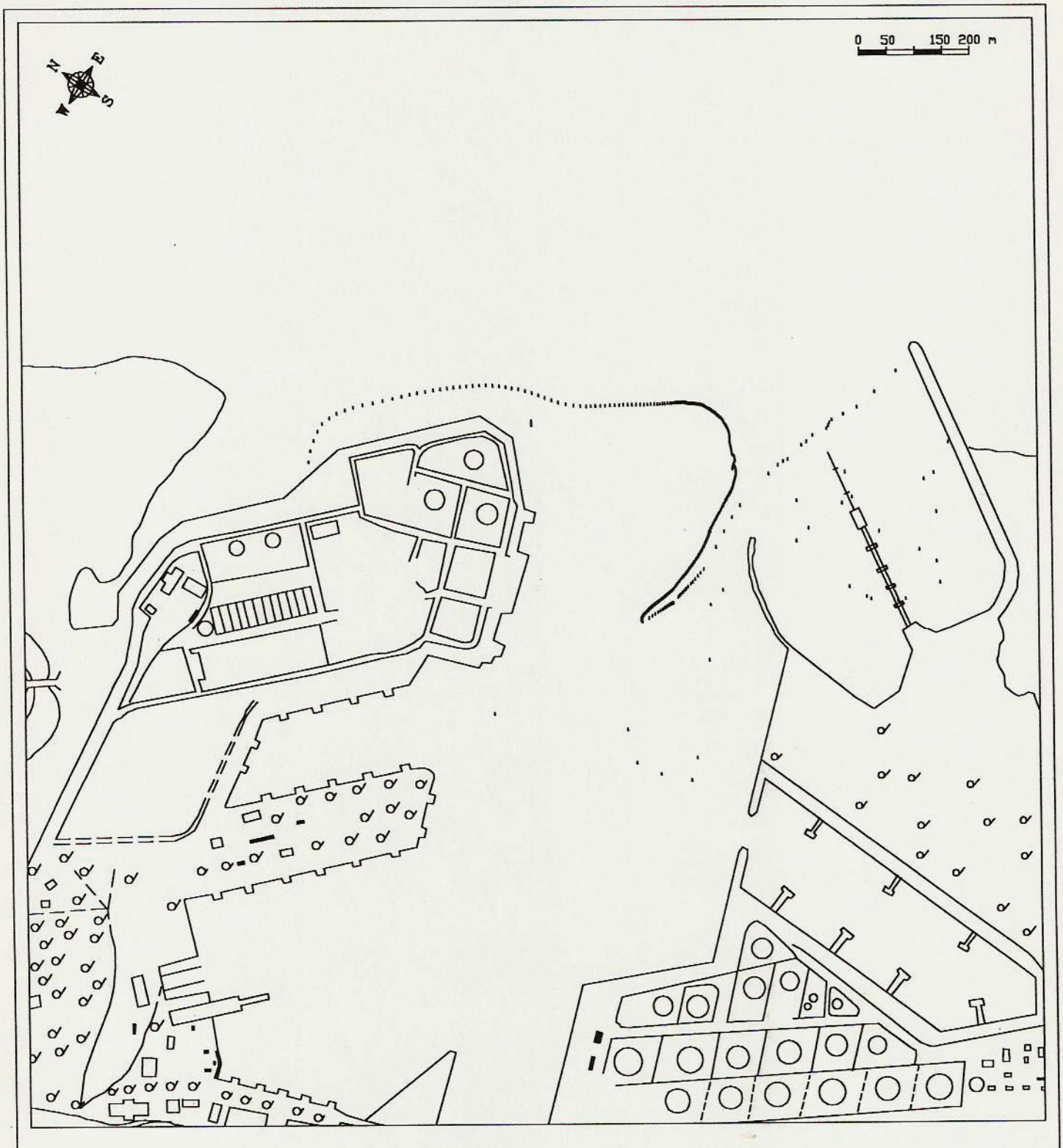

LOCATION OF WATER PARTICLES EMERGING FROM THE MAIN DISCHARGE LOCATION AT T=0 HOURS. SCENARIO A. ACTUAL CONDITIONS.

FIGURE 3.7

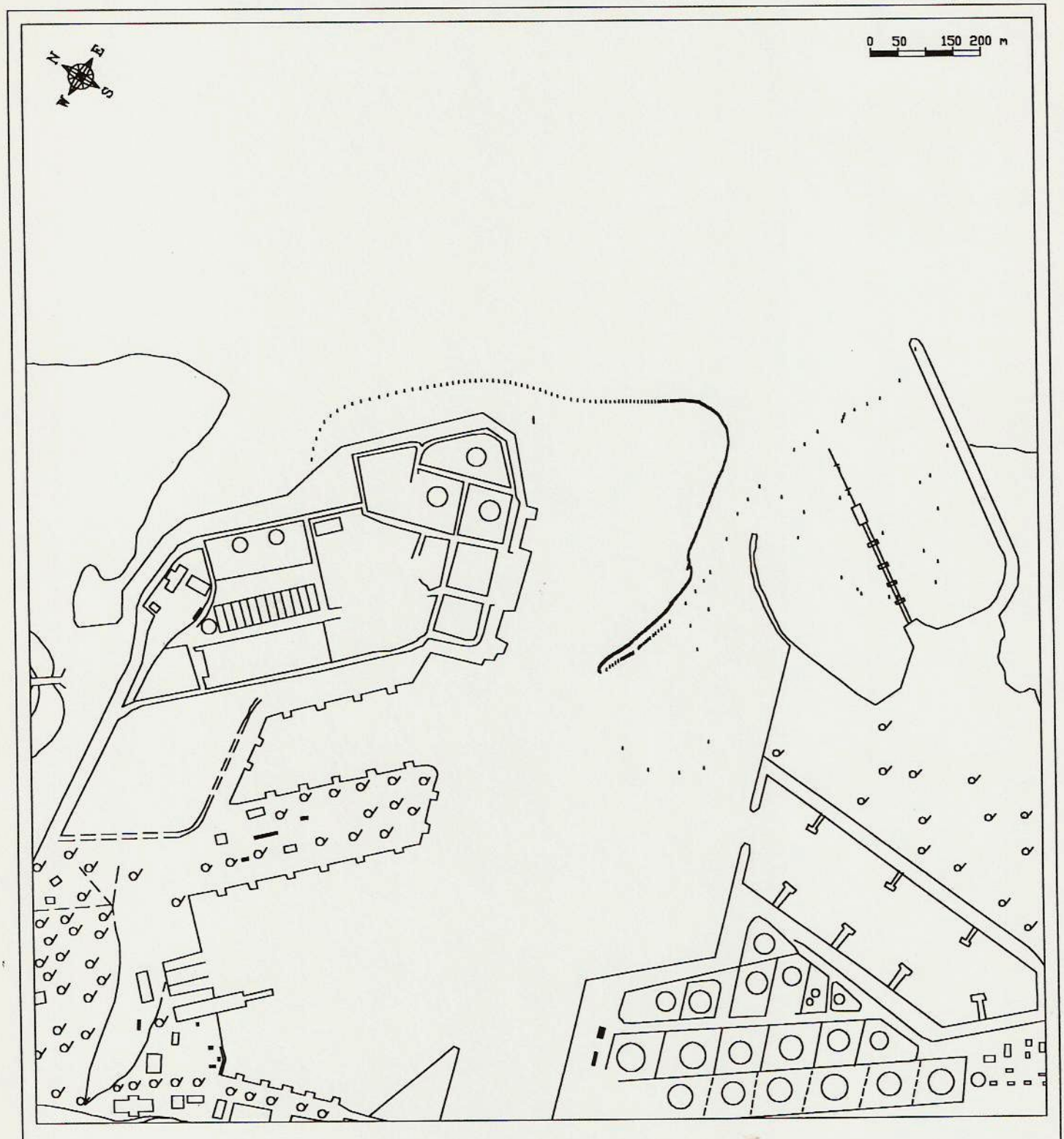

LOCATION OF WATER PARTICLES EMERGING FROM THE MAIN DISCHARGE LOCATION AT T=0.8 HOURS. SCENARIO A. ACTUAL CONDITIONS.

FIGURE 3.8

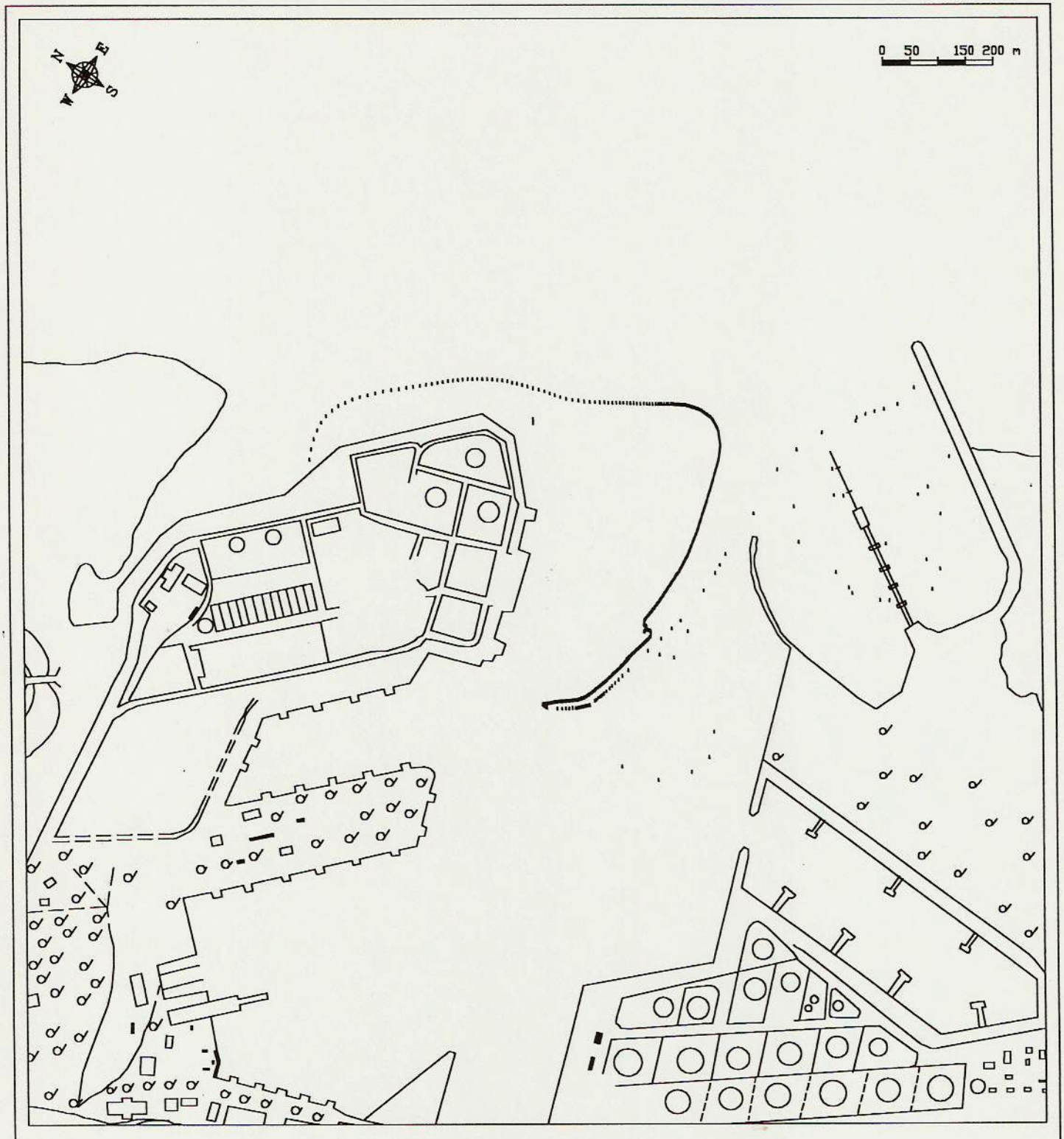

LOCATION OF WATER PARTICLES EMERGING FROM THE MAIN DISCHARGE LOCATION AT T=1.5 HOURS. SCENARIO A. ACTUAL CONDITIONS.

FIGURE 3.9

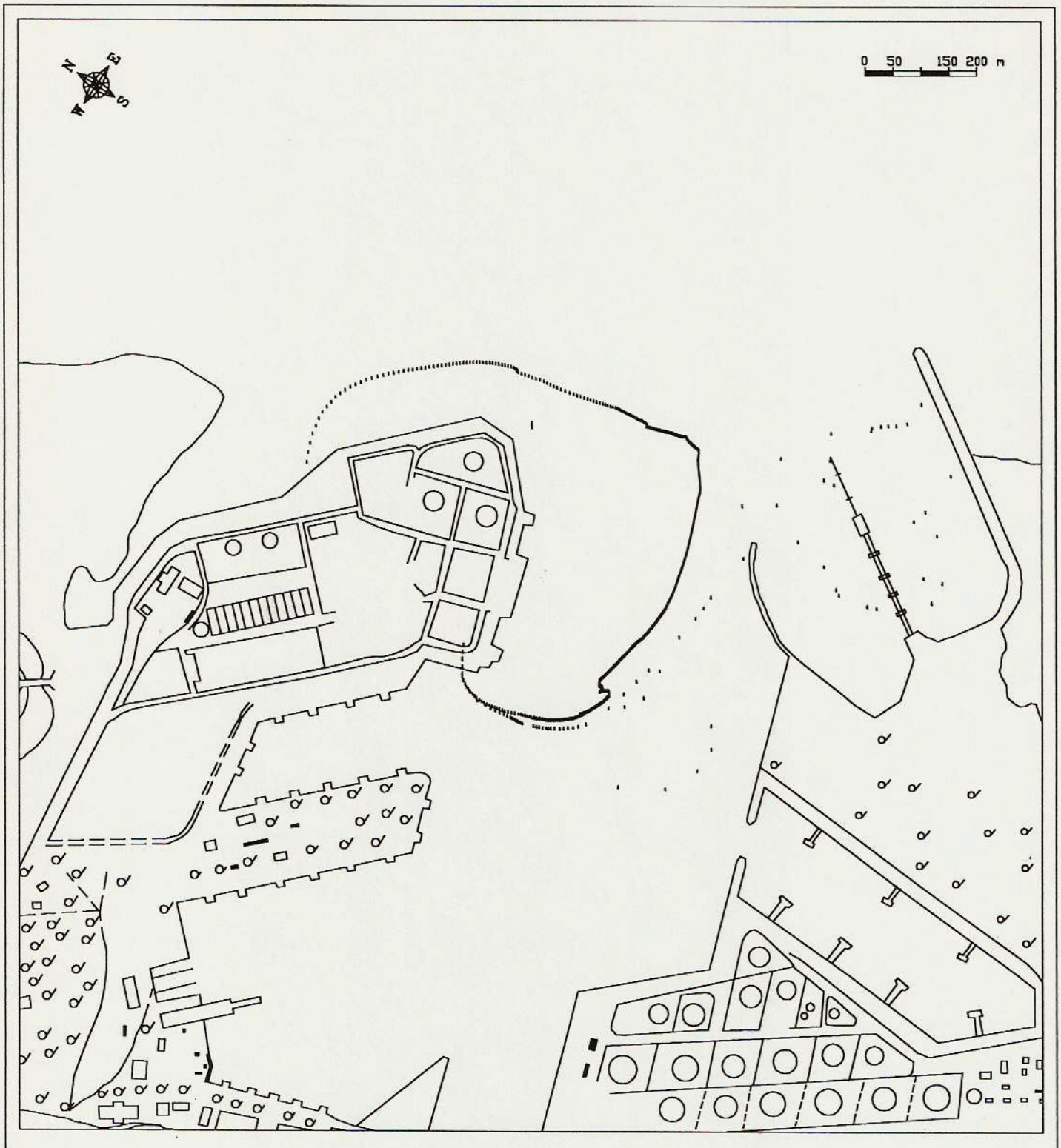

LOCATION OF WATER PARTICLES EMERGING FROM THE MAIN DISCHARGE LOCATION AT T=2.2 HOURS. SCENARIO A. ACTUAL CONDITIONS.

FIGURE 3.10

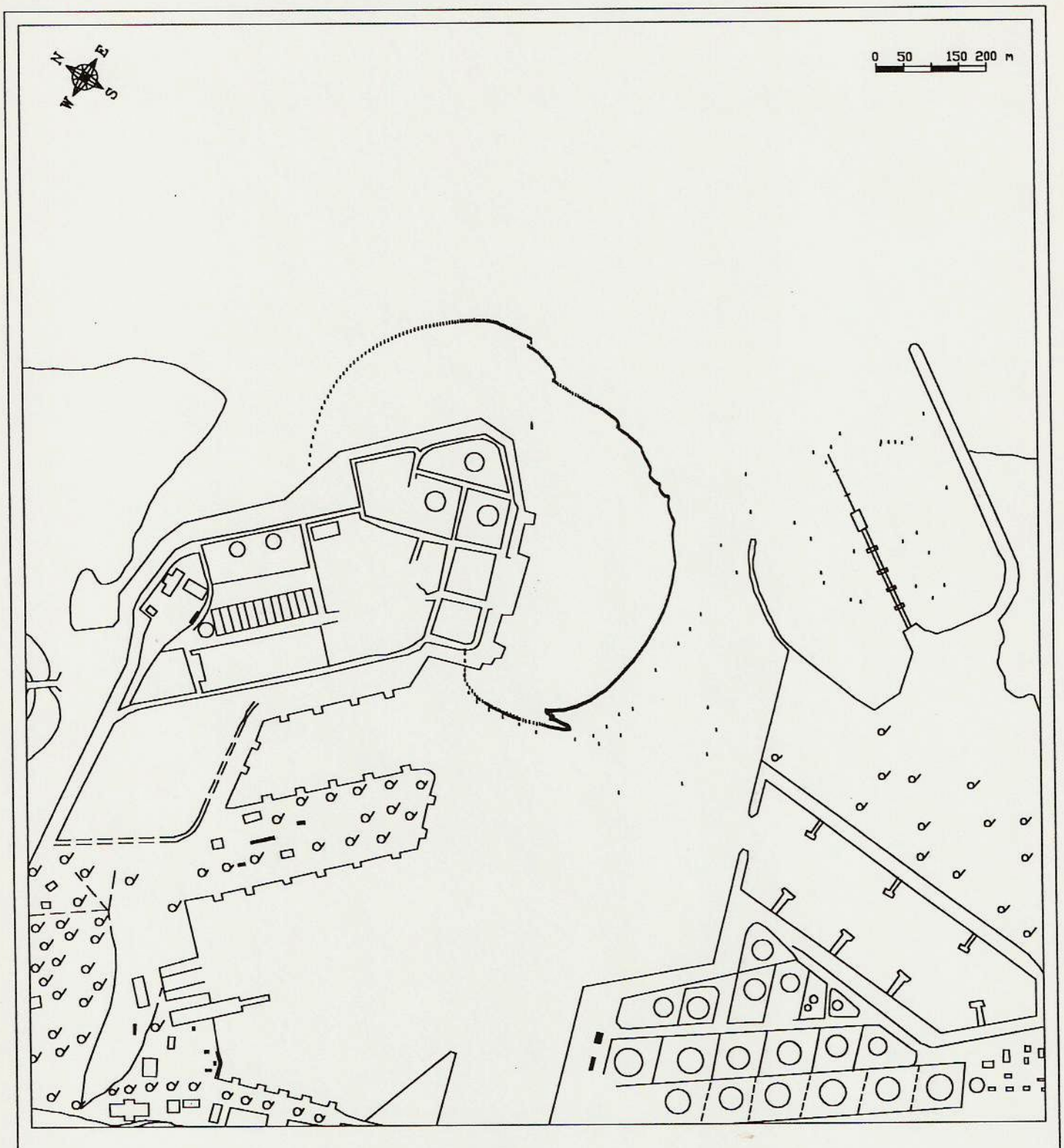

LOCATION OF WATER PARTICLES EMERGING FROM THE MAIN DISCHARGE LOCATION AT T=3 HOURS. SCENARIO A. ACTUAL CONDITIONS.

FIGURE 3.11

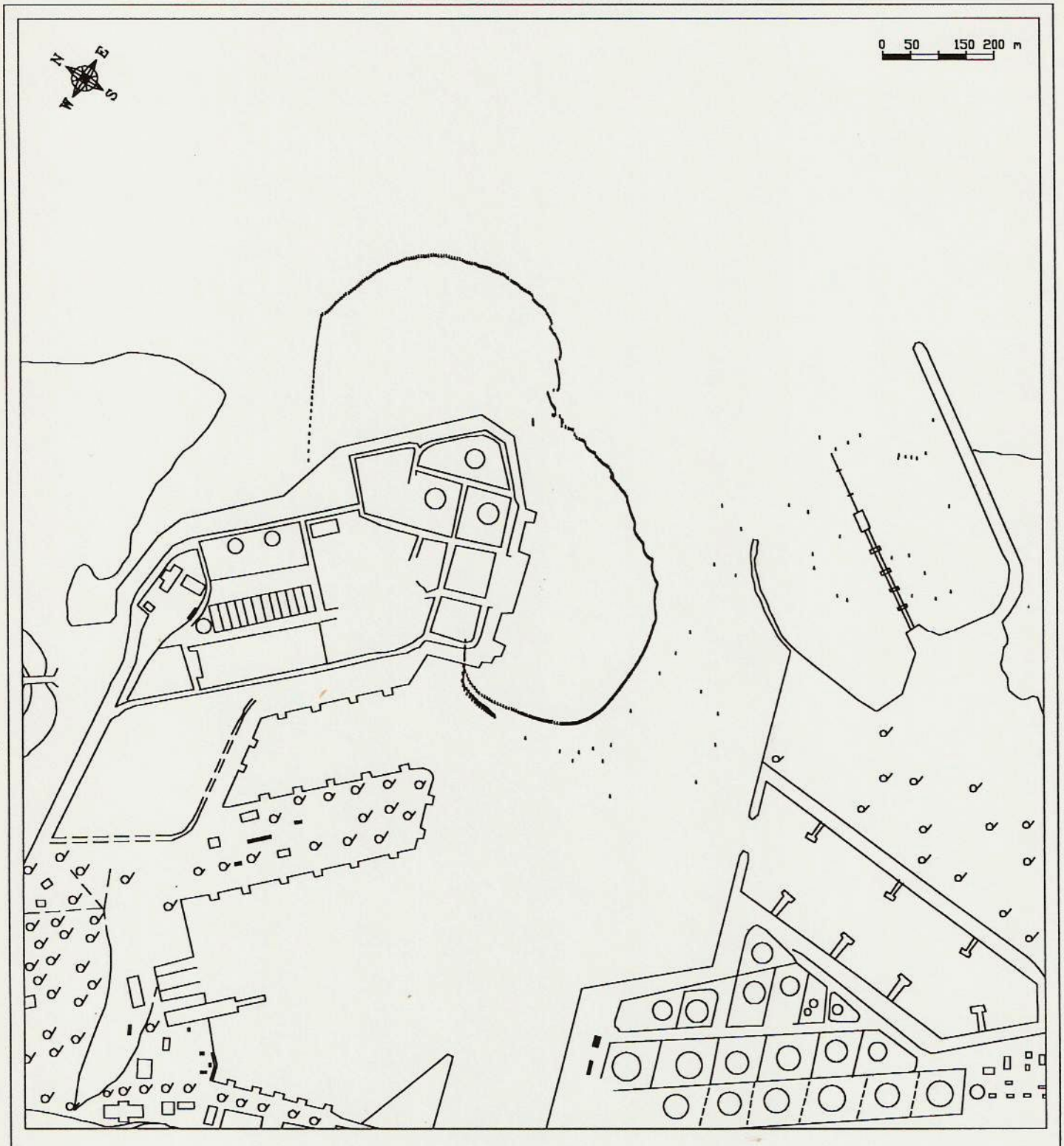

LOCATION OF WATER PARTICLES EMERGING FROM THE MAIN DISCHARGE LOCATION AT T=3.8 HOURS. SCENARIO A. ACTUAL CONDITIONS.

FIGURE 3.12

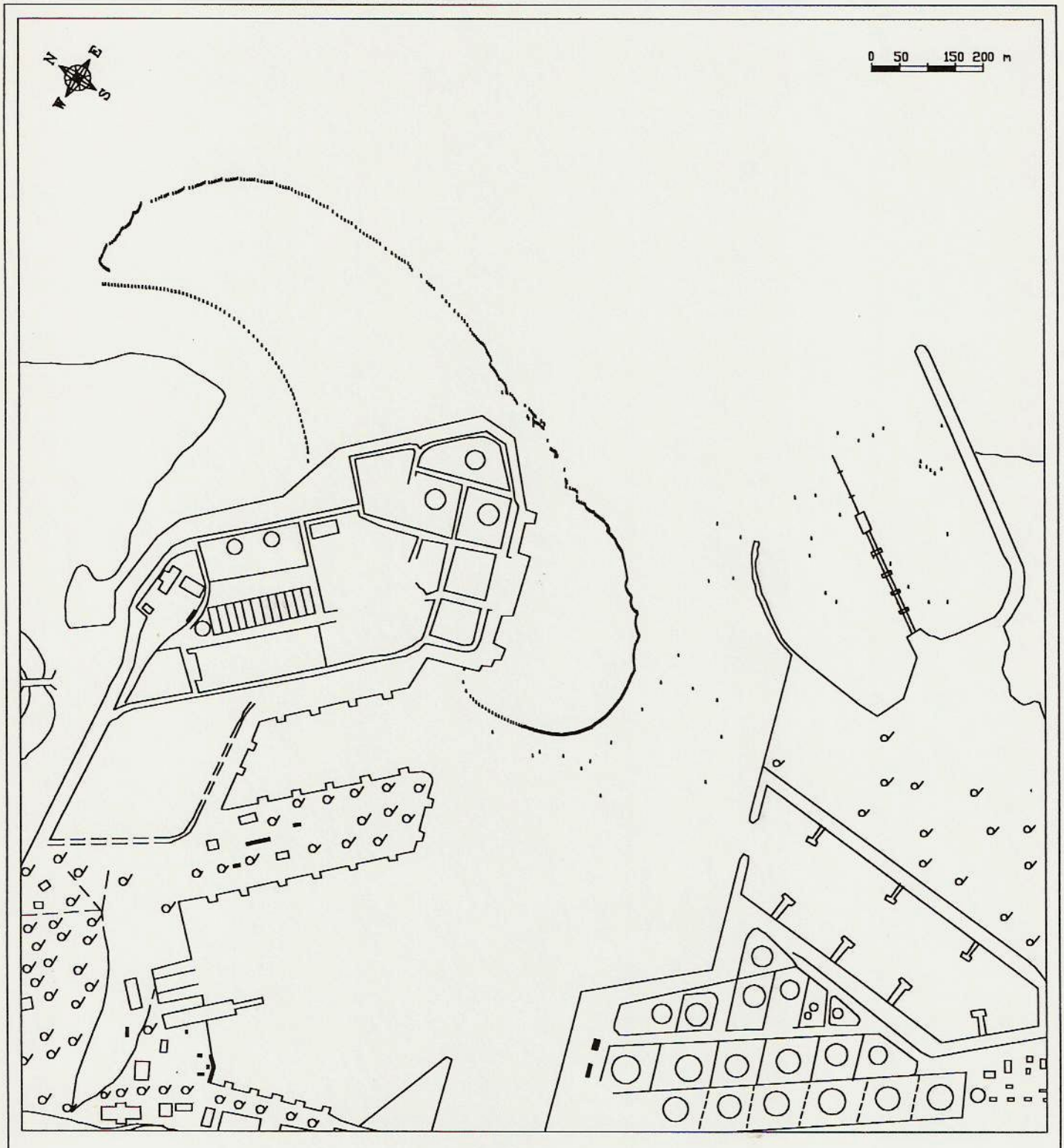

LOCATION OF WATER PARTICLES EMERGING FROM THE MAIN DISCHARGE LOCATION AT T=4.5 HOURS. SCENARIO A. ACTUAL CONDITIONS.

FIGURE 3.13

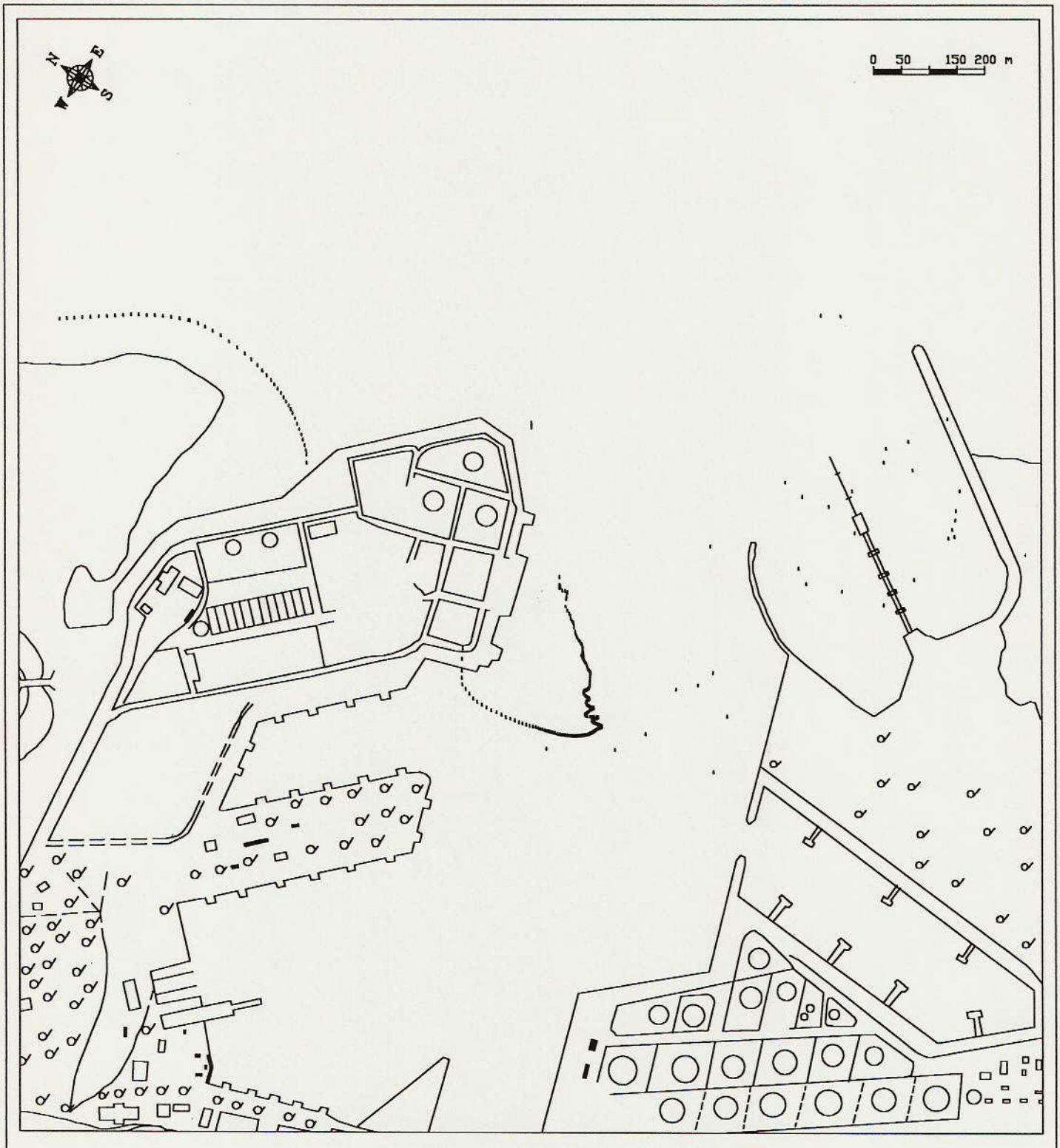

LOCATION OF WATER PARTICLES EMERGING FROM THE MAIN DISCHARGE LOCATION AT T=6 HOURS. SCENARIO A. ACTUAL CONDITIONS.

FIGURE 3.14

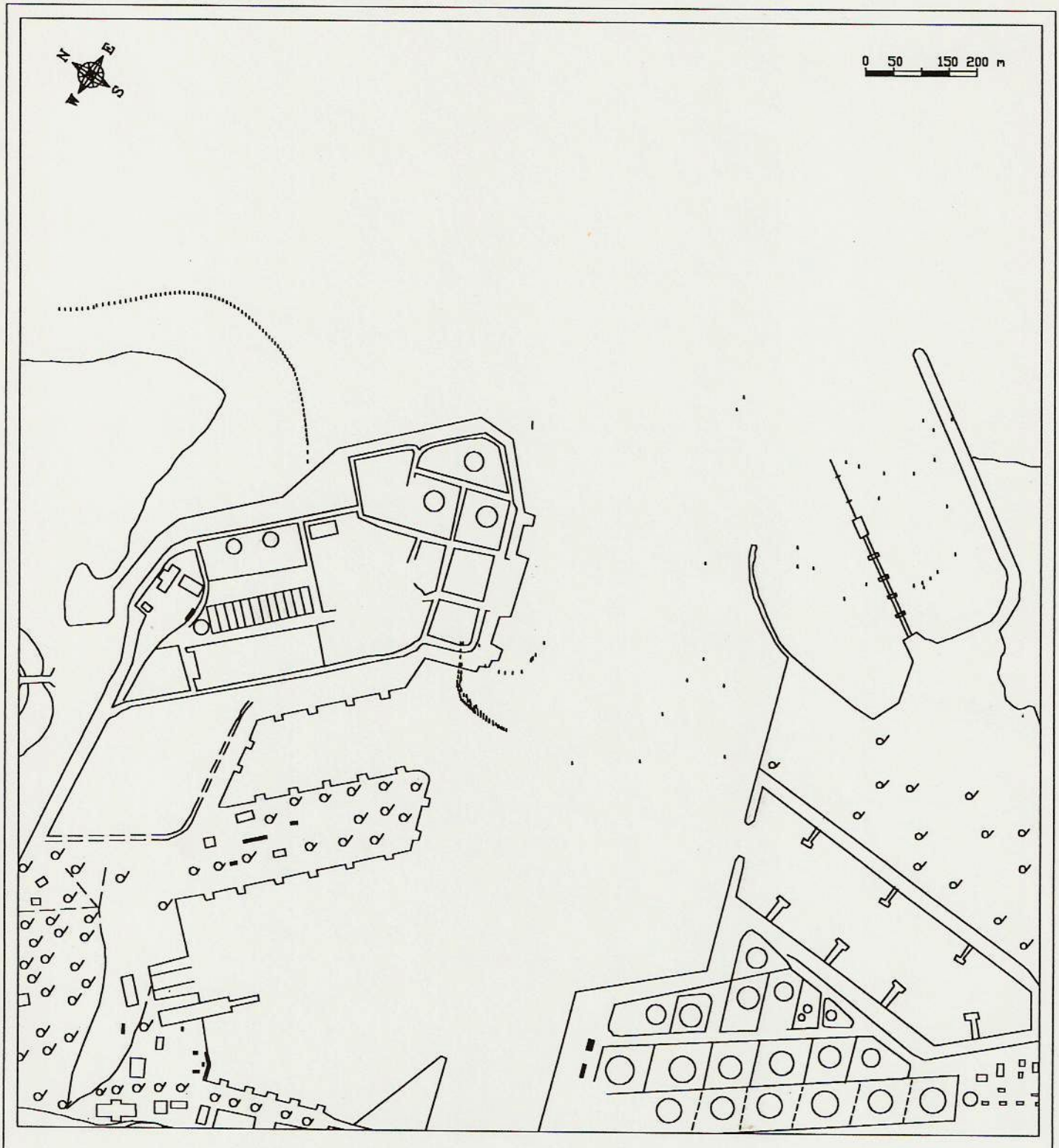

LOCATION OF WATER PARTICLES EMERGING FROM THE MAIN DISCHARGE LOCATION AT T=7.5 HOURS. SCENARIO A. ACTUAL CONDITIONS.

FIGURE 3.15

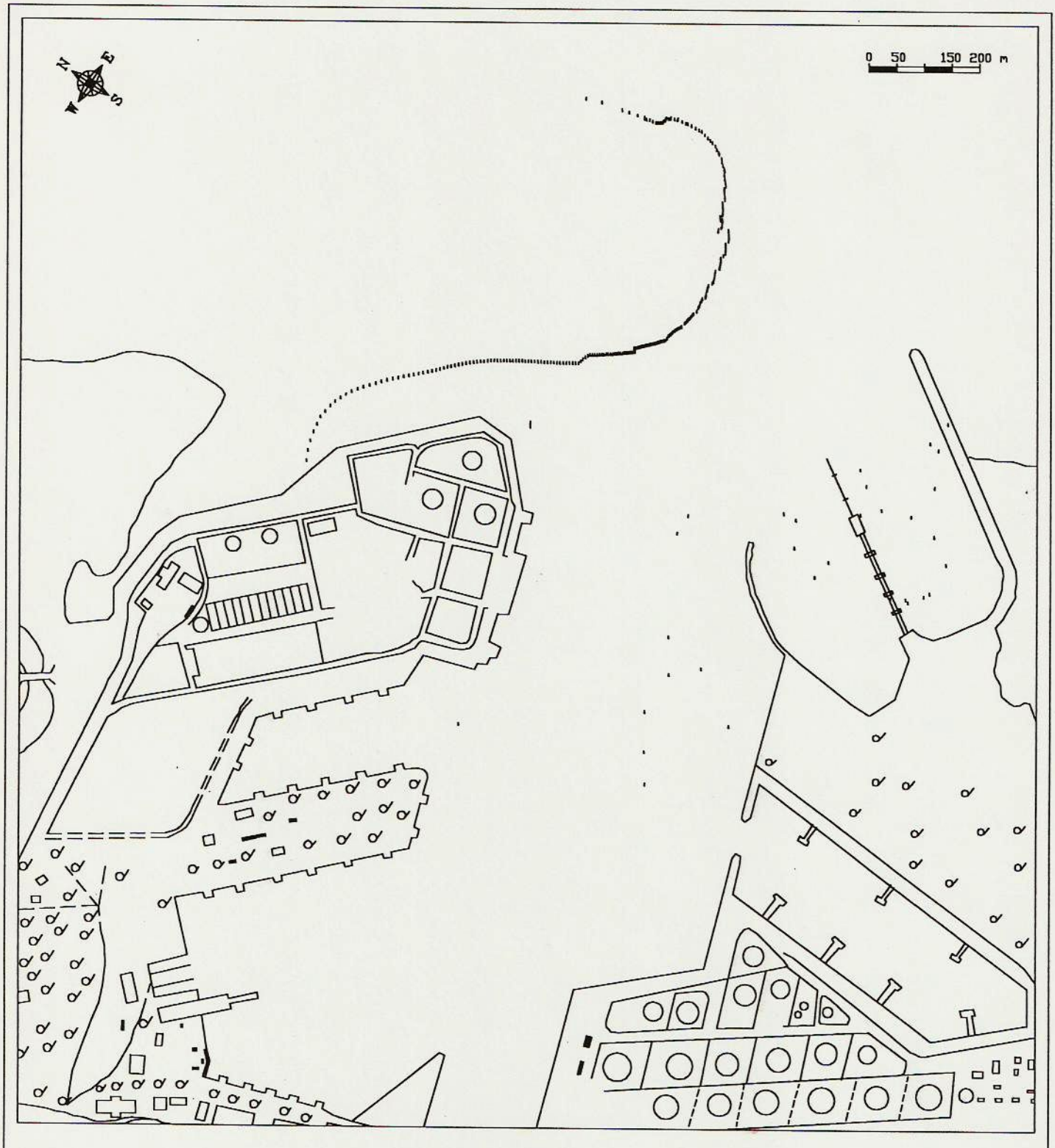

LOCATION OF WATER PARTICLES EMERGING FROM THE MAIN DISCHARGE LOCATION AT T=9 HOURS. SCENARIO A. ACTUAL CONDITIONS.

FIGURE 3.16

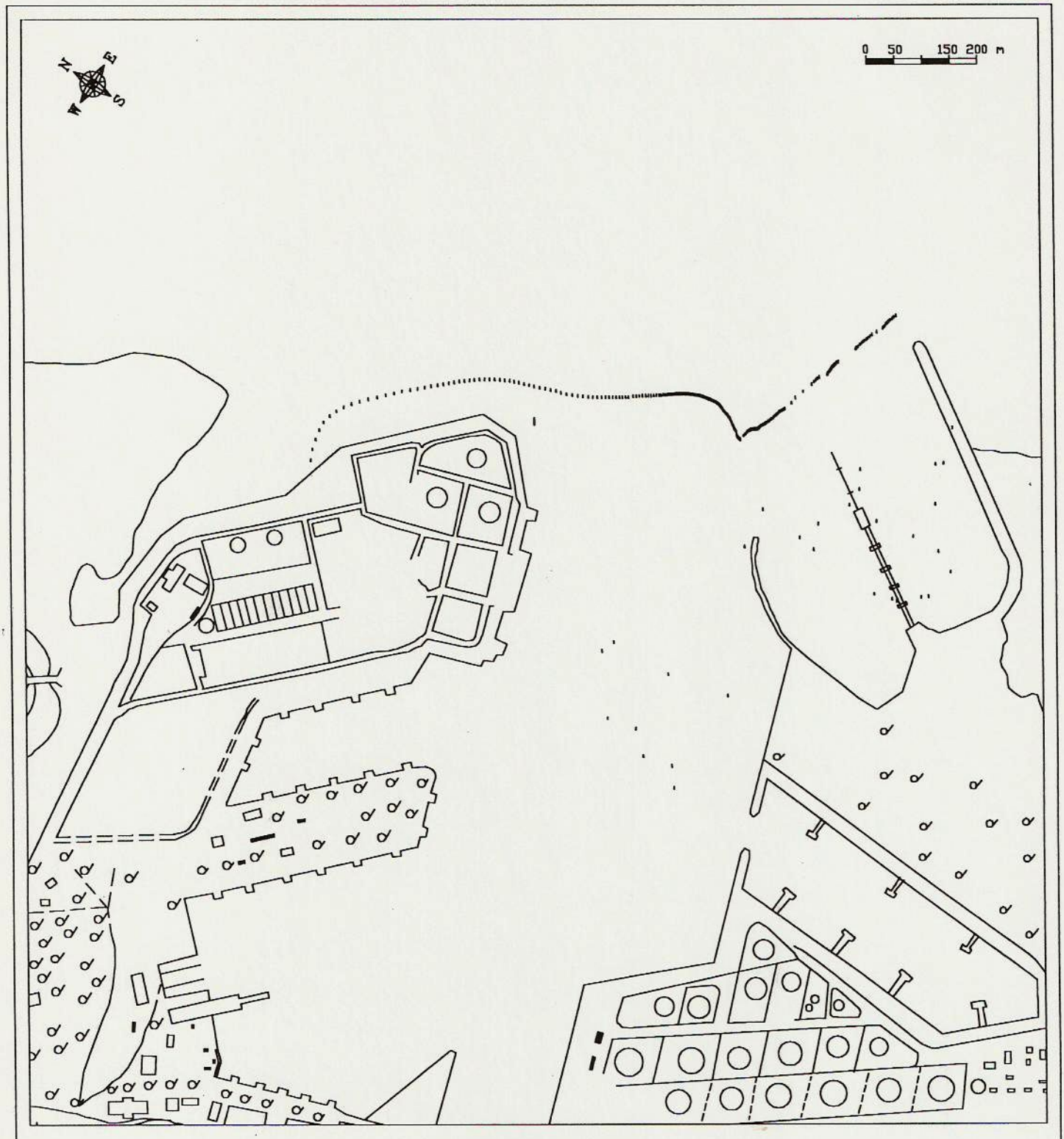

LOCATION OF WATER PARTICLES EMERGING FROM THE MAIN DISCHARGE LOCATION AT T=10.5 HOURS. SCENARIO A. ACTUAL CONDITIONS.

FIGURE 3.17

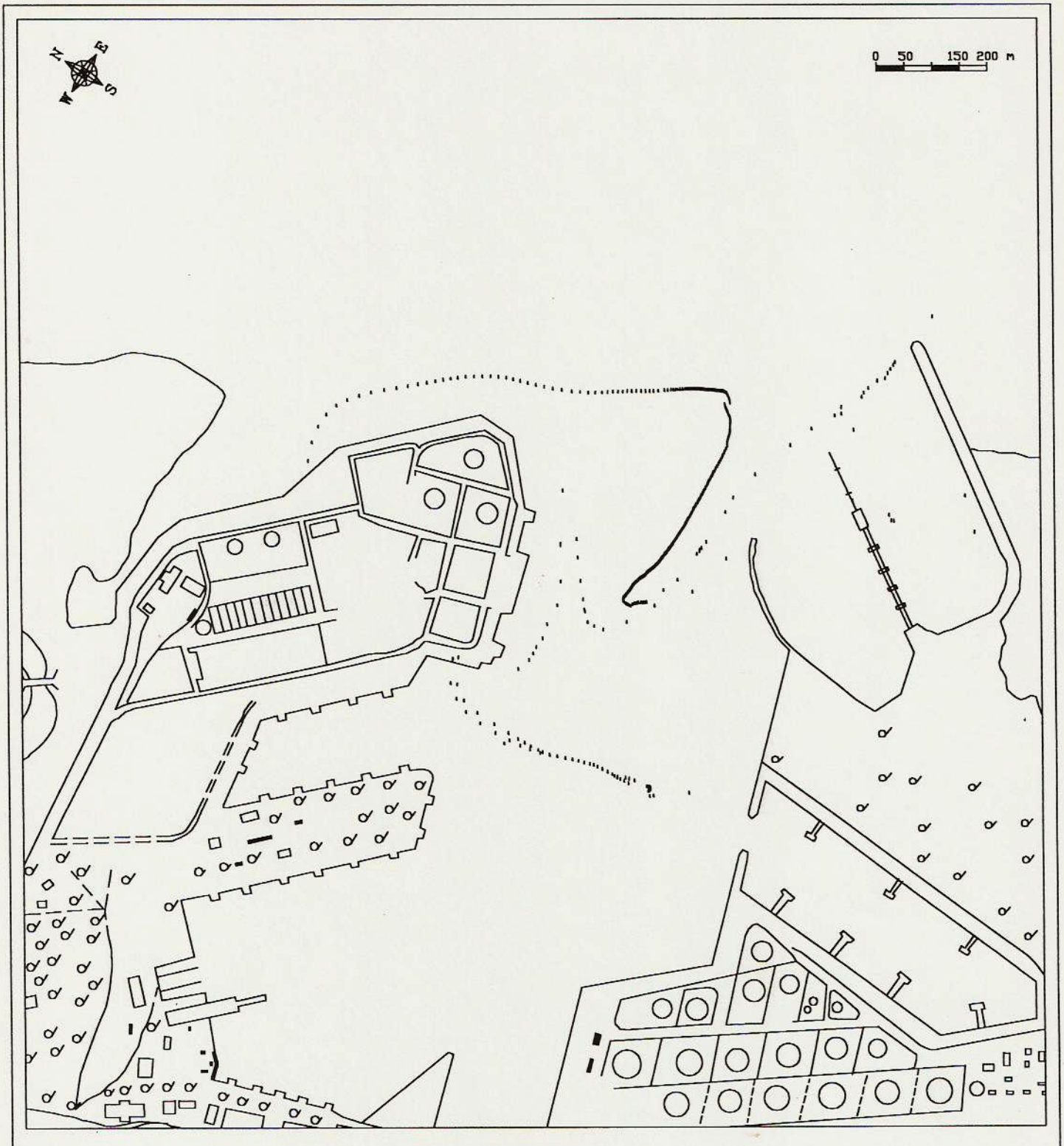

LOCATION OF WATER PARTICLES EMERGING FROM THE MAIN DISCHARGE LOCATION AT T=0 HOURS. SCENARIO A. FUTURE CONDITIONS.

FIGURE 3.18

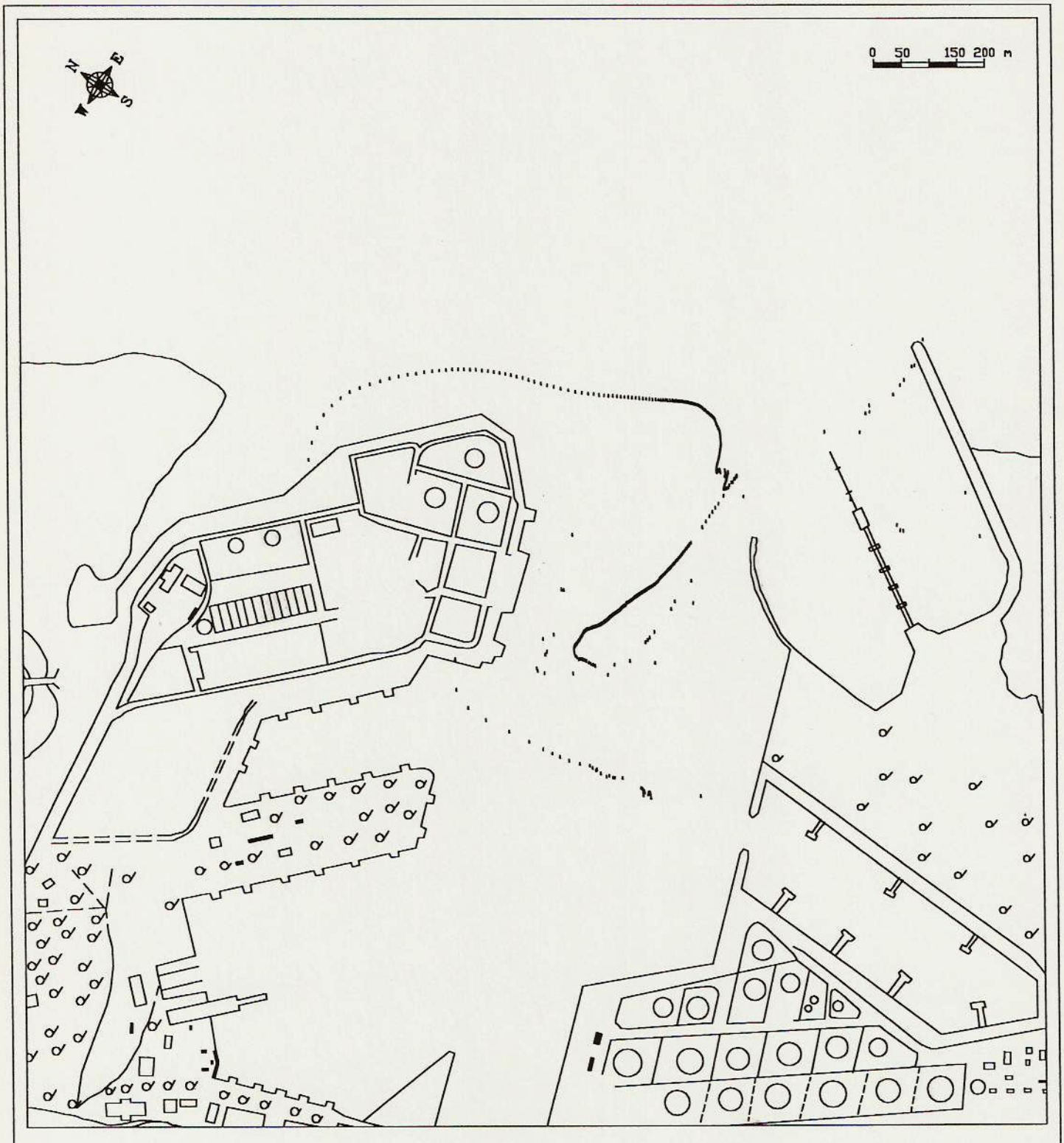

LOCATION OF WATER PARTICLES EMERGING FROM THE MAIN DISCHARGE LOCATION AT T=1 HOUR. SCENARIO A. FUTURE CONDITIONS.

FIGURE 3.19

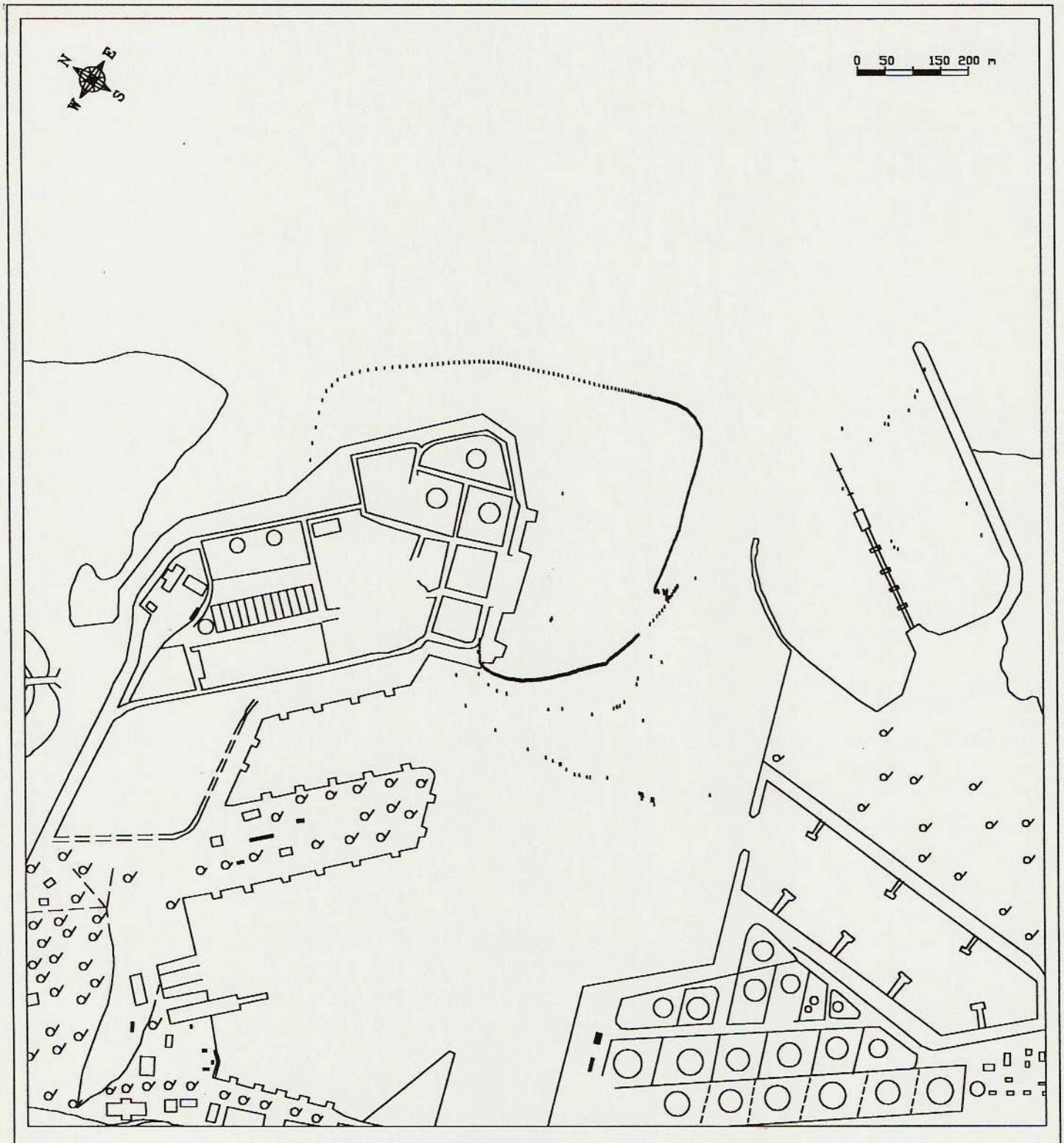

LOCATION OF WATER PARTICLES EMERGING FROM THE MAIN DISCHARGE LOCATION AT T=2 HOURS. SCENARIO A. FUTURE CONDITIONS.

FIGURE 3.20

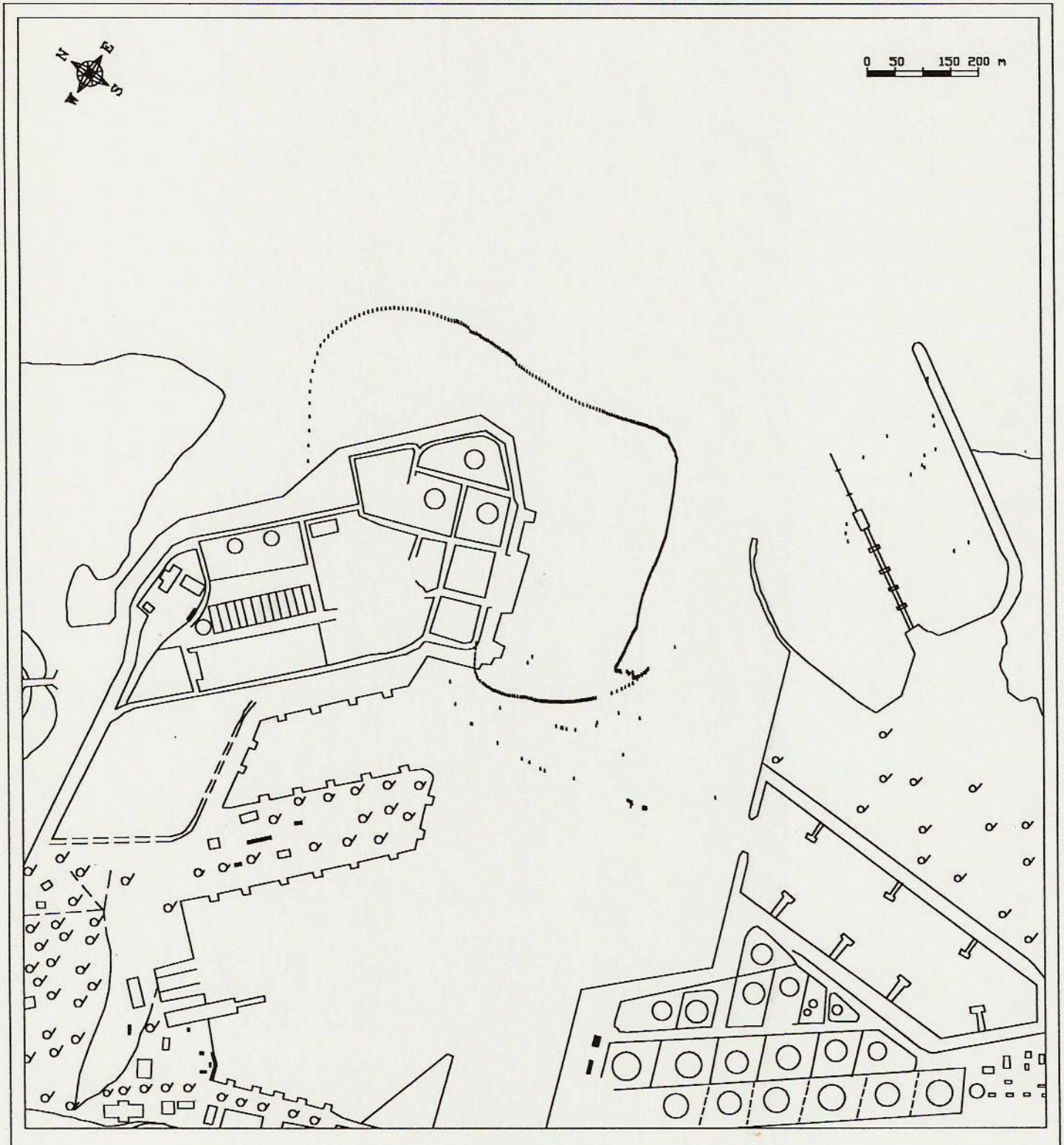

LOCATION OF WATER PARTICLES EMERGING FROM THE MAIN DISCHARGE LOCATION AT T=3 HOURS. SCENARIO A. FUTURE CONDITIONS.

FIGURE 3.21

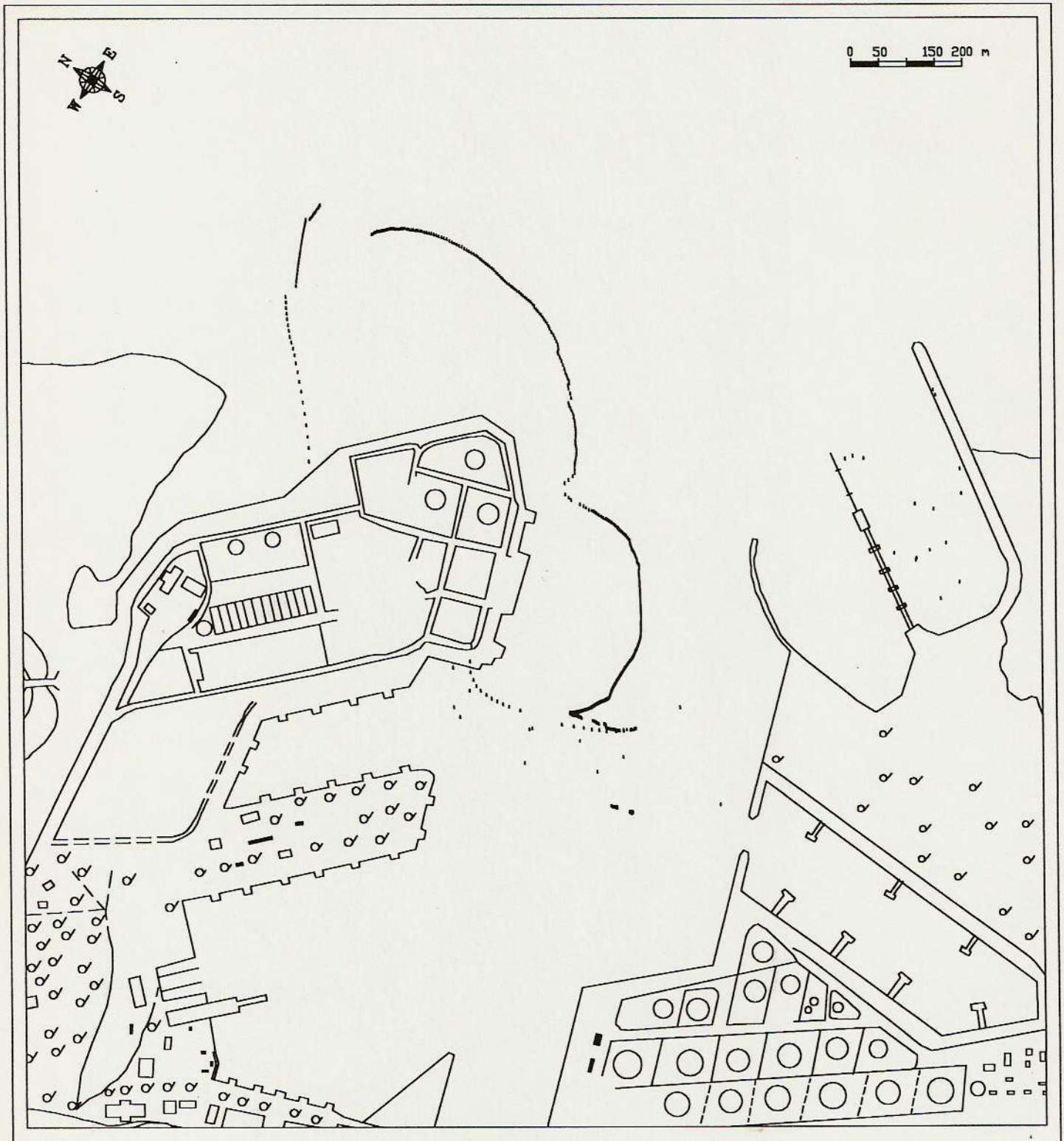

LOCATION OF WATER PARTICLES EMERGING FROM THE MAIN DISCHARGE LOCATION AT T=4 HOURS. SCENARIO A. FUTURE CONDITIONS.

FIGURE 3.22

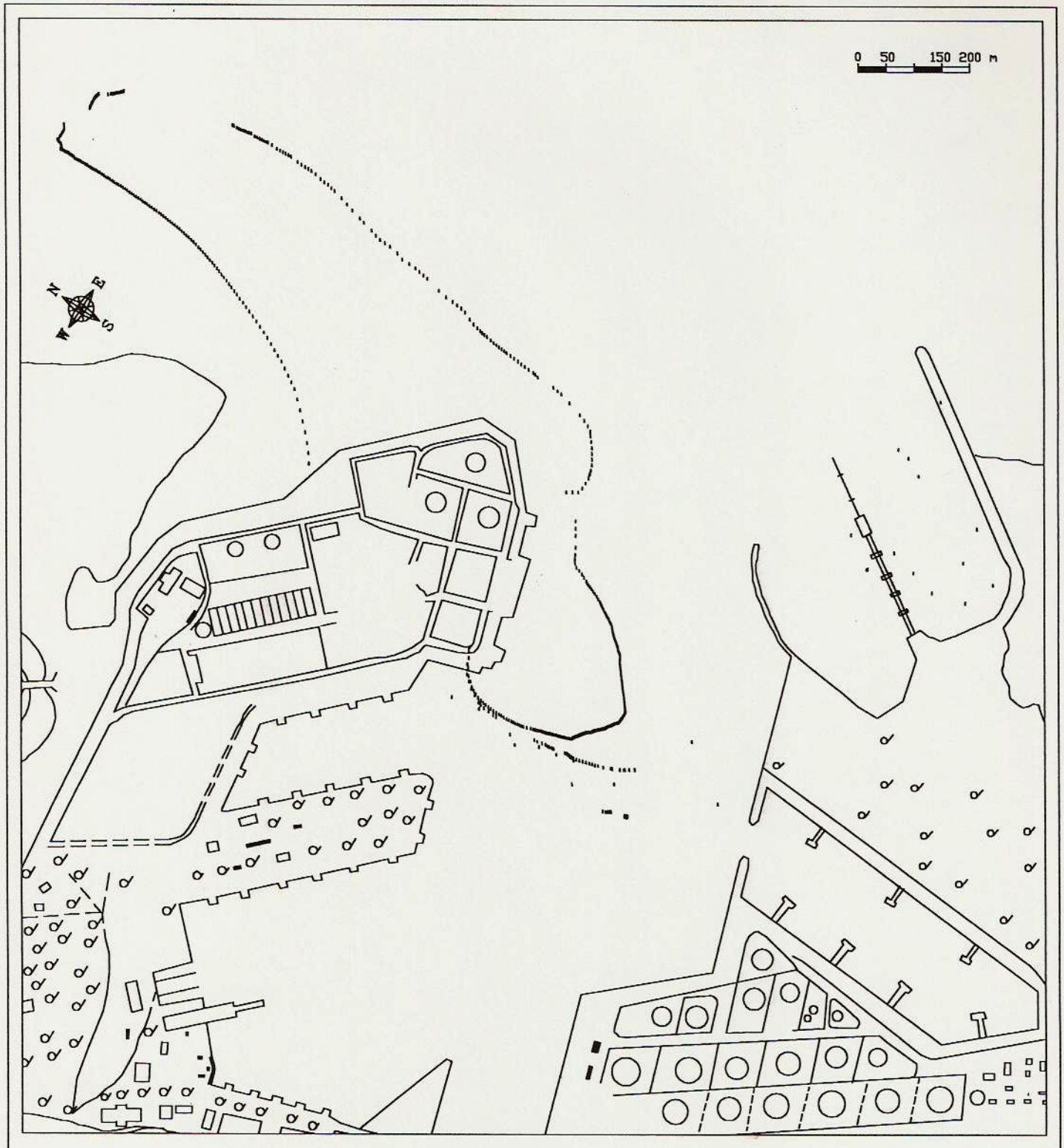

LOCATION OF WATER PARTICLES EMERGING FROM THE MAIN DISCHARGE LOCATION AT T=5 HOURS. SCENARIO A. FUTURE CONDITIONS.

FIGURE 3.23

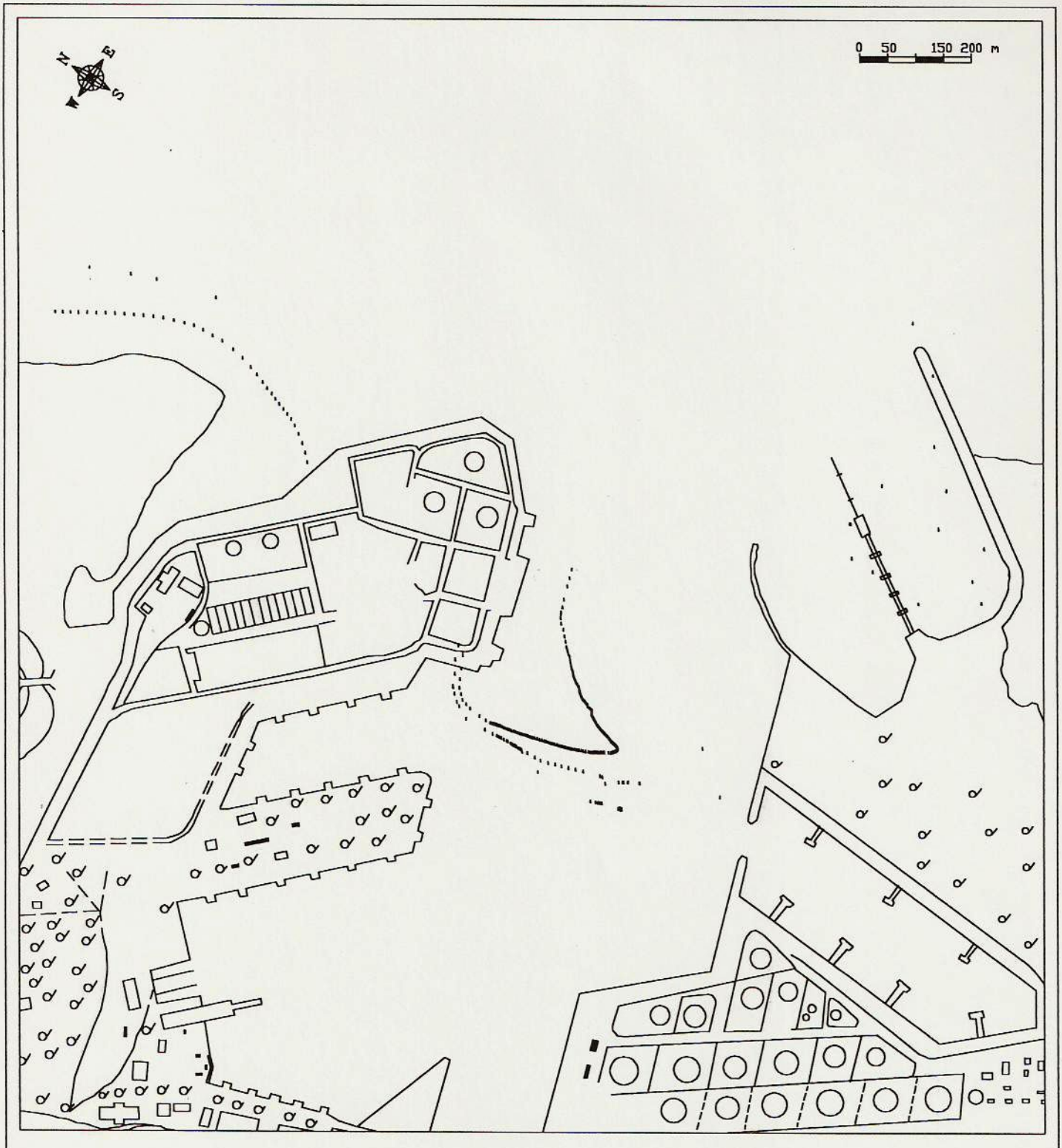

LOCATION OF WATER PARTICLES EMERGING FROM THE MAIN DISCHARGE LOCATION AT T=6 HOURS. SCENARIO A. FUTURE CONDITIONS.

FIGURE 3.24

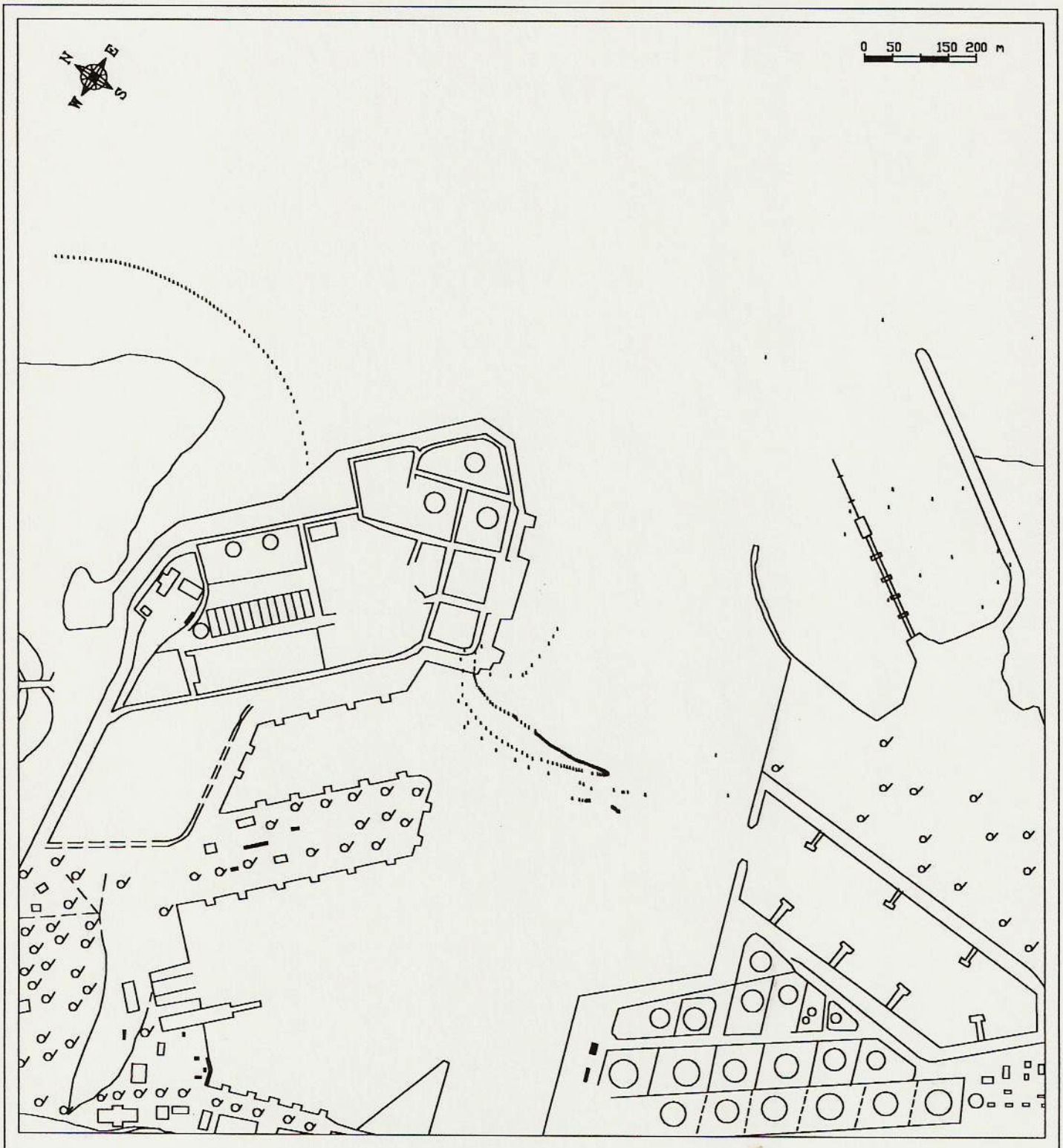

LOCATION OF WATER PARTICLES EMERGING FROM THE MAIN DISCHARGE LOCATION AT T=7 HOURS. SCENARIO A. FUTURE CONDITIONS.

FIGURE 3.25

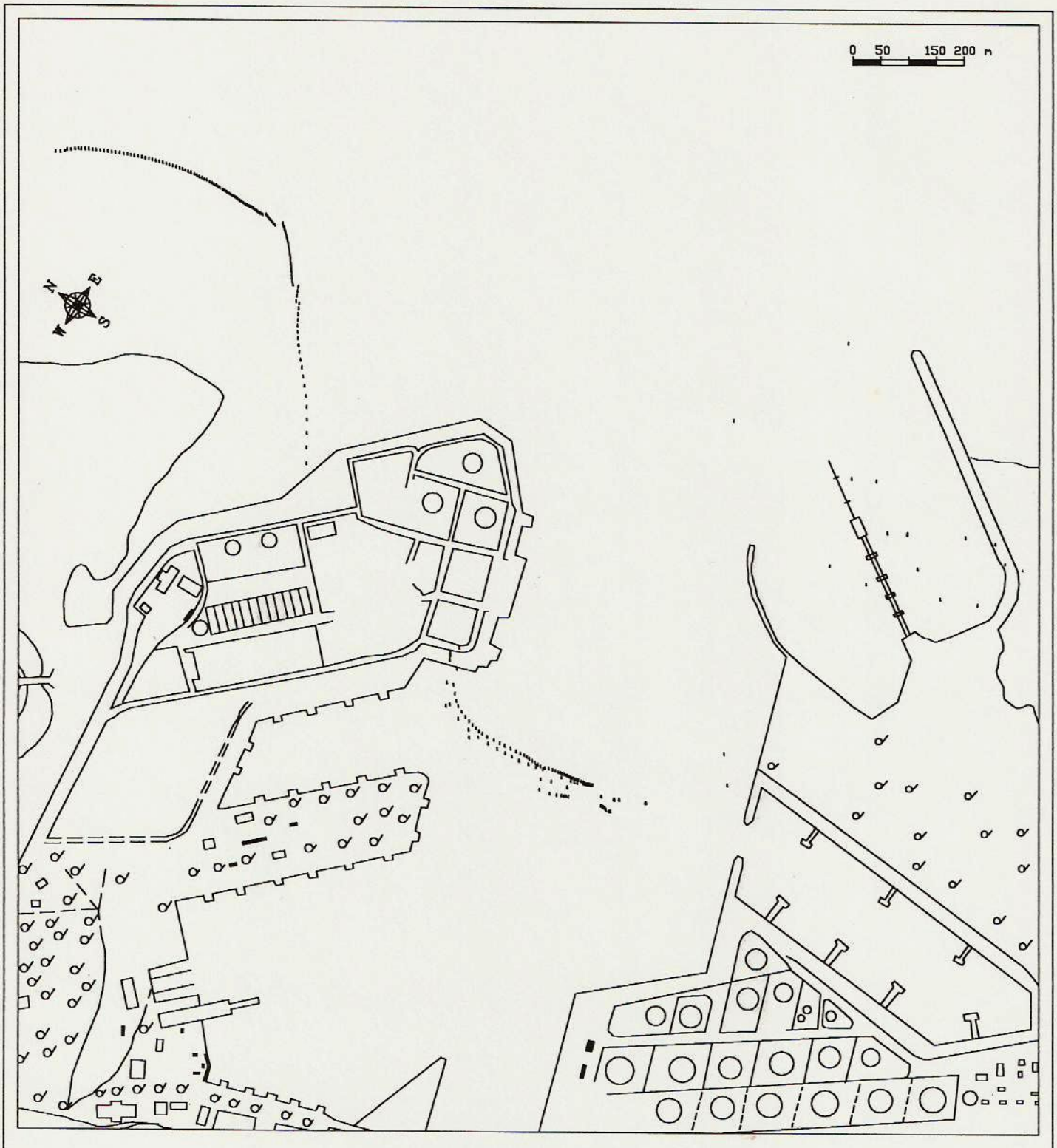

LOCATION OF WATER PARTICLES EMERGING FROM THE MAIN DISCHARGE LOCATION AT T=8 HOURS. SCENARIO A. FUTURE CONDITIONS.

FIGURE 3.26

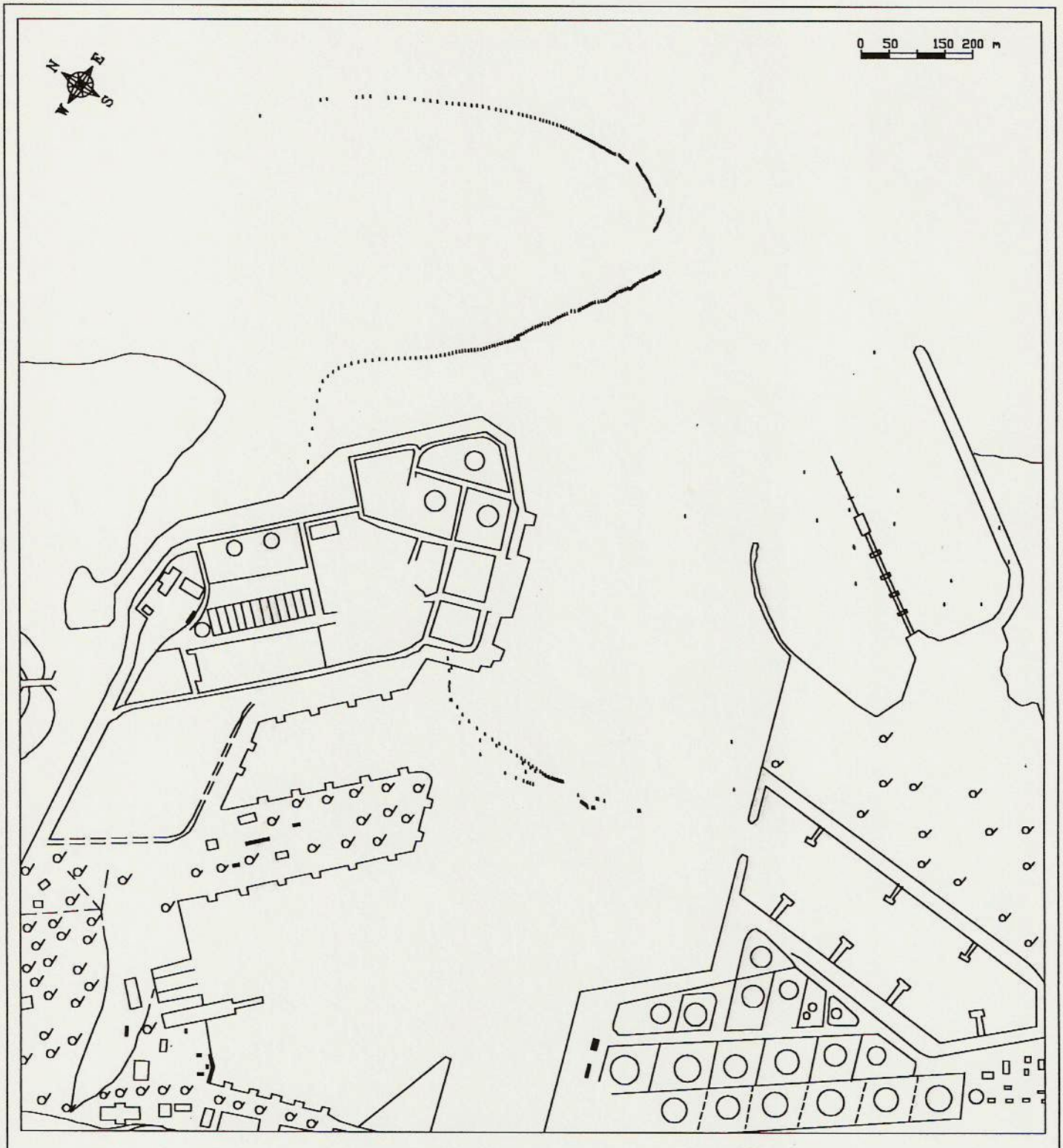

LOCATION OF WATER PARTICLES EMERGING FROM THE MAIN DISCHARGE LOCATION AT T=9 HOURS. SCENARIO A. FUTURE CONDITIONS.

FIGURE 3.27

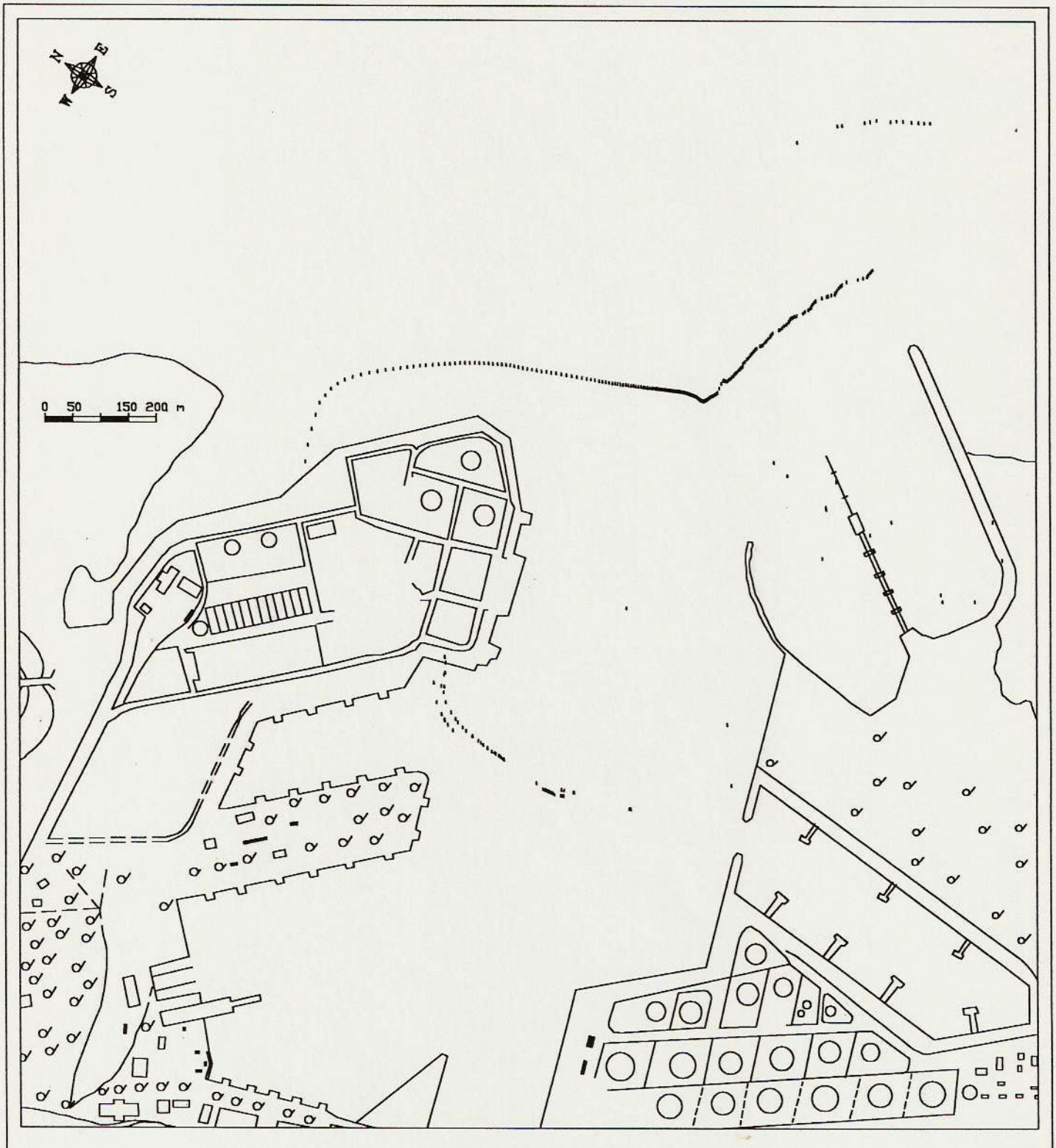

LOCATION OF WATER PARTICLES EMERGING FROM THE MAIN DISCHARGE LOCATION AT T=10 HOURS. SCENARIO A. FUTURE CONDITIONS.

FIGURE 3.28

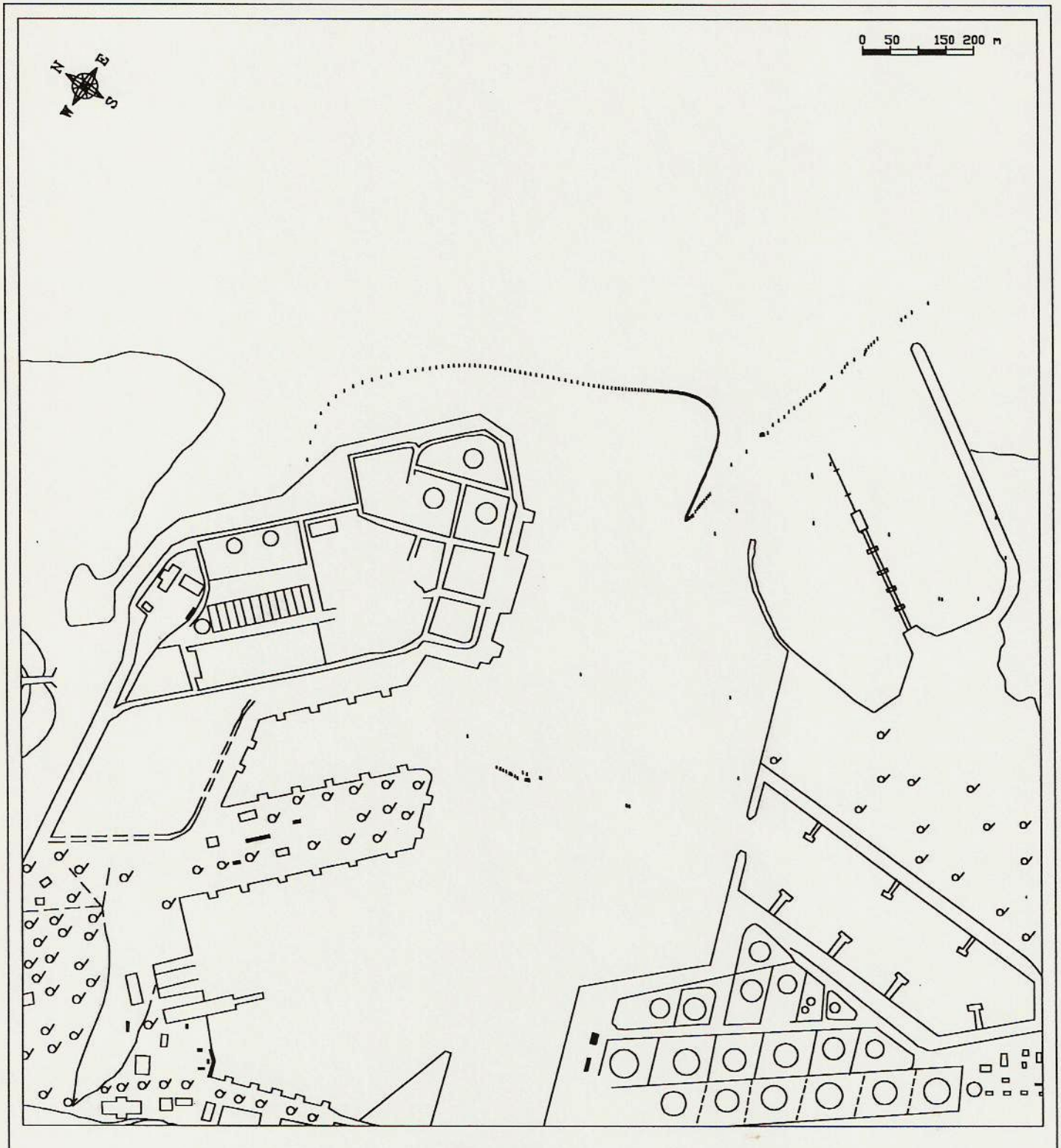

LOCATION OF WATER PARTICLES EMERGING FROM THE MAIN DISCHARGE LOCATION AT T=11 HOURS. SCENARIO A. FUTURE CONDITIONS.

FIGURE 3.29

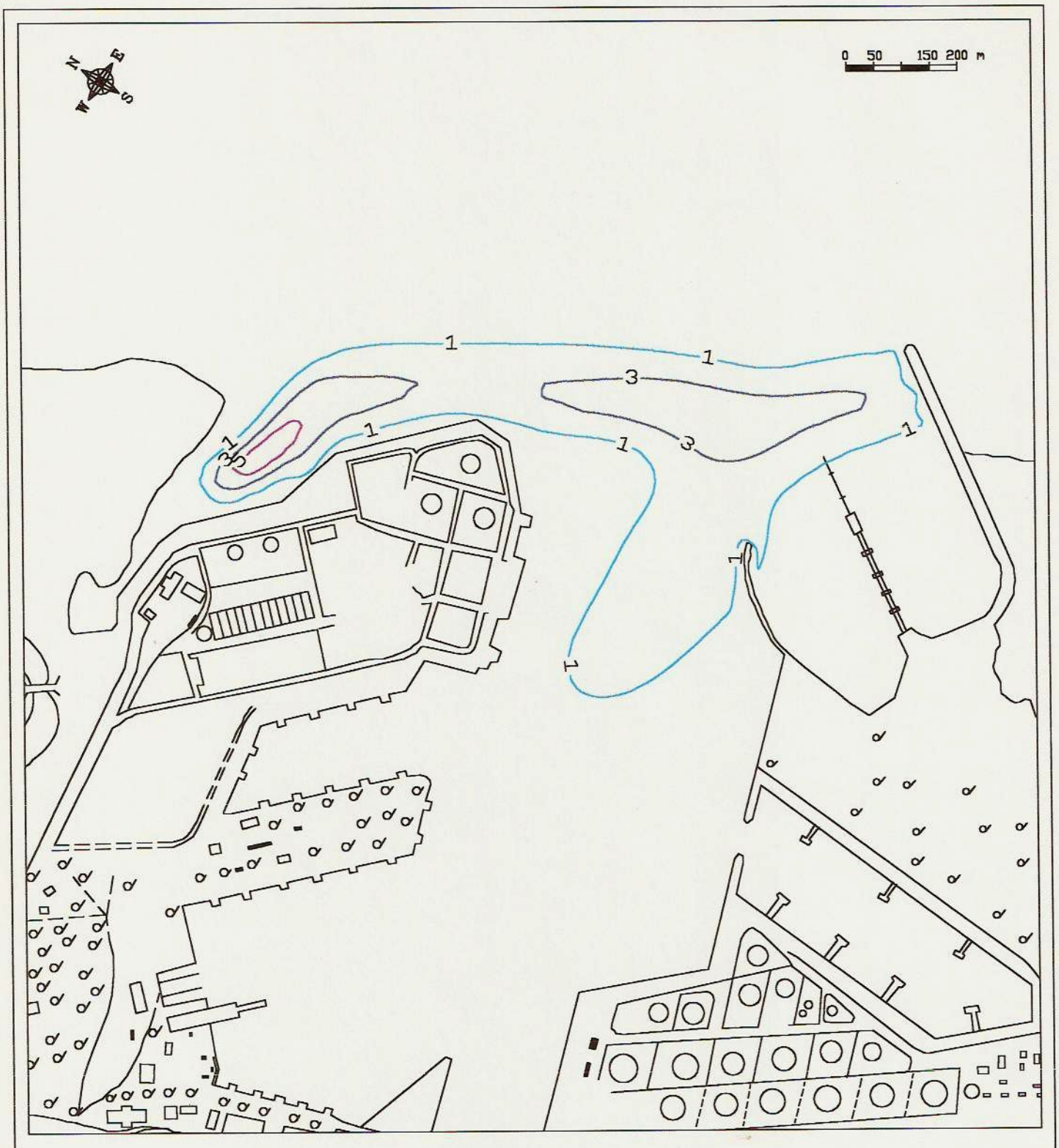

THERMAL PLUME FOR T=0.5 HOURS.
SCENARIO A. ACTUAL CONDITIONS.

FIGURE 3.30

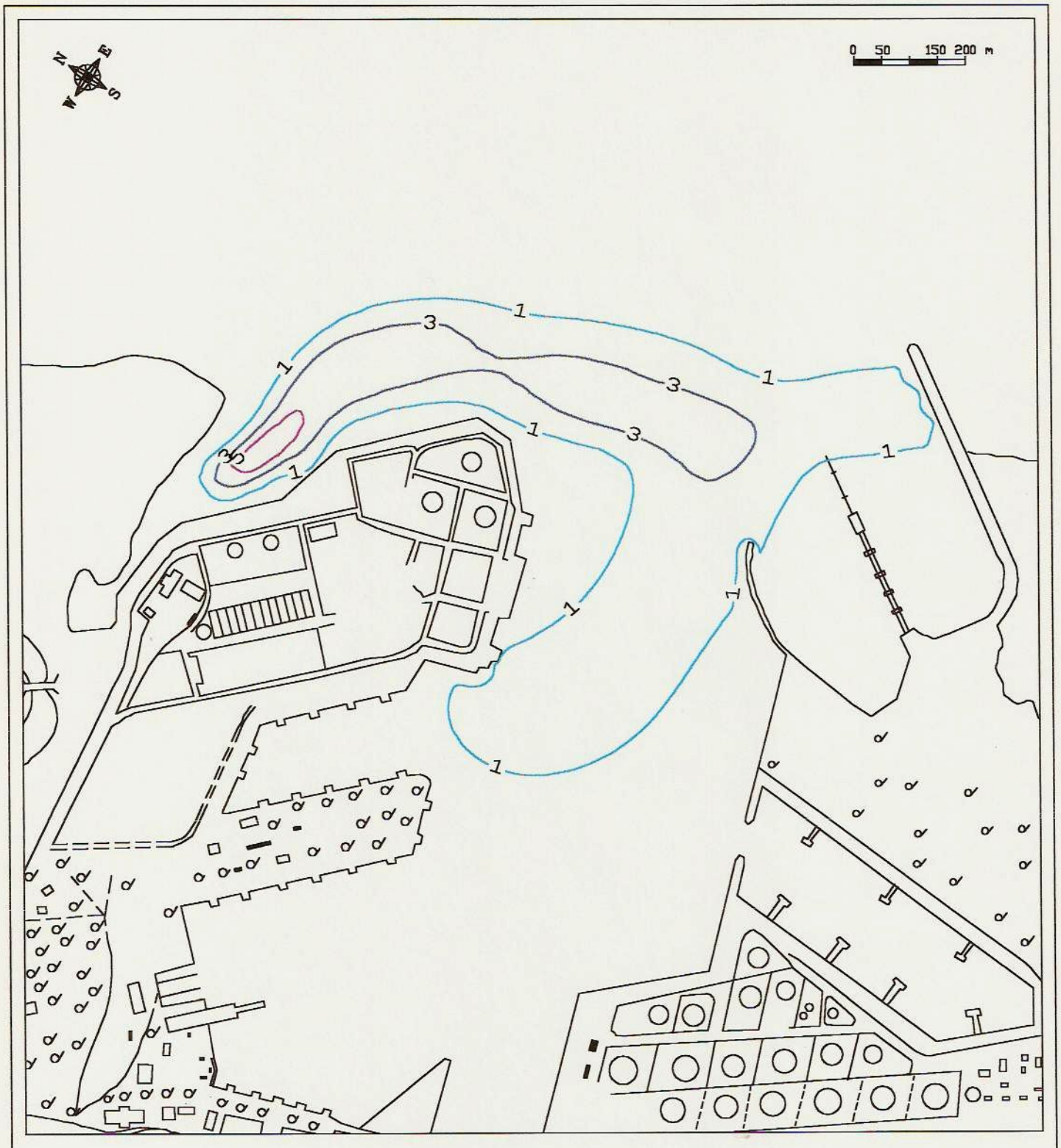

THERMAL PLUME FOR T=2 HOURS.
SCENARIO A. ACTUAL CONDITIONS.

FIGURE 3.31

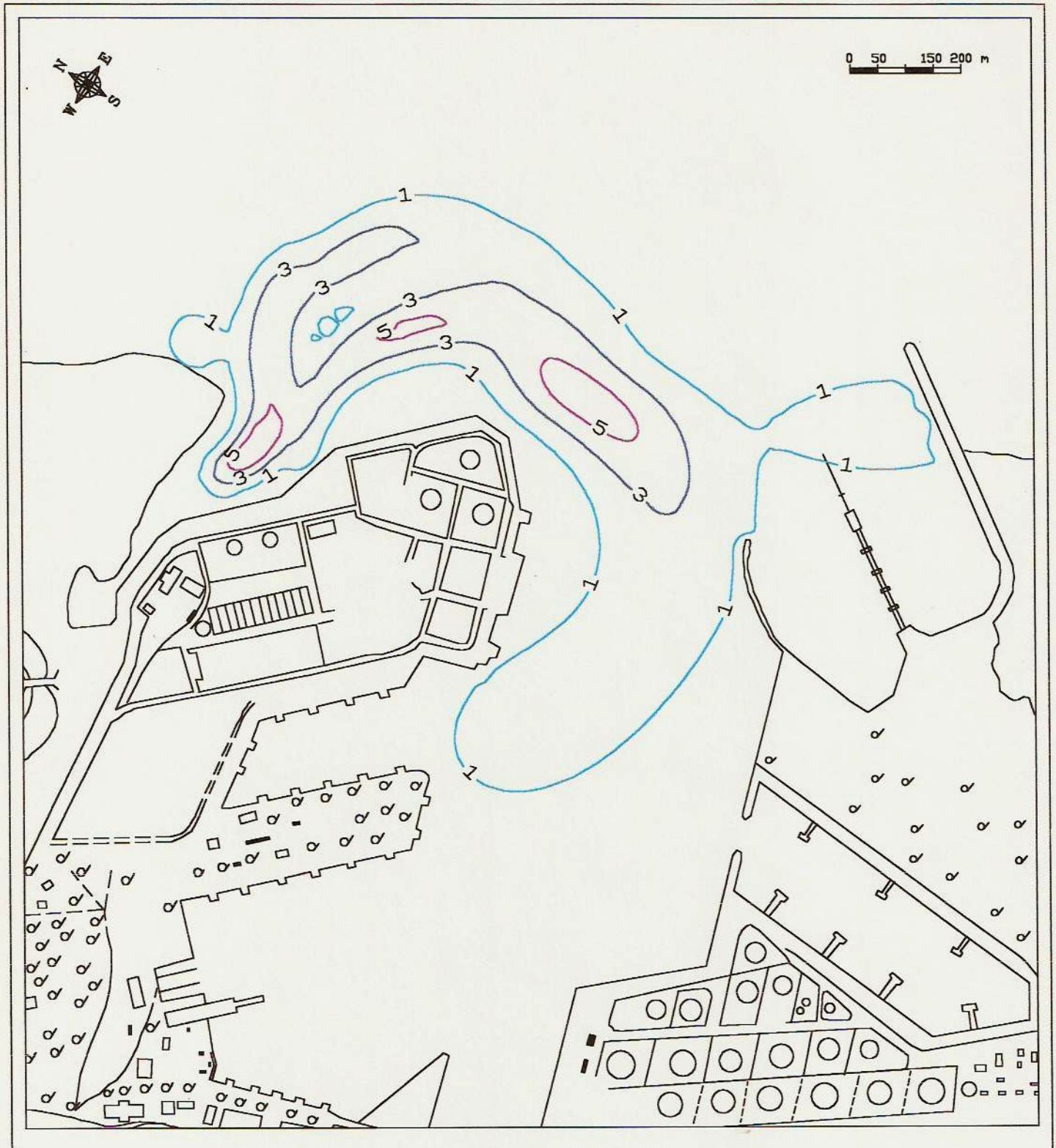

THERMAL PLUME FOR T=3 HOURS.
SCENARIO A. ACTUAL CONDITIONS.

FIGURE 3.32

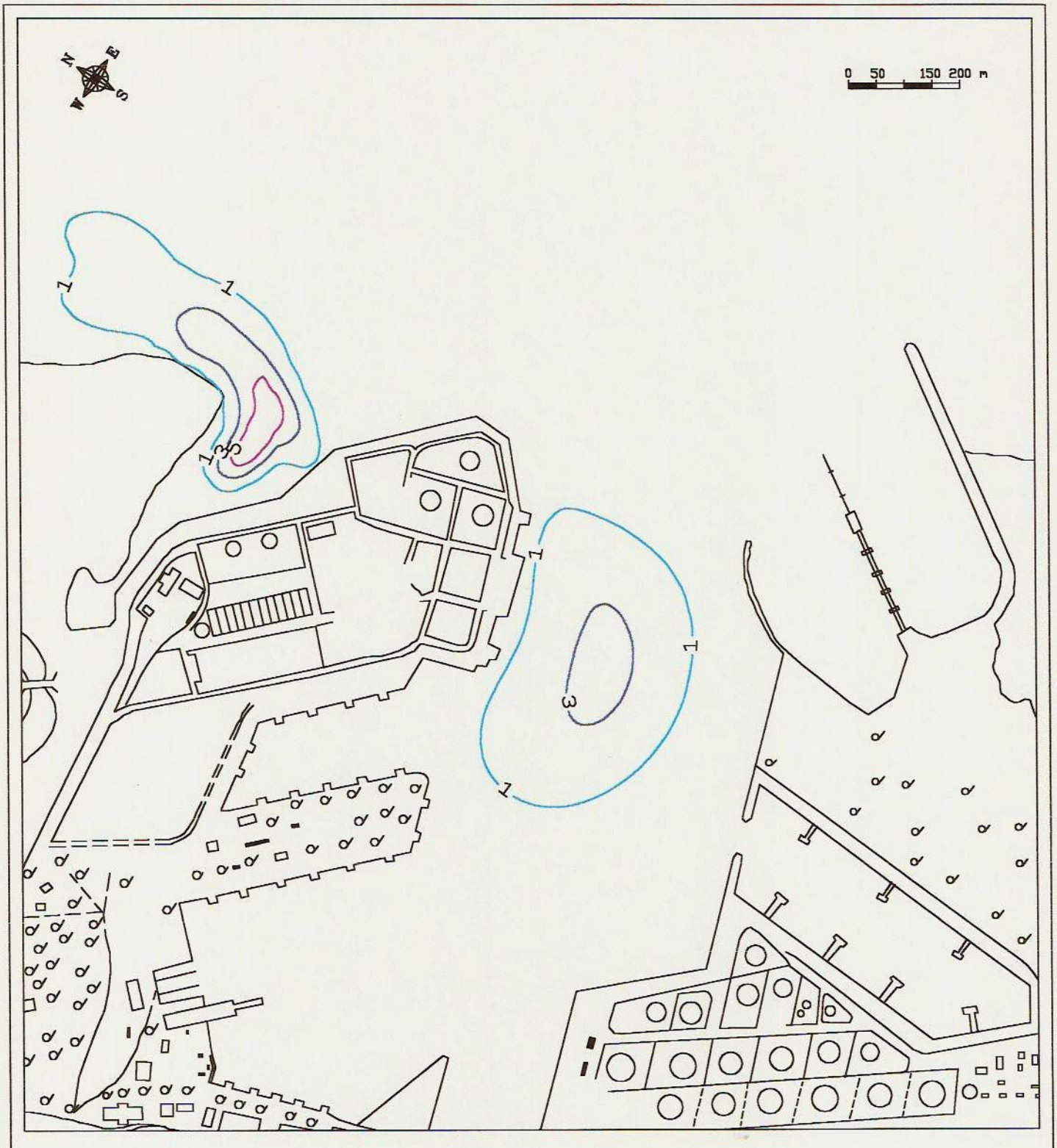

THERMAL PLUME FOR T=5 HOURS.
SCENARIO A. ACTUAL CONDITIONS.

FIGURE 3.33

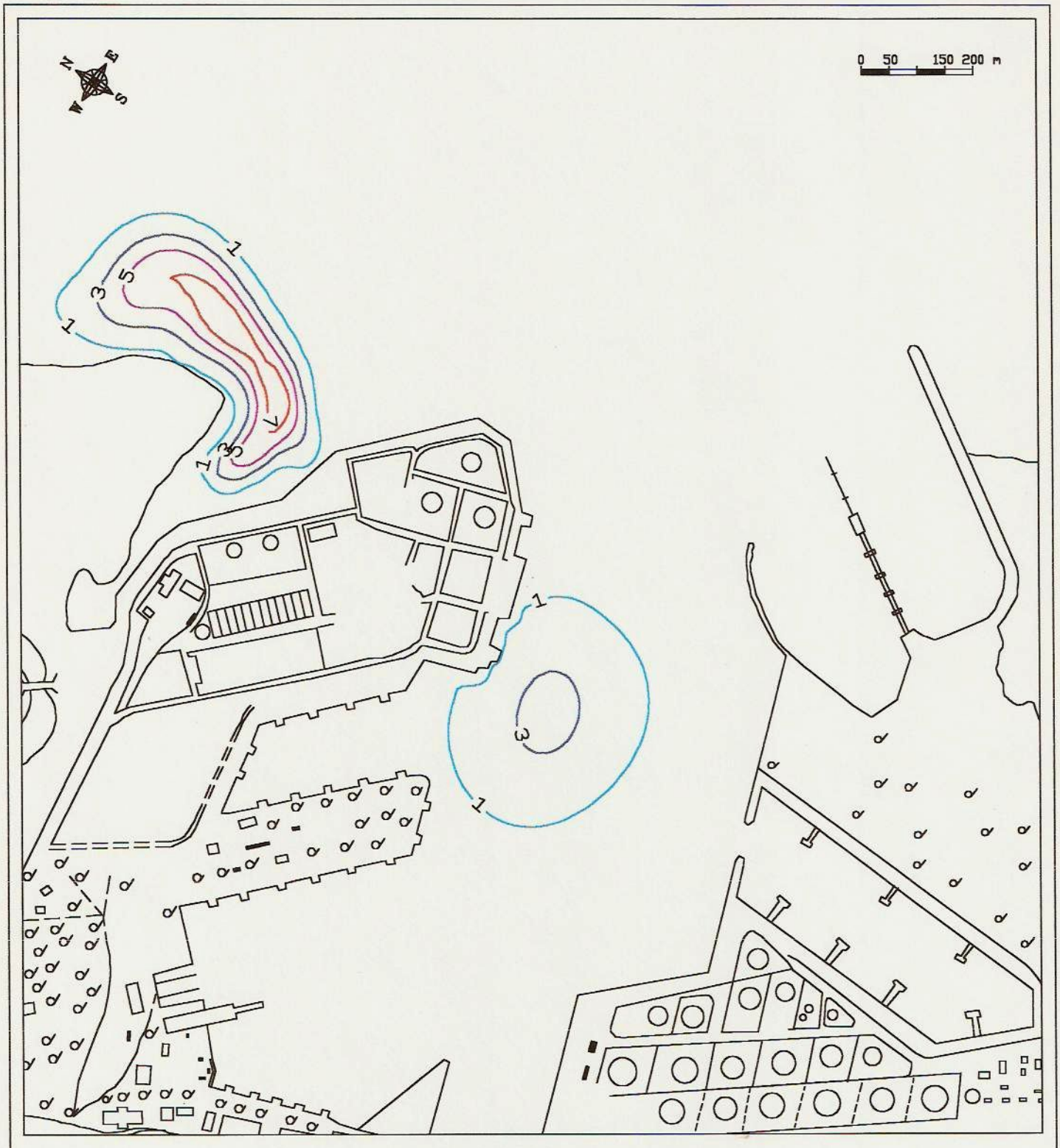

THERMAL PLUME FOR T=6.5 HOURS.
SCENARIO A. ACTUAL CONDITIONS.

FIGURE 3.34

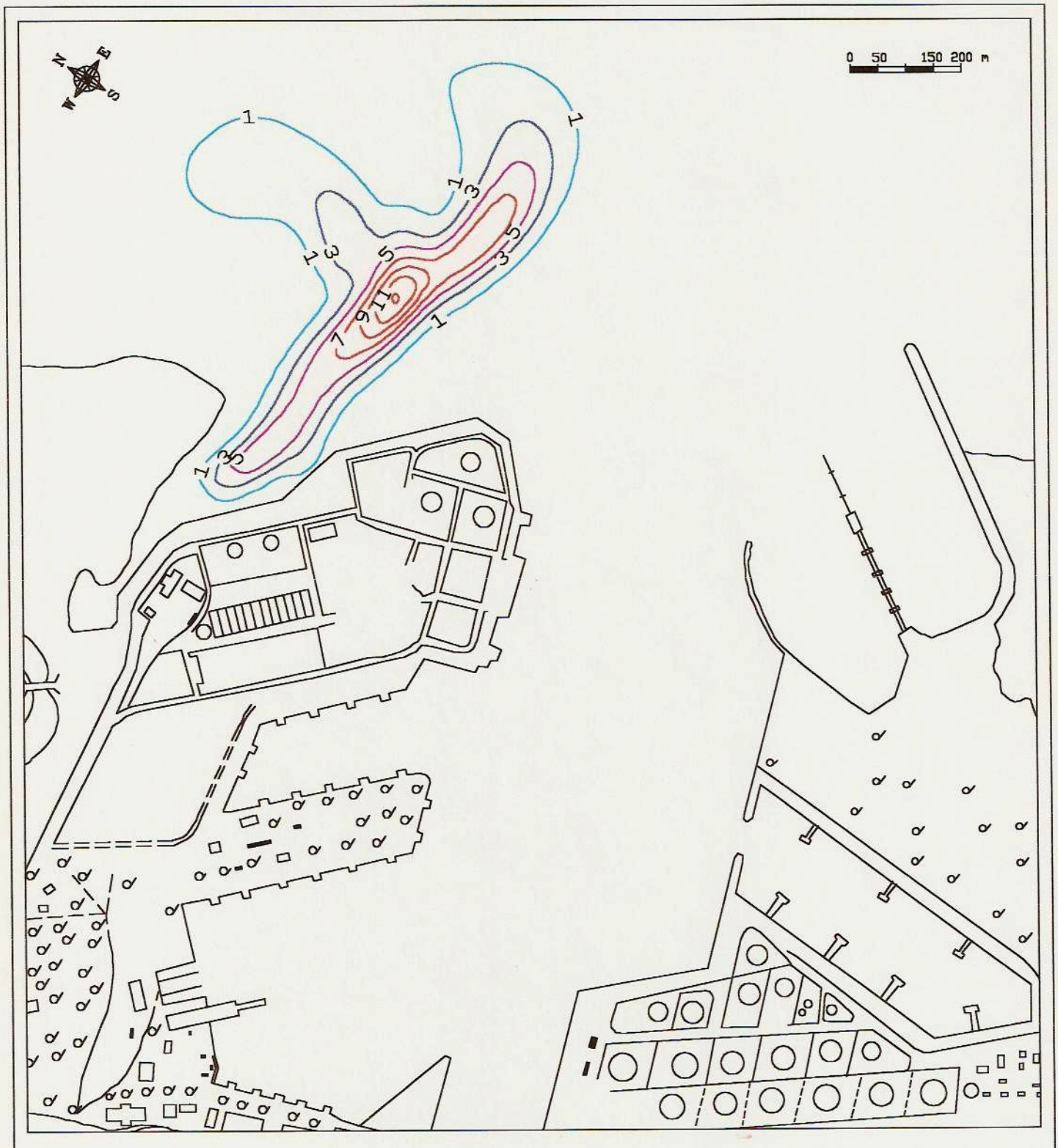

THERMAL PLUME FOR T=8 HOURS.
SCENARIO A. ACTUAL CONDITIONS.

FIGURE 3.35

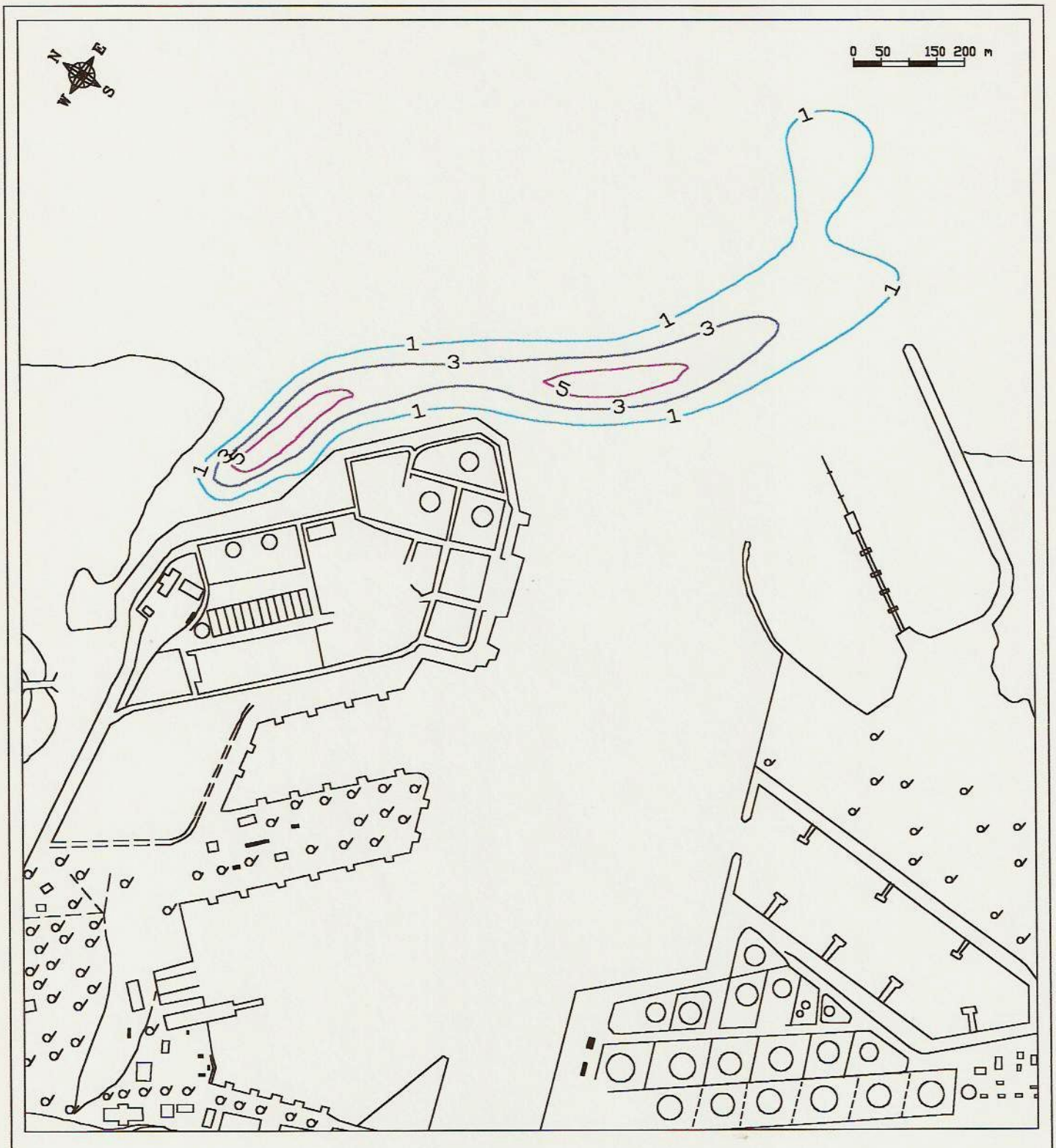

THERMAL PLUME FOR T=9.5 HOURS.
SCENARIO A. ACTUAL CONDITIONS.

FIGURE 3.36

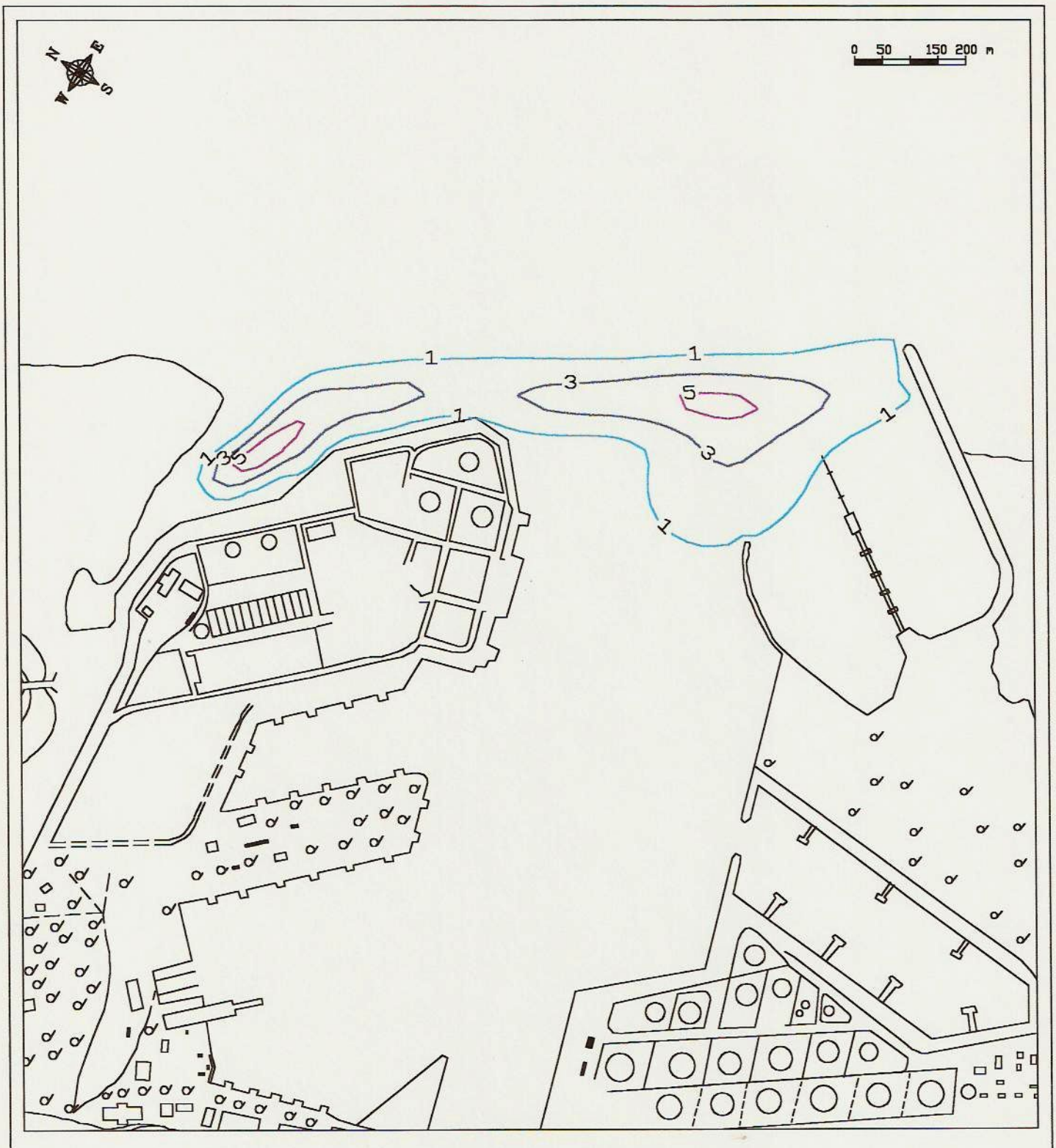

THERMAL PLUME FOR T=11 HOURS.
SCENARIO A. ACTUAL CONDITIONS.

FIGURE 3.37

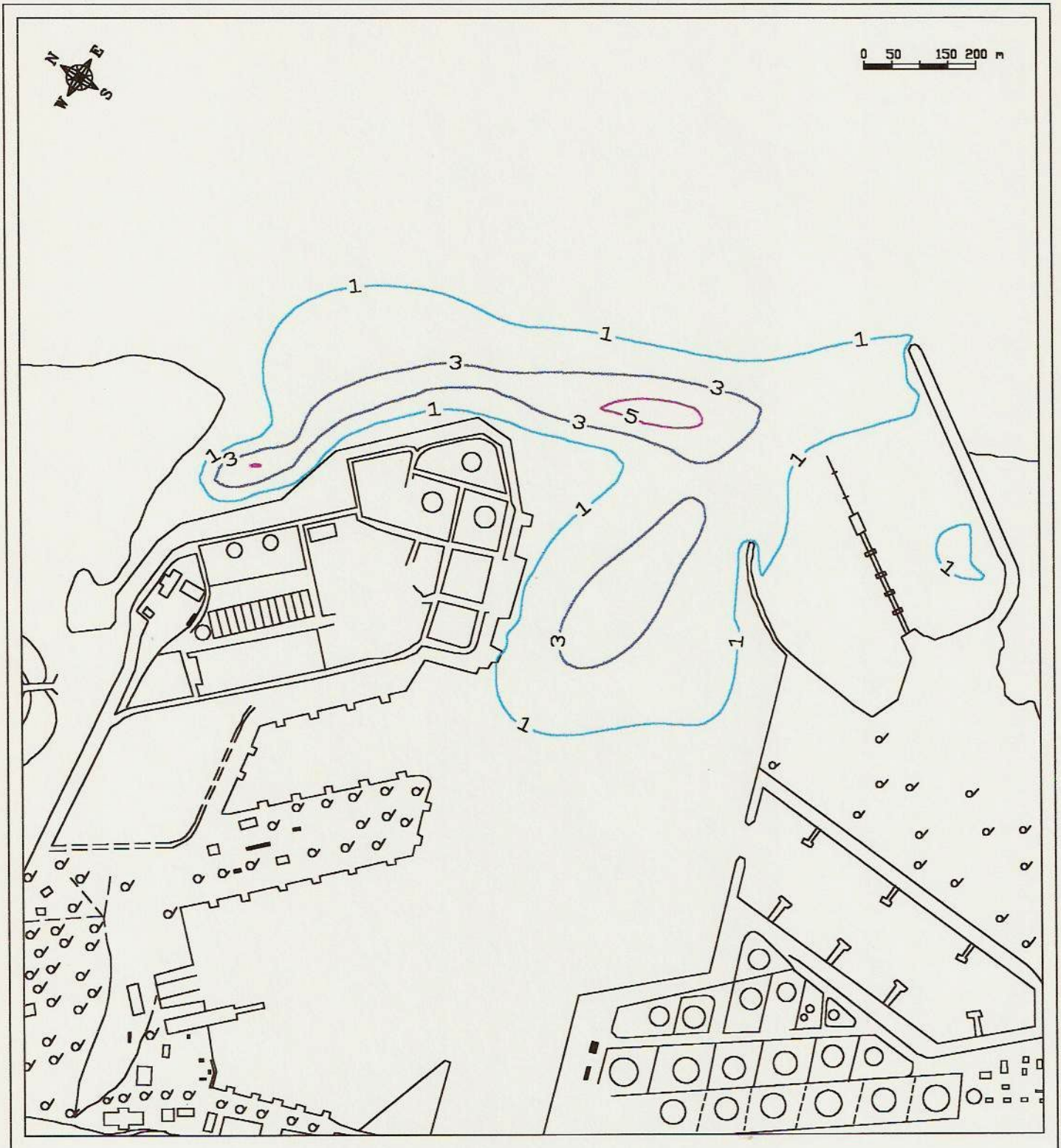

THERMAL PLUME FOR T=0.5 HOURS.
SCENARIO A. FUTURE CONDITIONS.

FIGURE 3.38

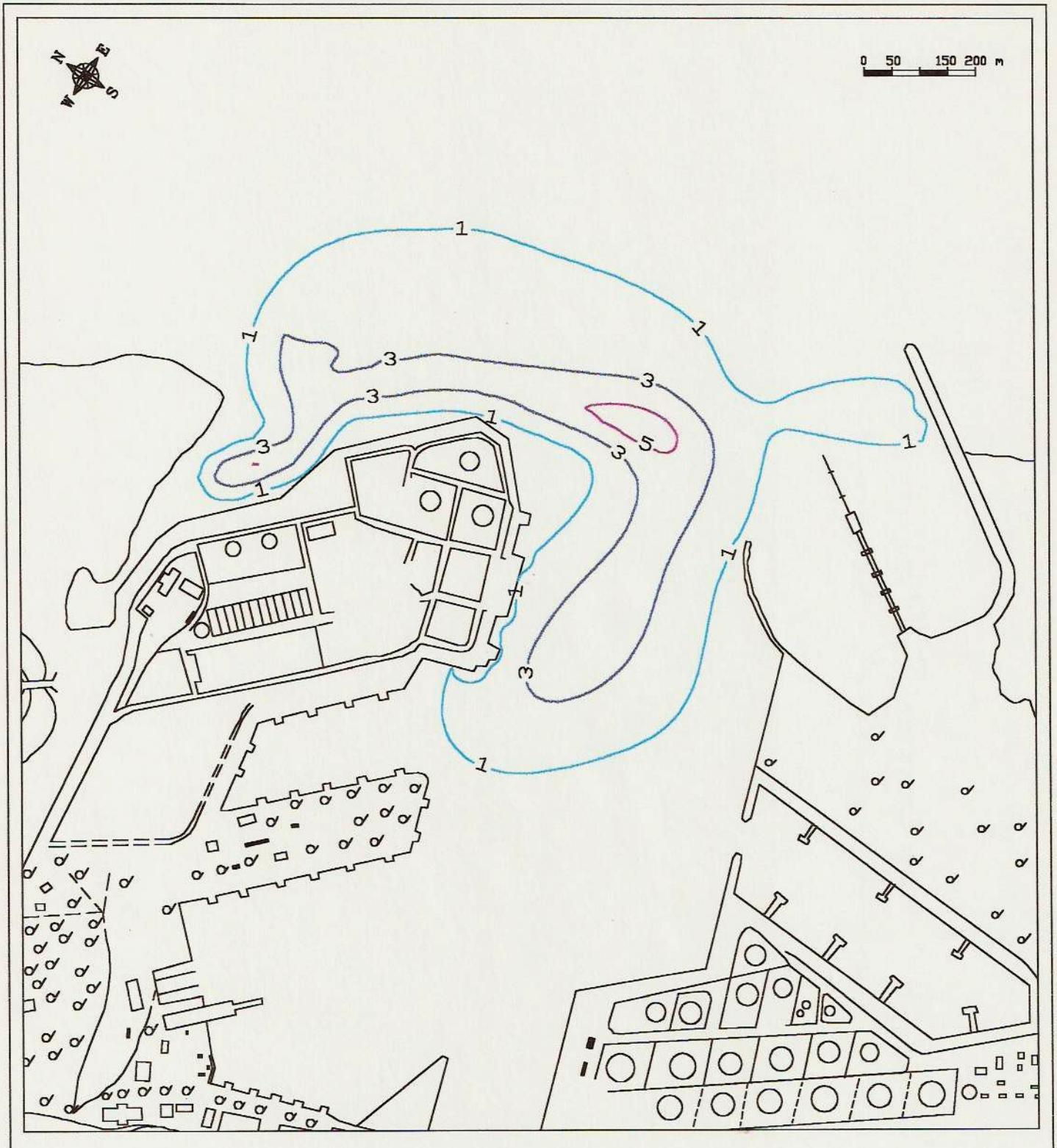

THERMAL PLUME FOR T=2 HOURS.
SCENARIO A. FUTURE CONDITIONS.

FIGURE 3.39

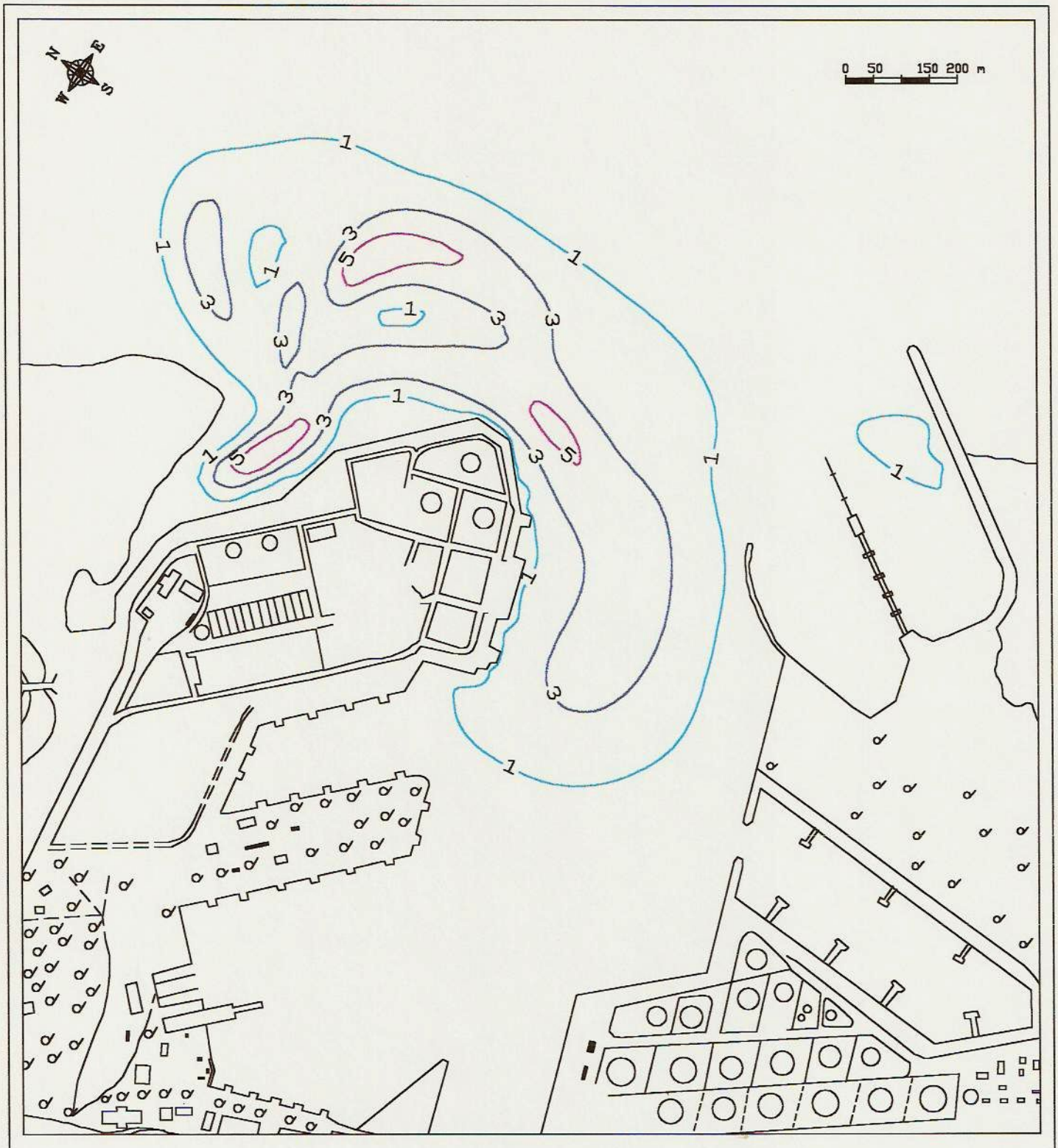

THERMAL PLUME FOR T=3 HOURS.
SCENARIO A. FUTURE CONDITIONS.

FIGURE 3.40

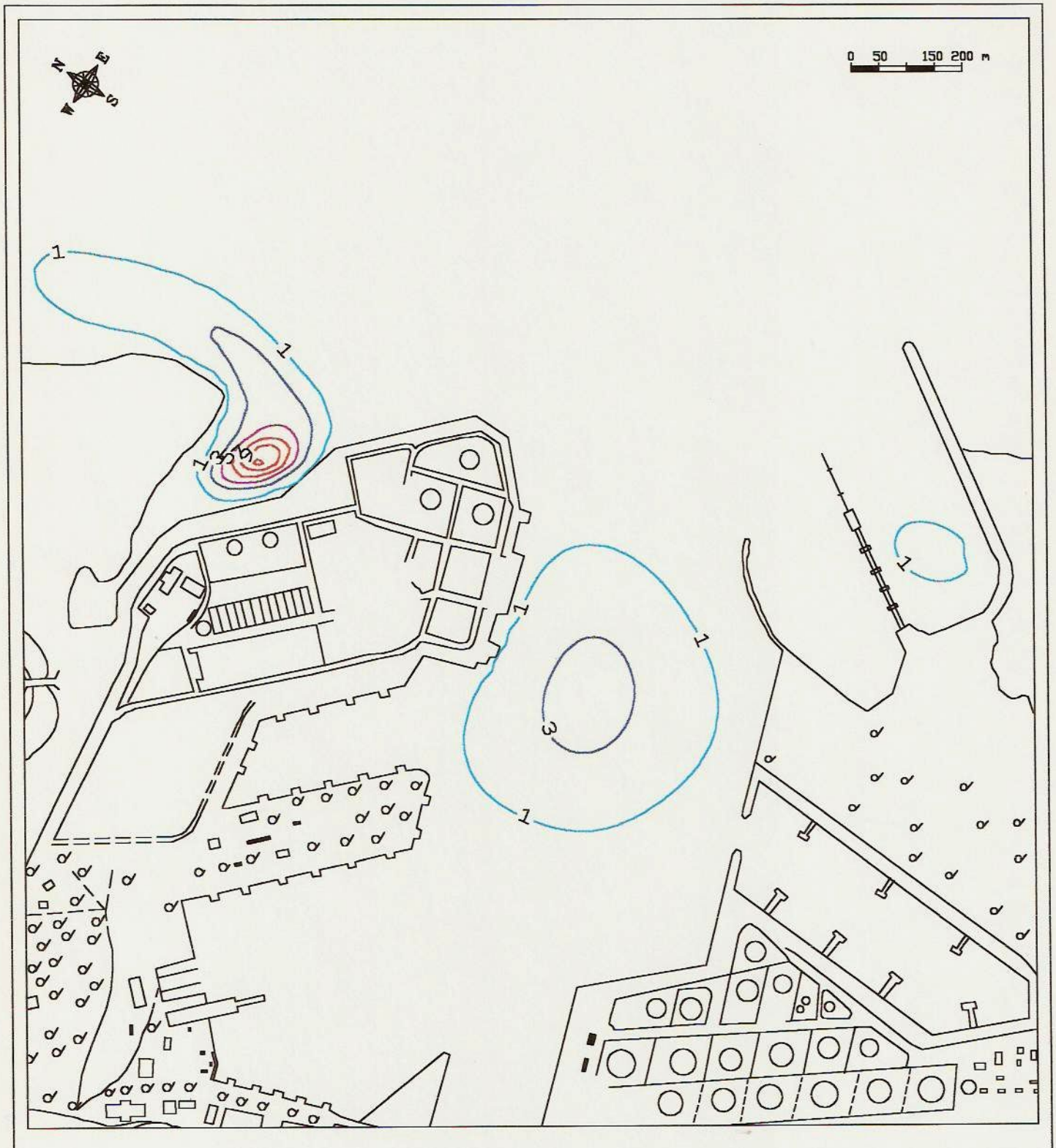

THERMAL PLUME FOR T=5 HOURS.
SCENARIO A. FUTURE CONDITIONS.

FIGURE 3.41

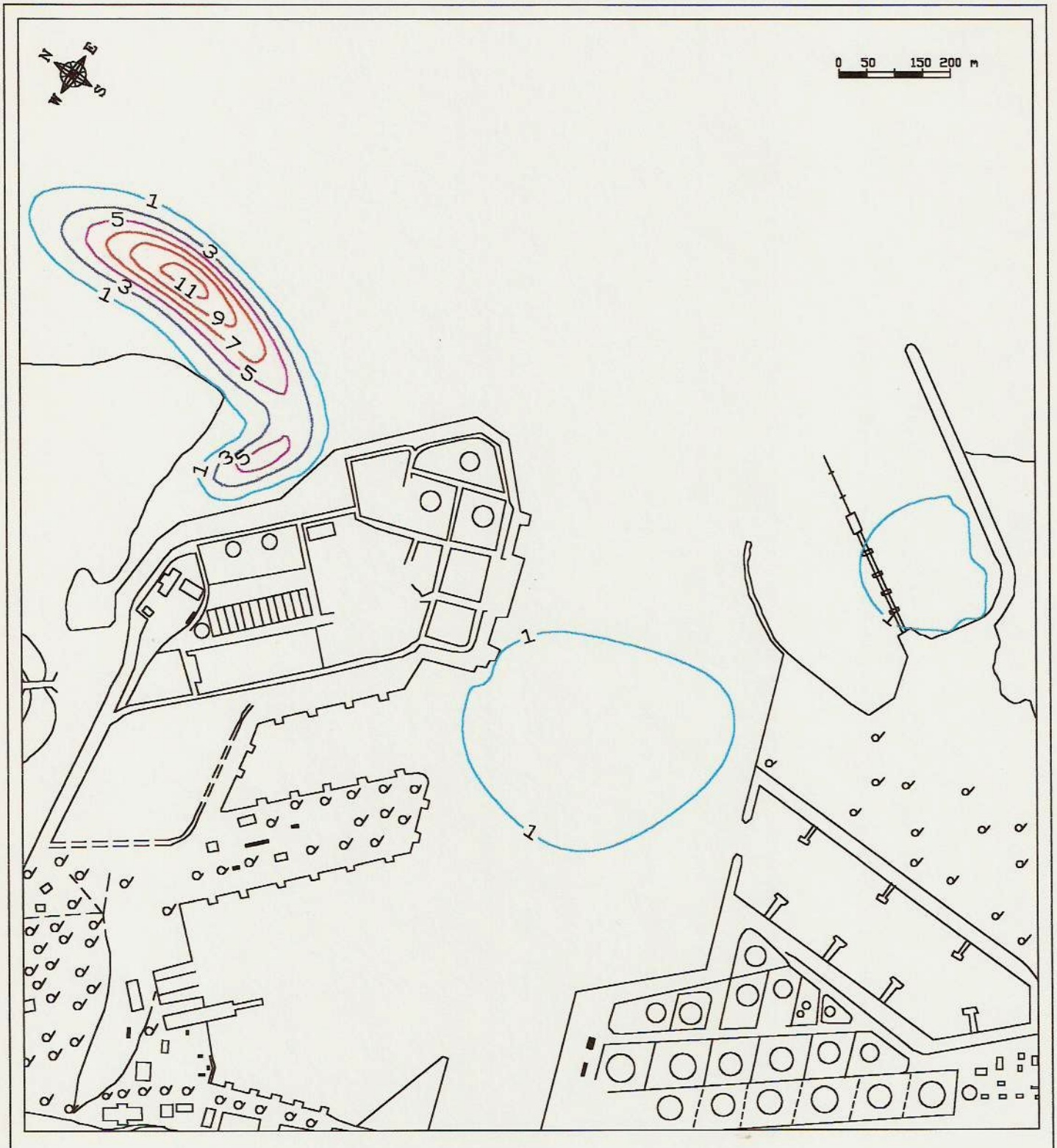

THERMAL PLUME FOR T=6.5 HOURS.
SCENARIO A. FUTURE CONDITIONS.

FIGURE 3.42

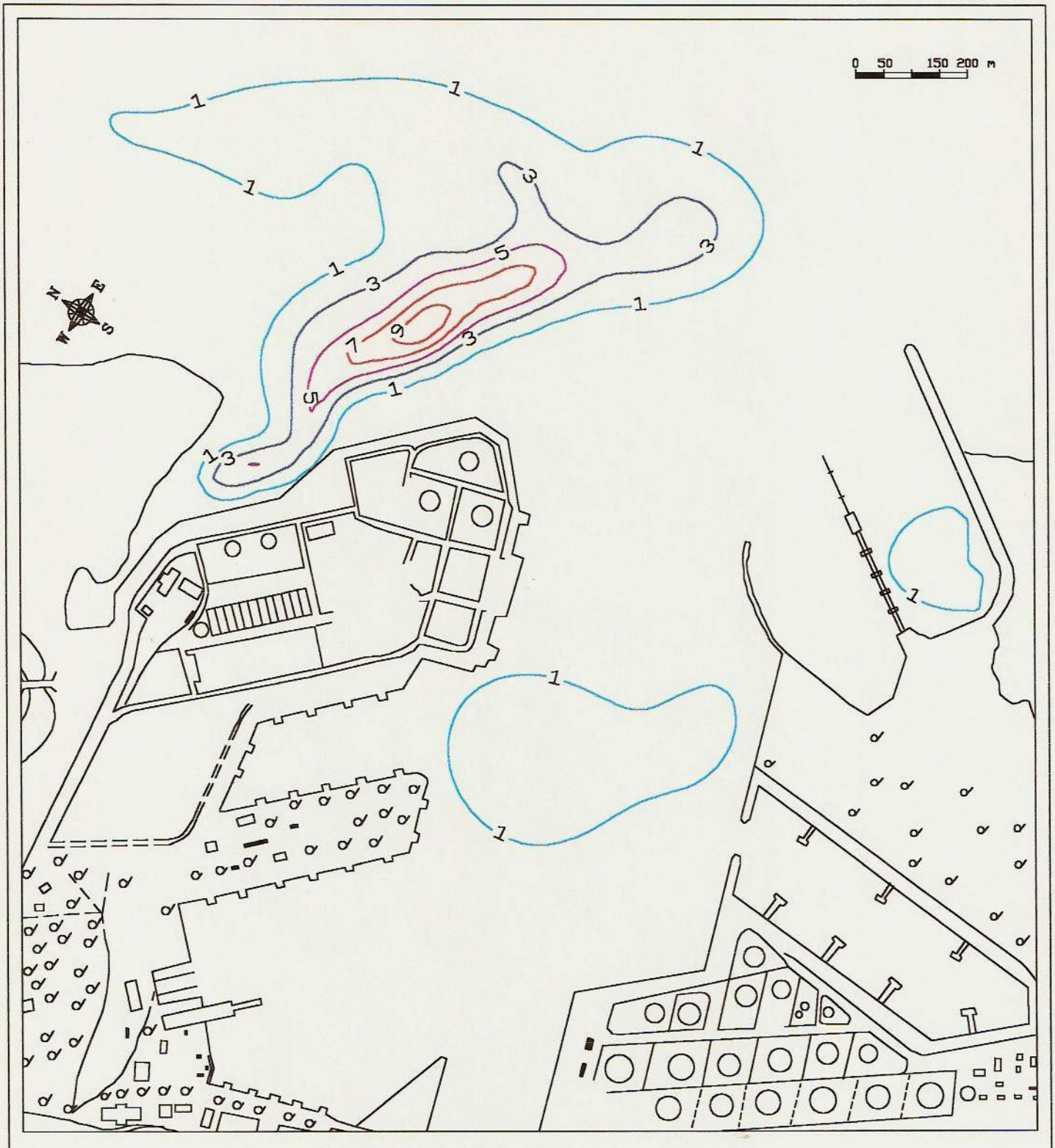

THERMAL PLUME FOR T=8 HOURS.
SCENARIO A. FUTURE CONDITIONS.

FIGURE 3.43

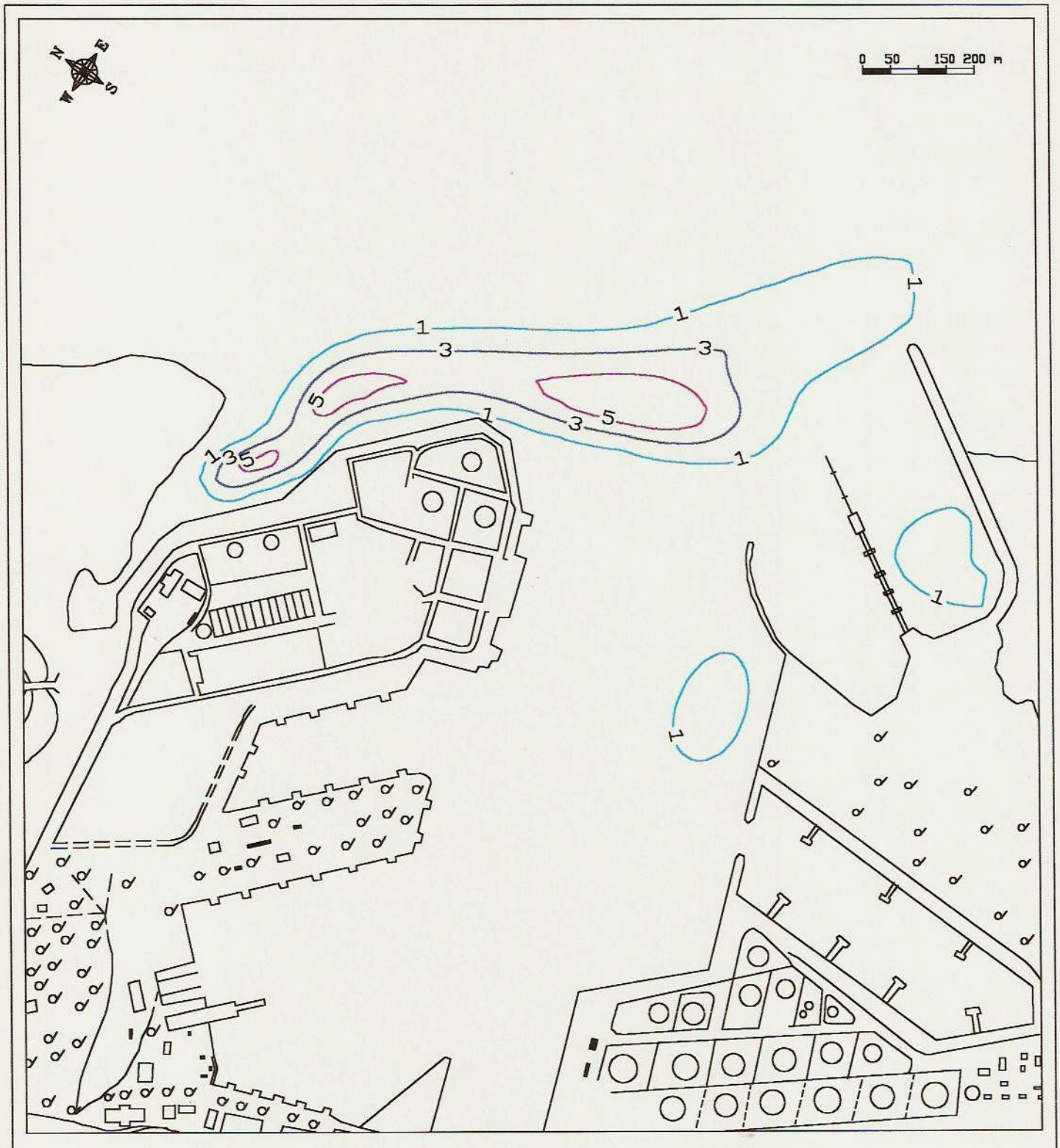

THERMAL PLUME FOR T=9.5 HOURS.
SCENARIO A. FUTURE CONDITIONS.

FIGURE 3.44

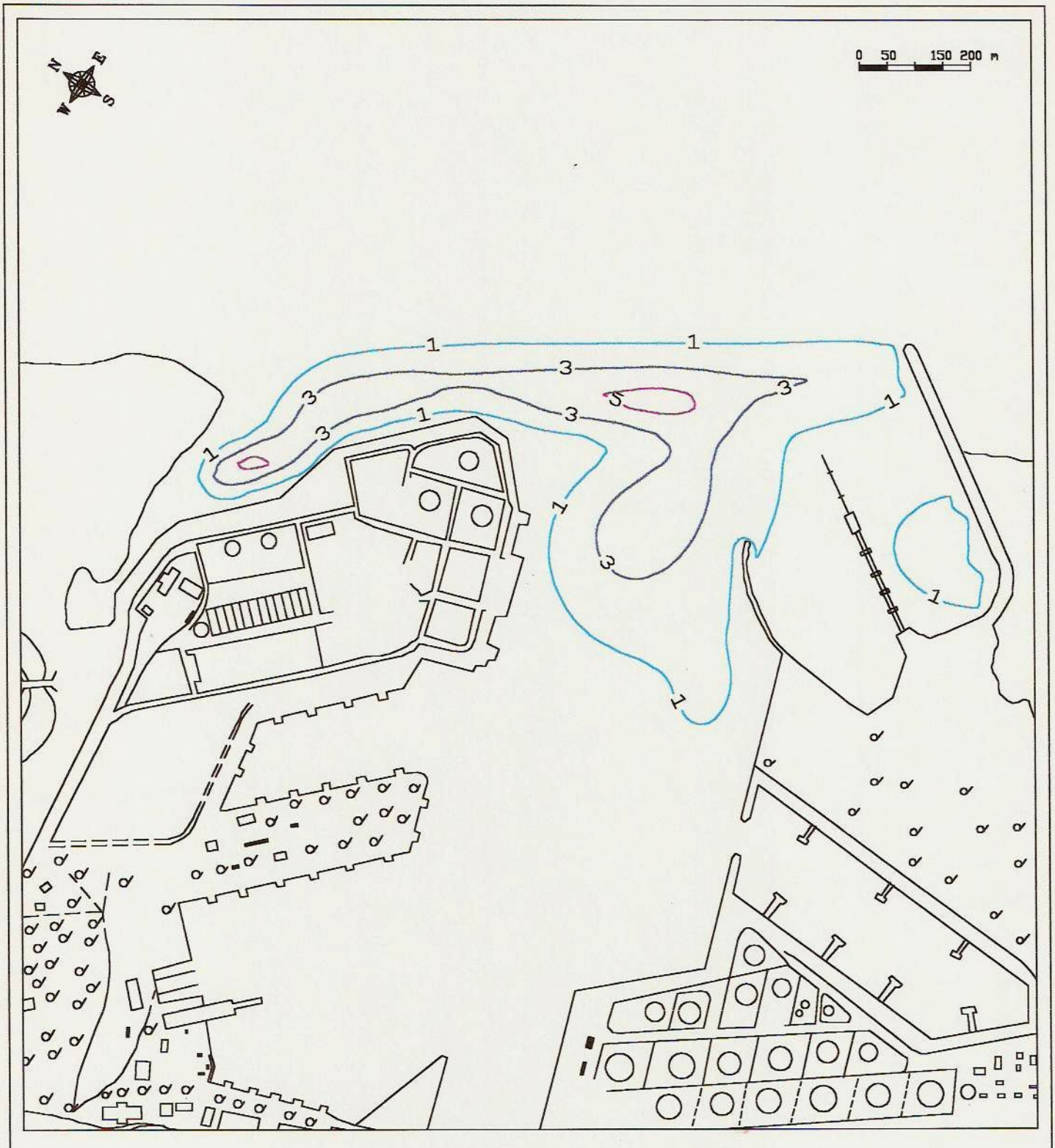

THERMAL PLUME FOR T=11 HOURS.
SCENARIO A. FUTURE CONDITIONS.

FIGURE 3.45

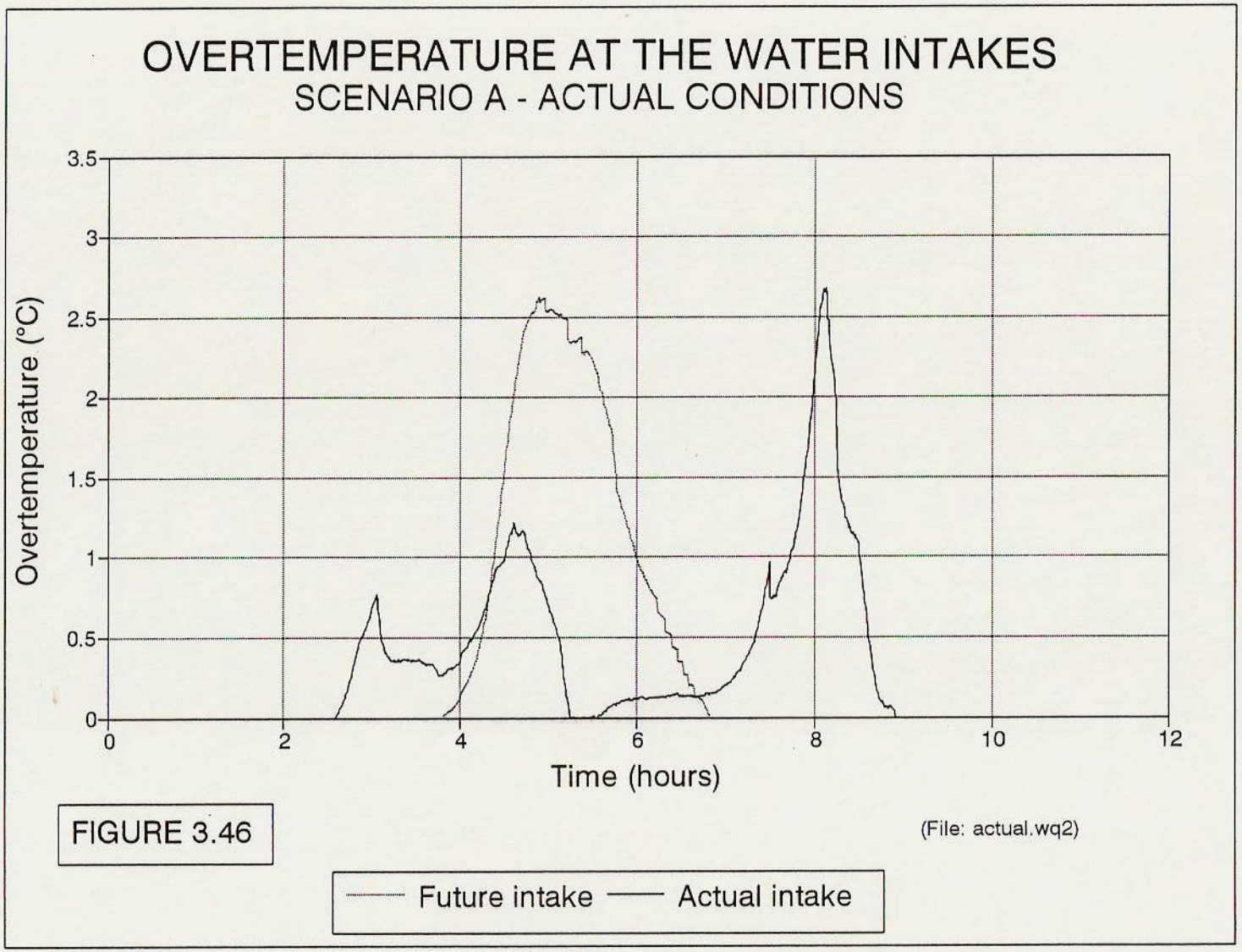
OVERTEMPERATURE AT THE WATER INTAKES
SCENARIO A - ACTUAL CONDITIONS
Overtemperature (°C)
3.5
3
2.5
2
1.5
1
0.5
0
0
2
4
6
8
10
12
Time (hours)
(File: actual.wq2)
Future intake
Actual intake

FIGURE 3.46

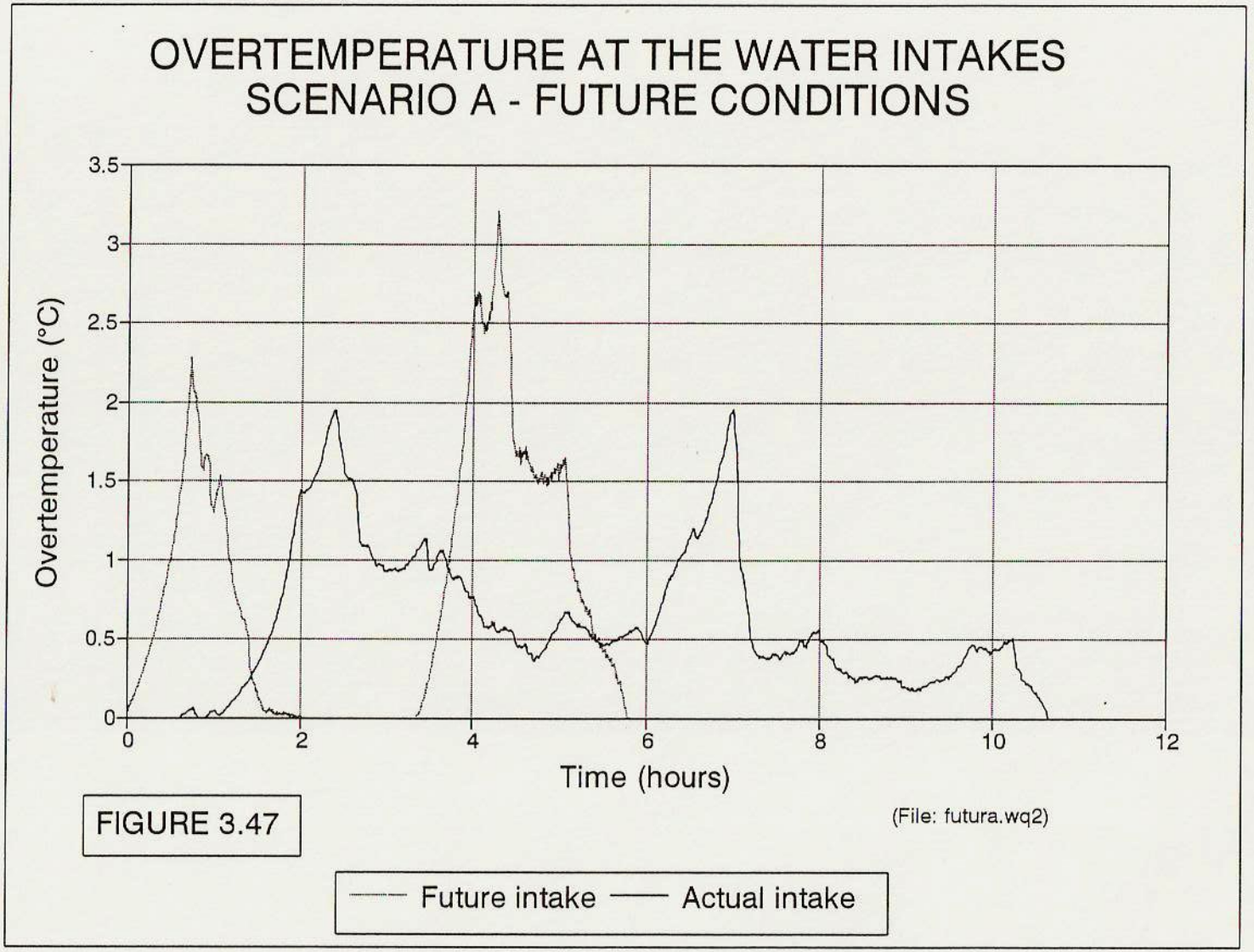
OVERTEMPERATURE AT THE WATER INTAKES
SCENARIO A - FUTURE CONDITIONS
Overtemperature (°C)
3.5
3
2.5
2
1.5
1
0.5
0
0
2
4
6
8
10
12
Time (hours)
(File: futura.wq2)
Future intake
Actual intake

FIGURE 3.47

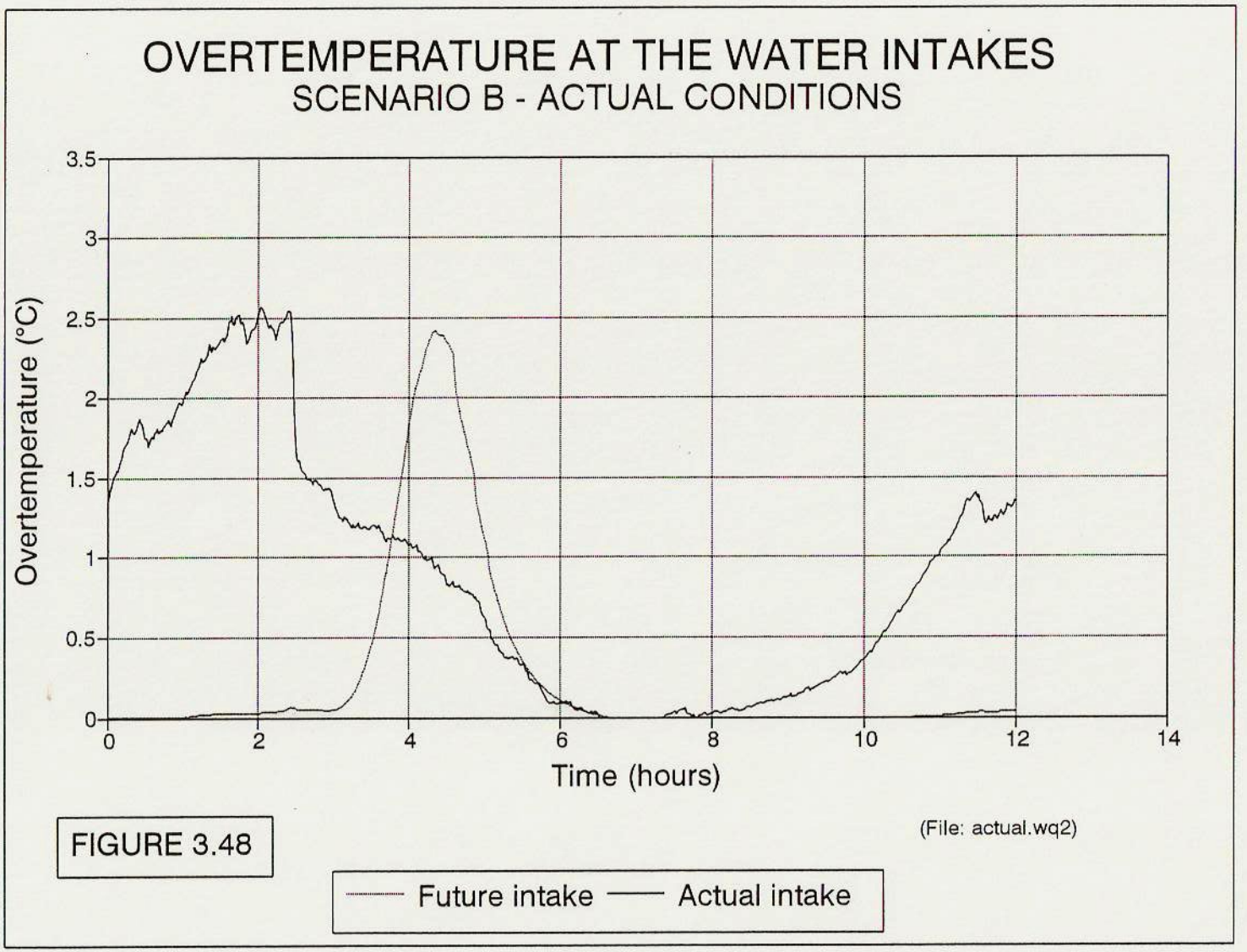
OVERTEMPERATURE AT THE WATER INTAKES
SCENARIO B - ACTUAL CONDITIONS
Overtemperature (°C)
3.5
3
2.5
2
1.5
1
0.5
0
0
2
4
6
8
10
12
14
Time (hours)
(File: actual.wq2)
Future intake
Actual intake

FIGURE 3.48

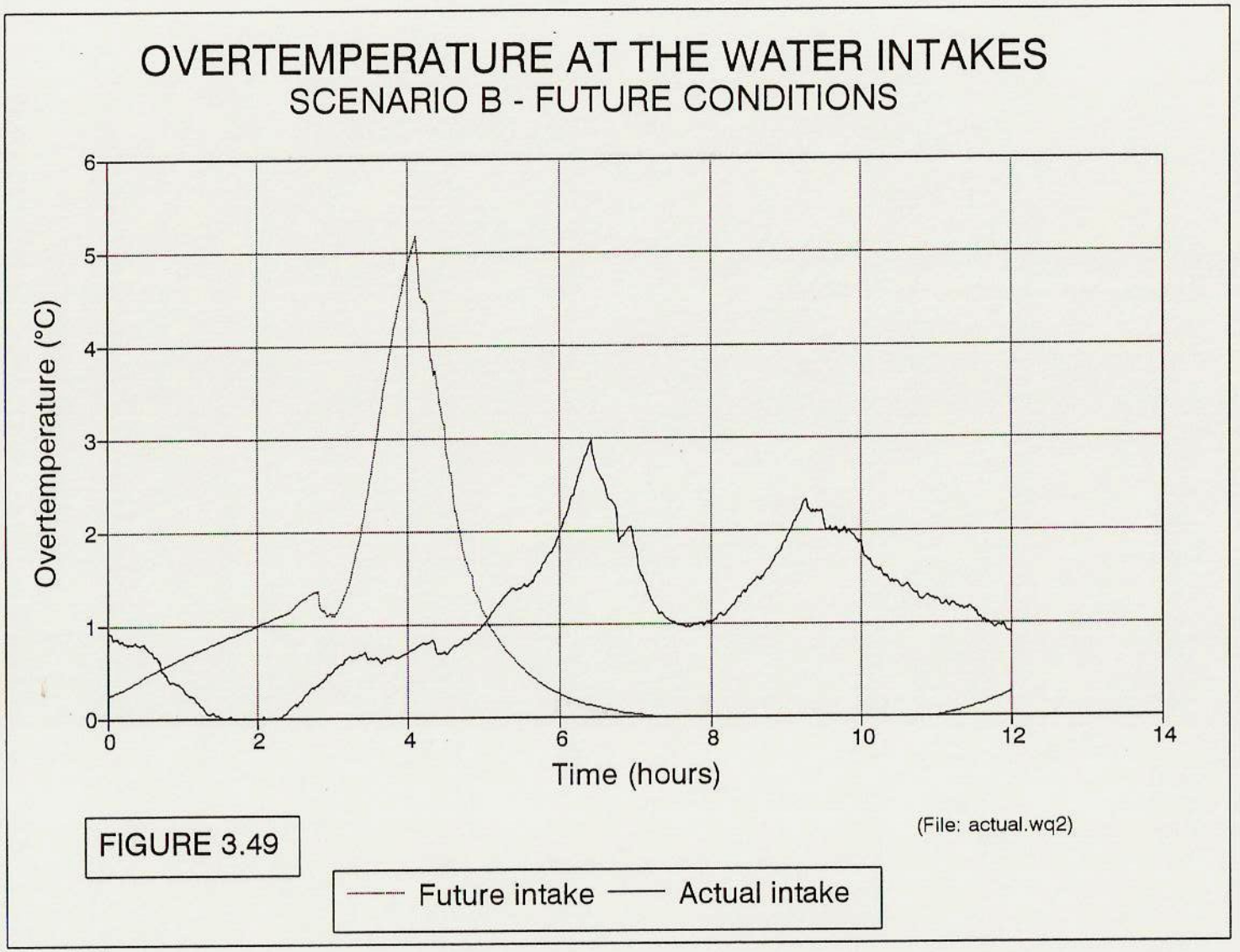
OVERTEMPERATURE AT THE WATER INTAKES
SCENARIO B - FUTURE CONDITIONS
Overtemperature (°C)
0
1
2
3
4
5
6
0
2
4
6
8
10
12
14
Time (hours)
(File: actual.wq2)
Future intake
Actual intake

FIGURE 3.49

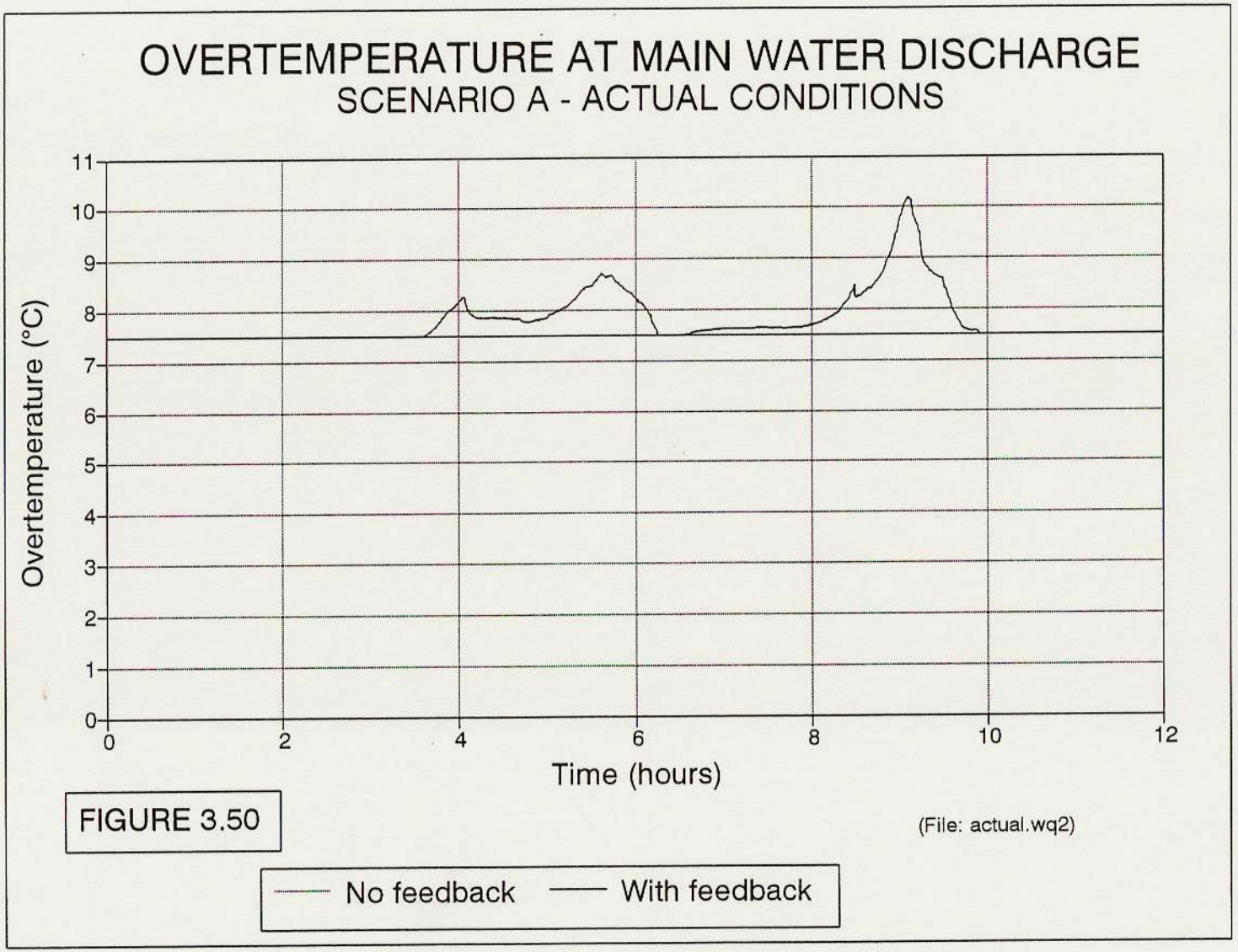
OVERTEMPERATURE AT MAIN WATER DISCHARGE
SCENARIO A - ACTUAL CONDITIONS
Overtemperature (°C)
0
1
2
3
4
5
6
7
8
9
10
11
0
2
4
6
8
10
12
Time (hours)
FIGURE 3.50
(File: actual.wq2)
No feedback
With feedback

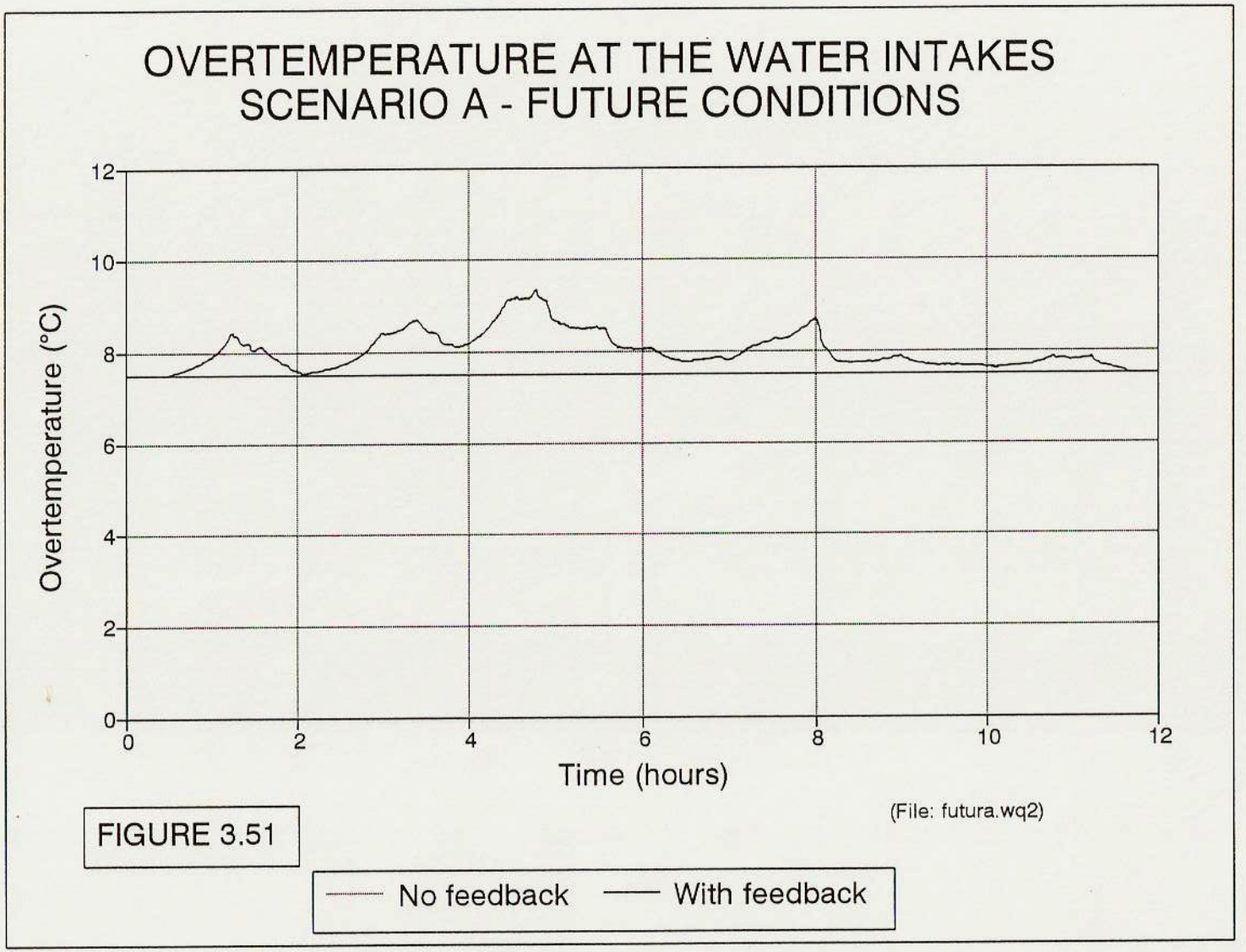
OVERTEMPERATURE AT THE WATER INTAKES
SCENARIO A - FUTURE CONDITIONS
Overtemperature (°C)
0
2
4
6
8
10
12
Time (hours)
(File: futura.wq2)
No feedback
With feedback

FIGURE 3.51

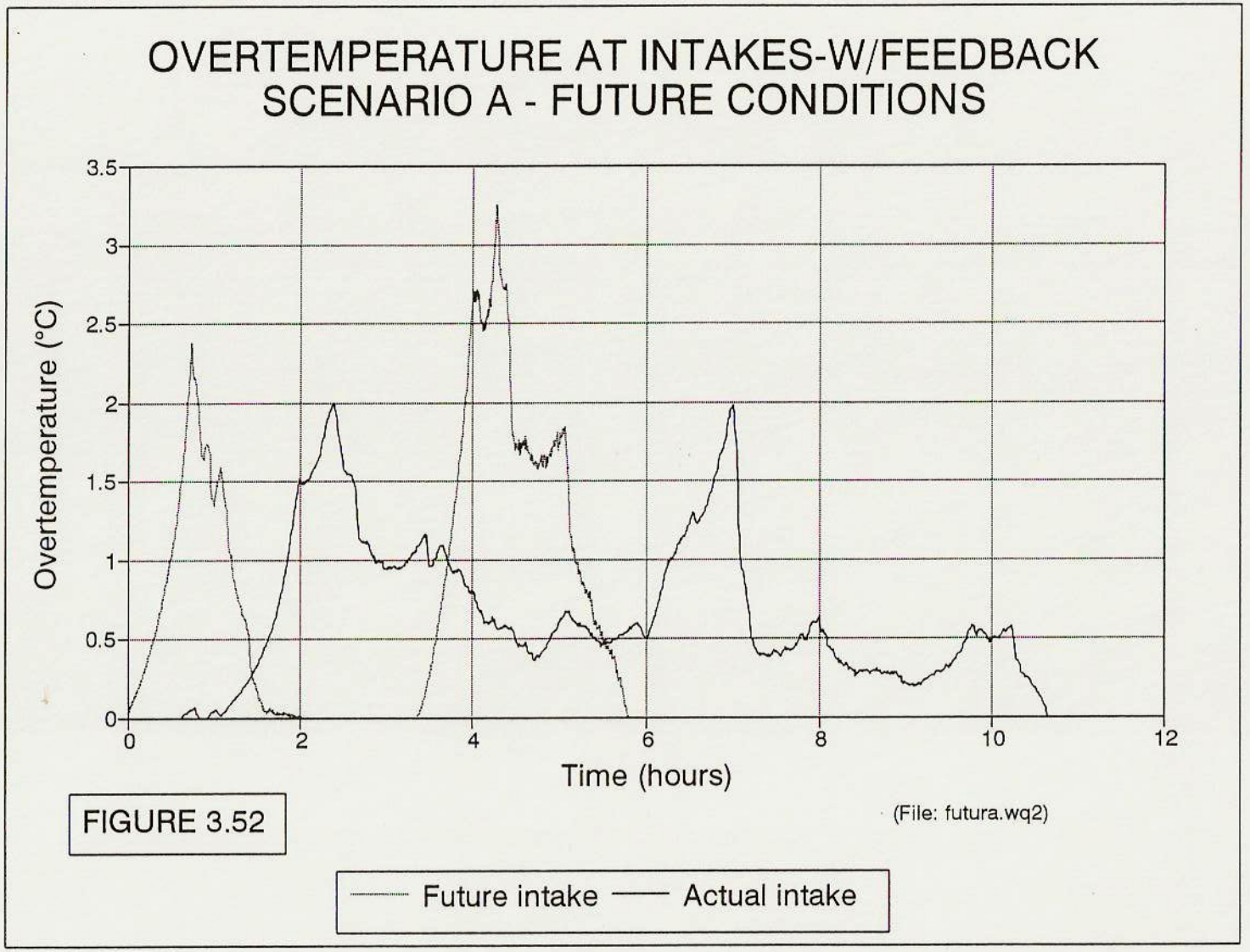
OVERTEMPERATURE AT INTAKES-W/FEEDBACK
SCENARIO A - FUTURE CONDITIONS
Overtemperature (°C)
3.5
3
2.5
2
1.5
1
0.5
0
0
2
4
6
8
10
12
Time (hours)
(File: futura.wq2)
Future intake
Actual intake

FIGURE 3.52

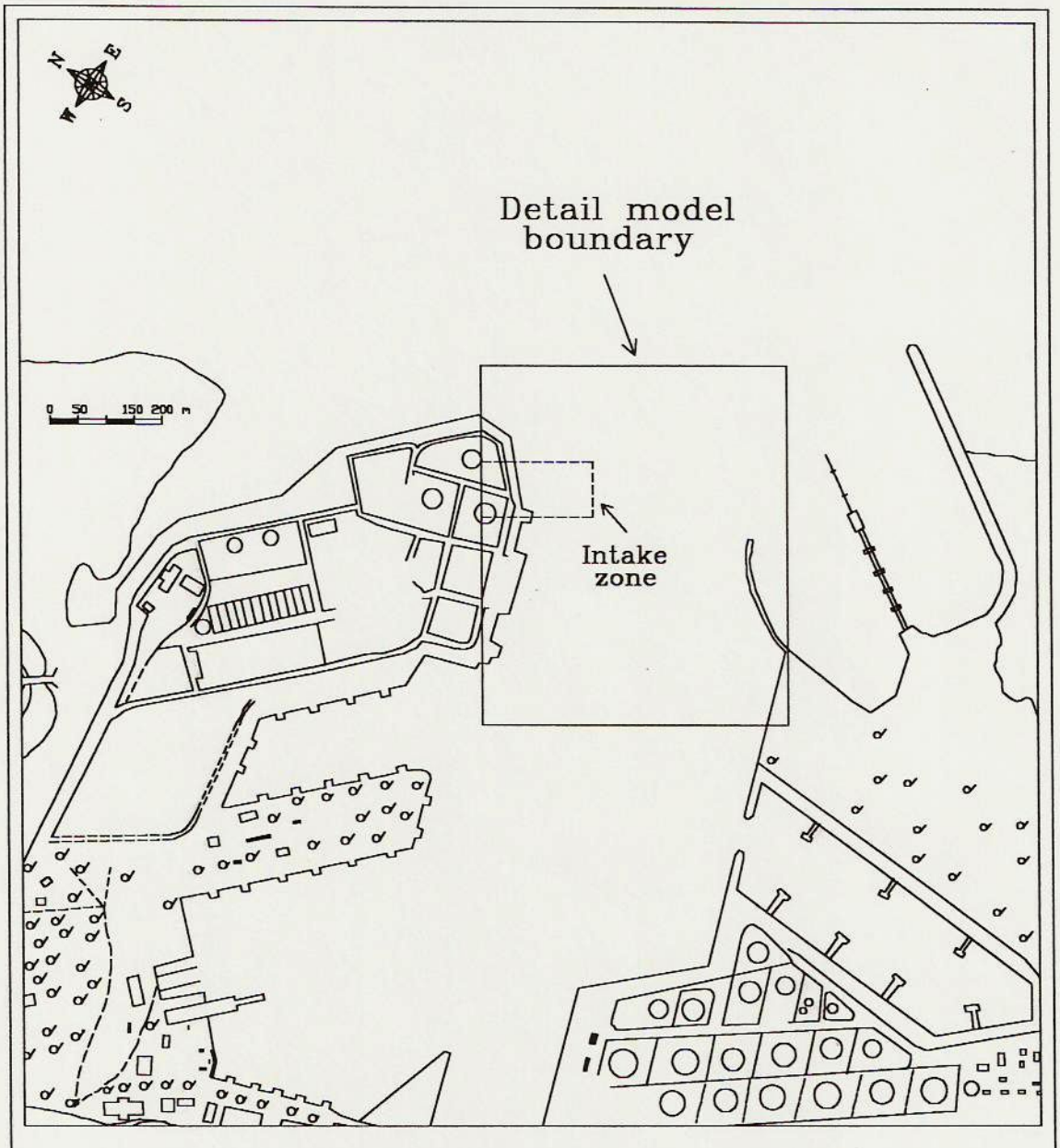

ZONE OF THE DETAIL MODEL | FIGURE 4.1

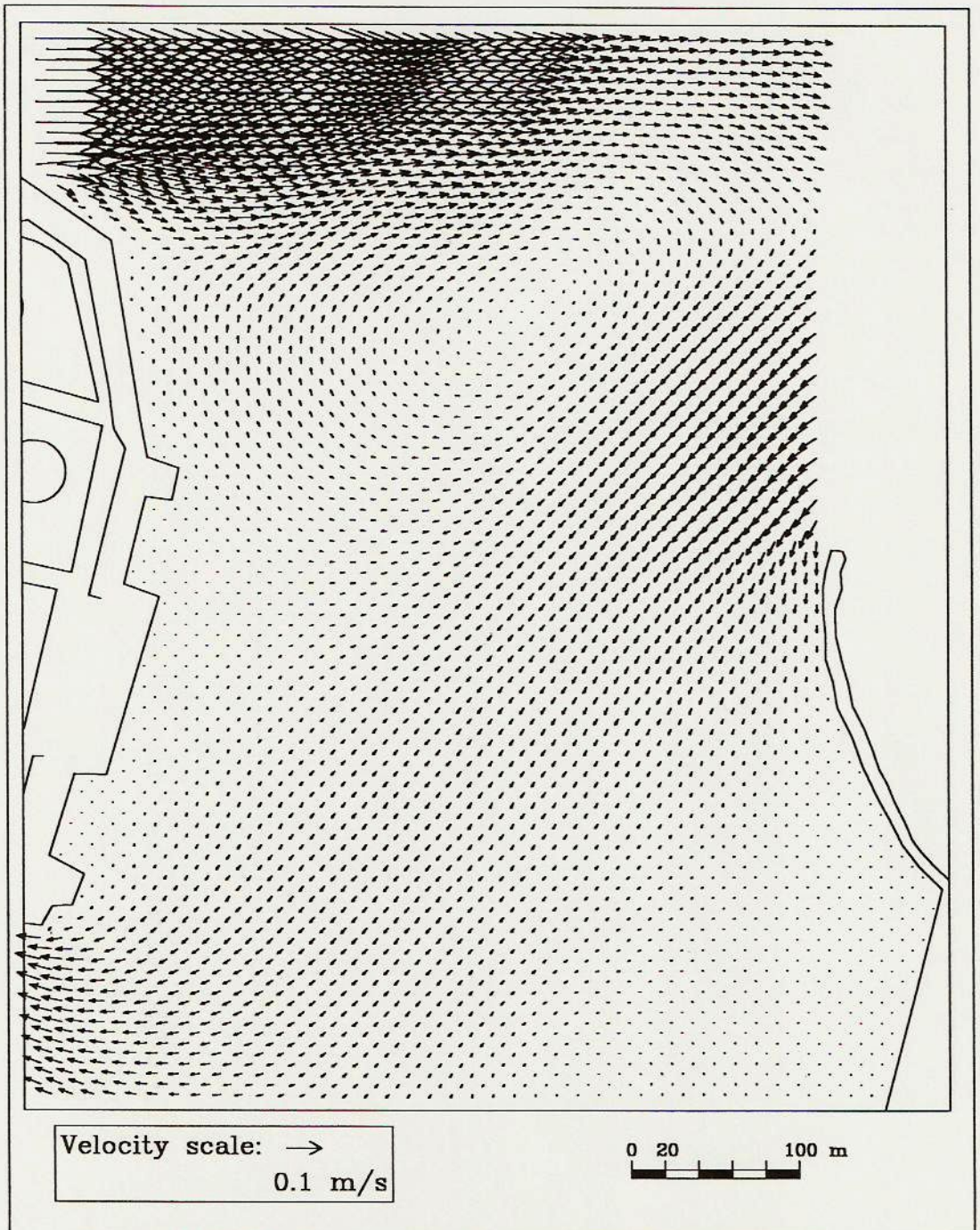

VELOCITY FIELD FOR THE DETAIL MODEL. SCENARIO A. T=0 AND T=12 HOURS. ACTUAL CONDITIONS.

FIGURE 4.2

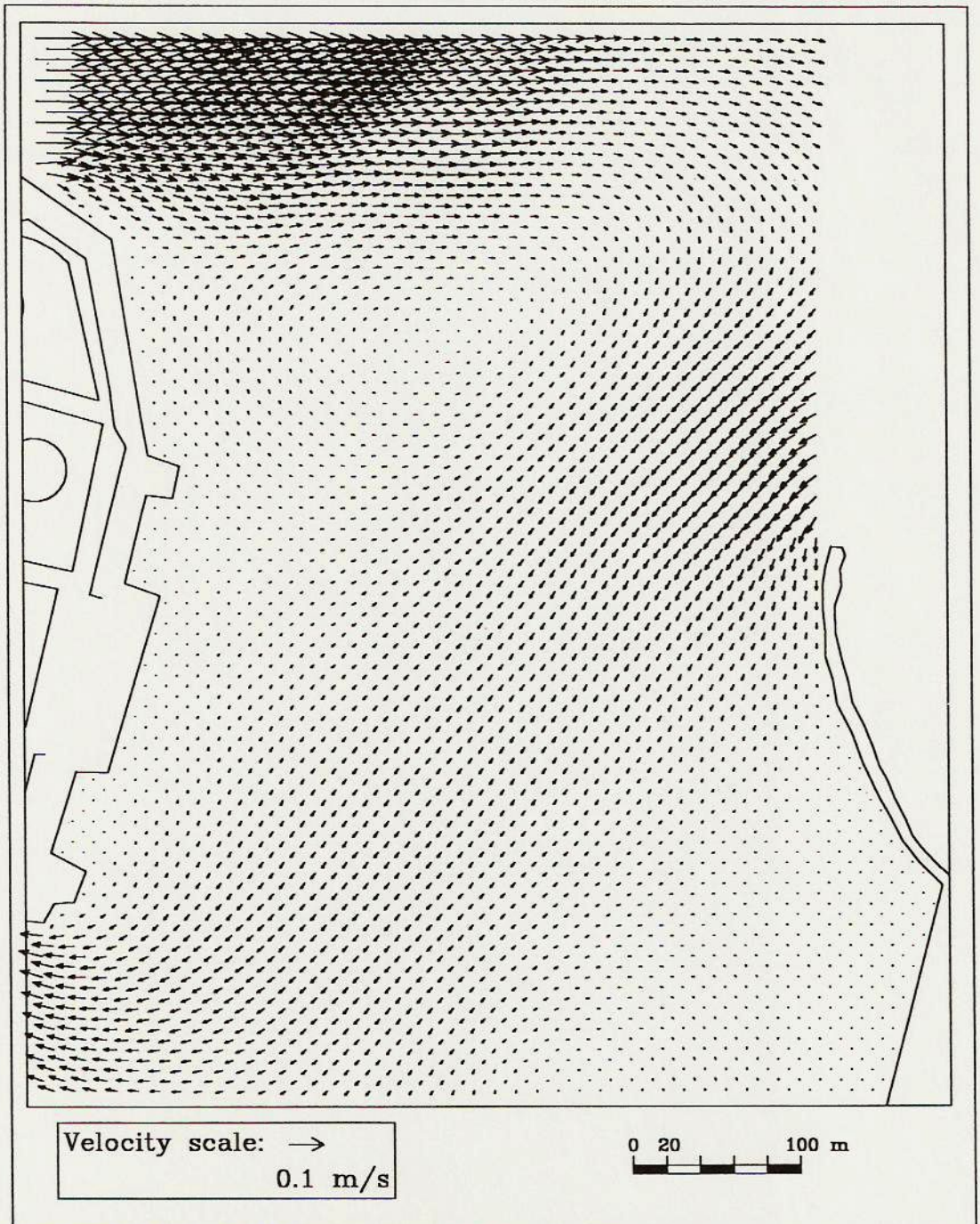

VELOCITY FIELD FOR THE DETAIL MODEL. SCENARIO A. T=1.7 AND T=8.9 HOURS. ACTUAL CONDITIONS.

FIGURE 4.3

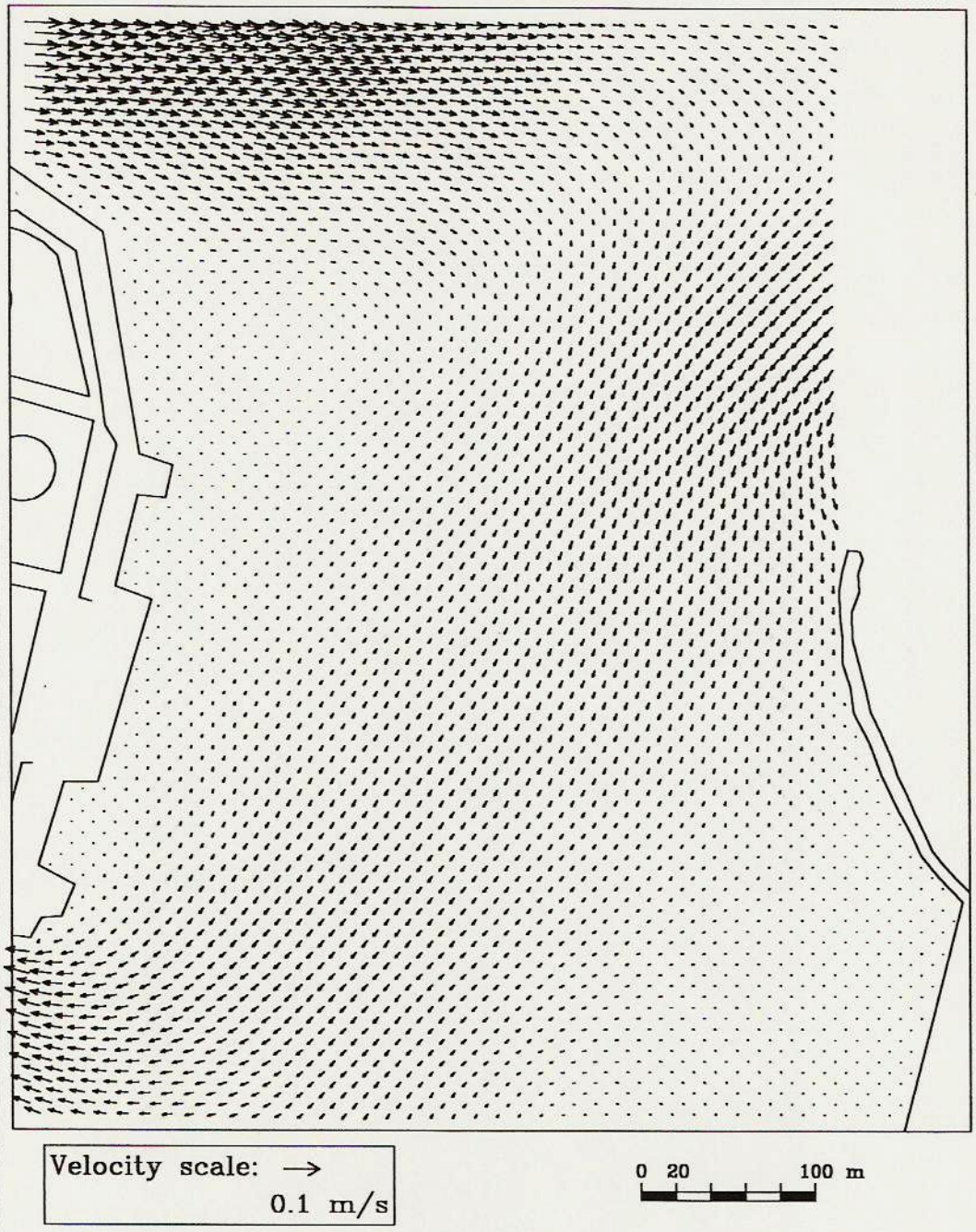

VELOCITY FIELD FOR THE DETAIL MODEL. SCENARIO A. T=2.3 AND T=8.2 HOURS. ACTUAL CONDITIONS.

FIGURE 4.4

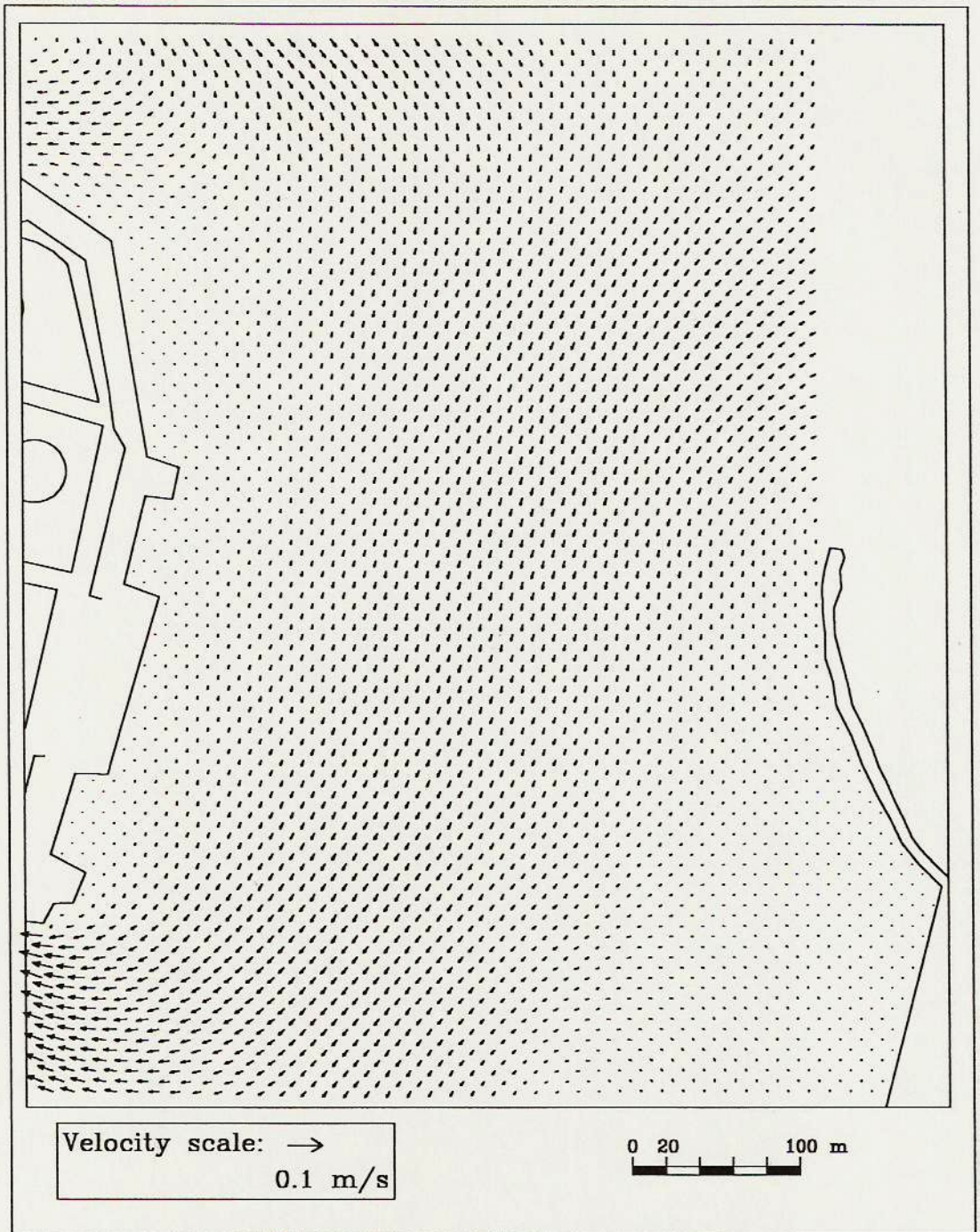

VELOCITY FIELD FOR THE DETAIL MODEL. SCENARIO A. T=2.7 AND T=7.7 HOURS. ACTUAL CONDITIONS.

FIGURE 4.5

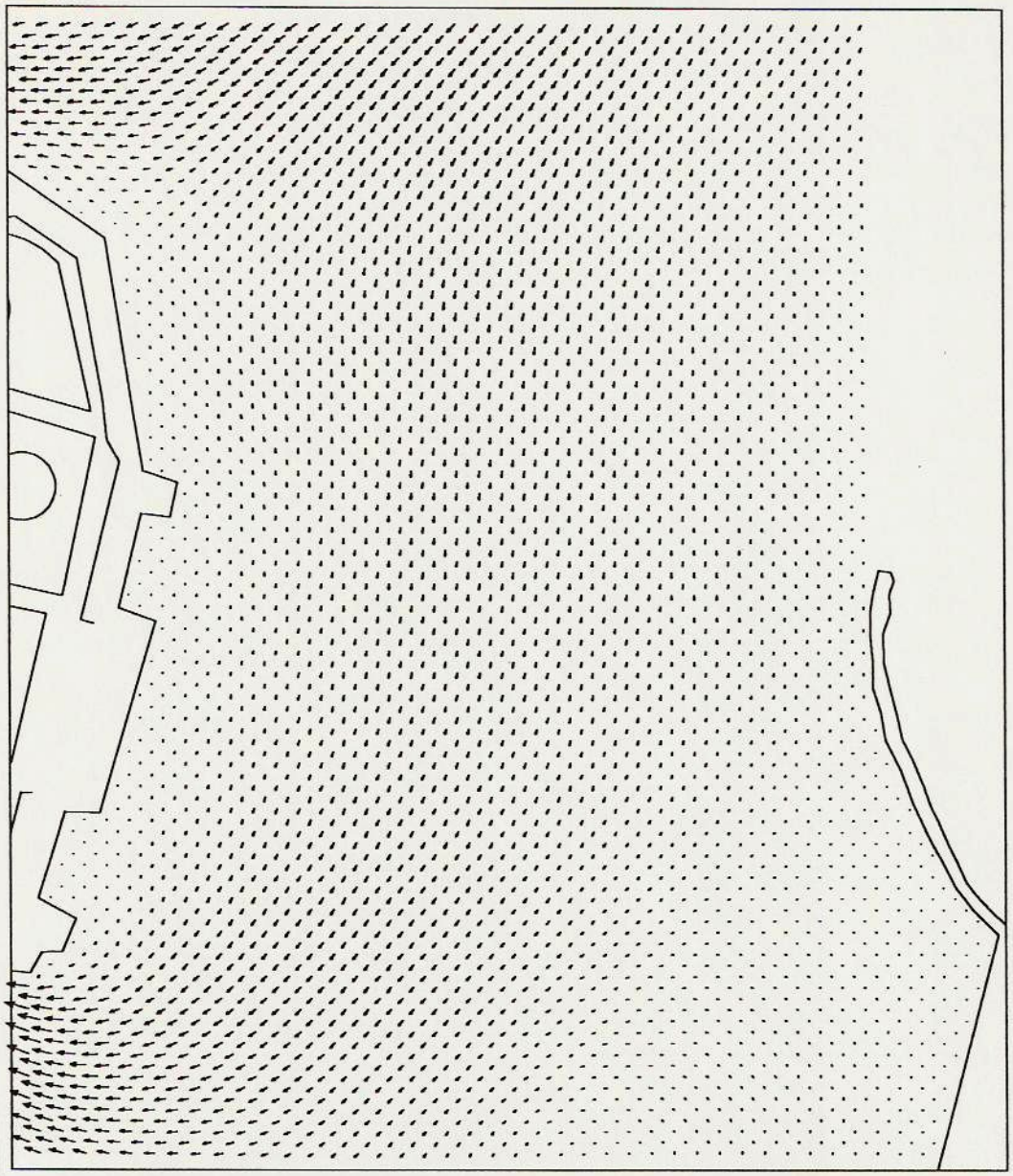

VELOCITY FIELD FOR THE DETAIL MODEL. SCENARIO A. T=3.3 AND T=7 HOURS. ACTUAL CONDITIONS.

FIGURE 4.6

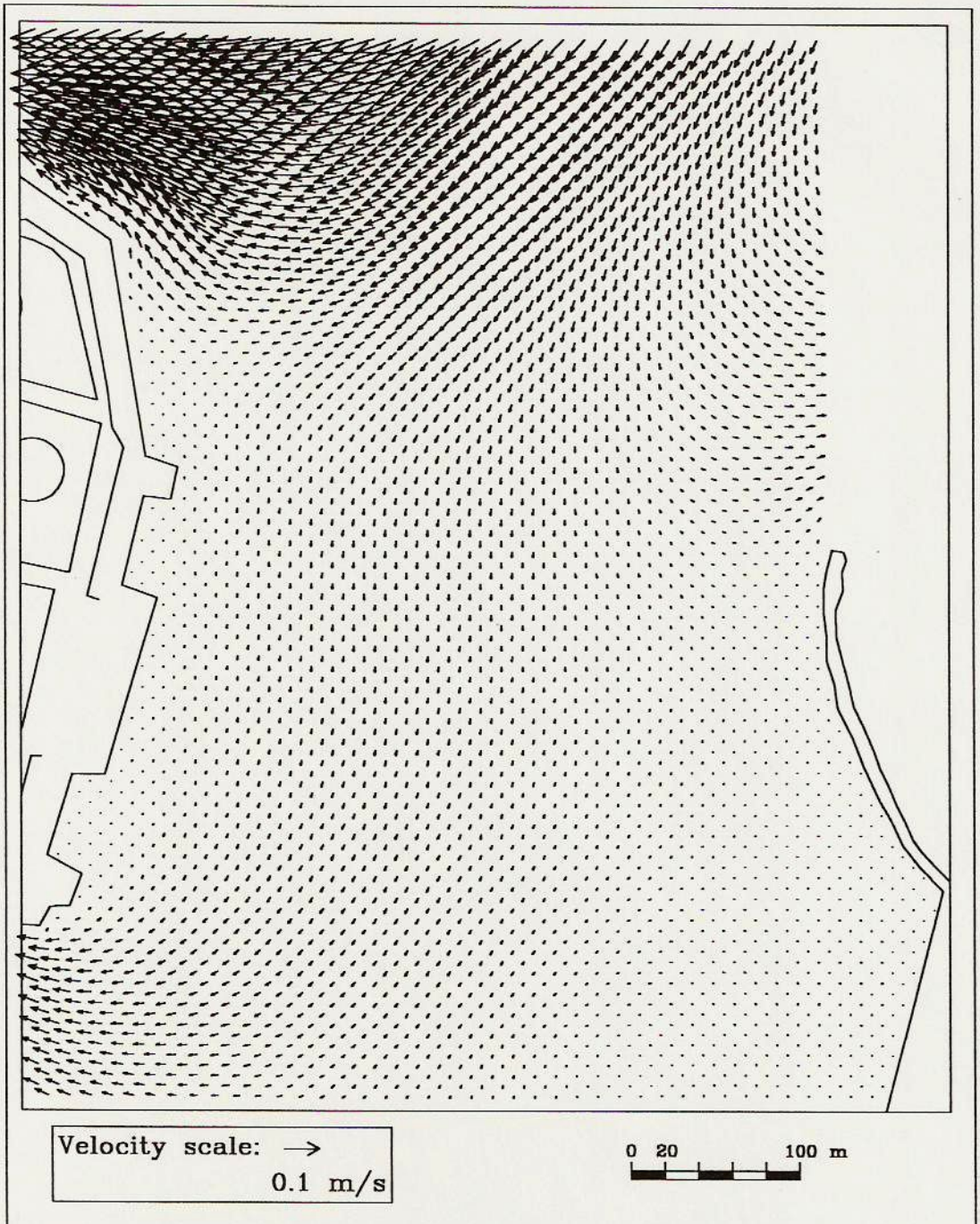

VELOCITY FIELD FOR THE DETAIL MODEL. SCENARIO A. T=5 HOURS. ACTUAL CONDITIONS.

FIGURE 4.7

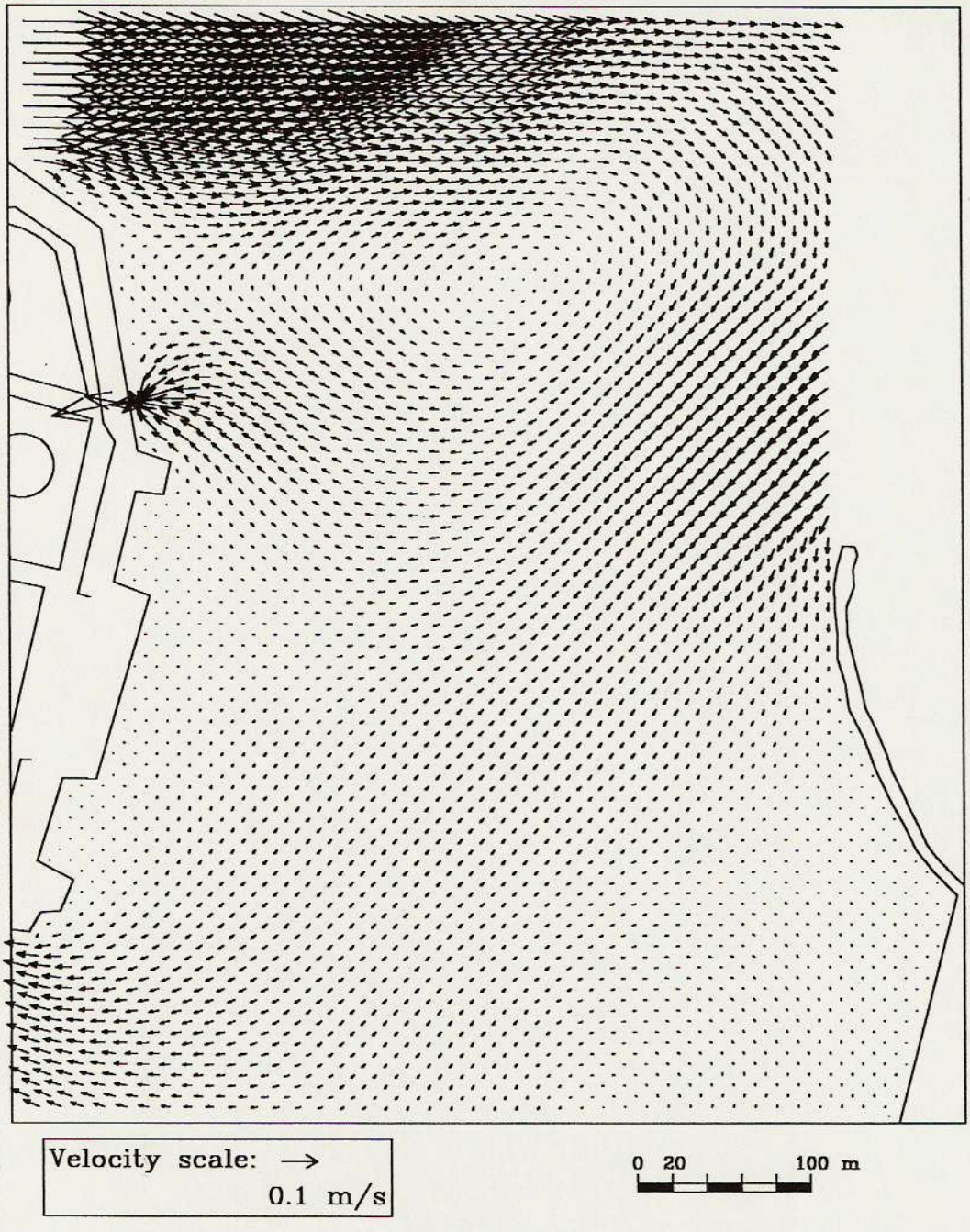

VELOCITY FIELD FOR THE DETAIL MODEL. SCENARIO A. T=0 AND T=12 HOURS. FUTURE CONDITIONS.

FIGURE 4.8

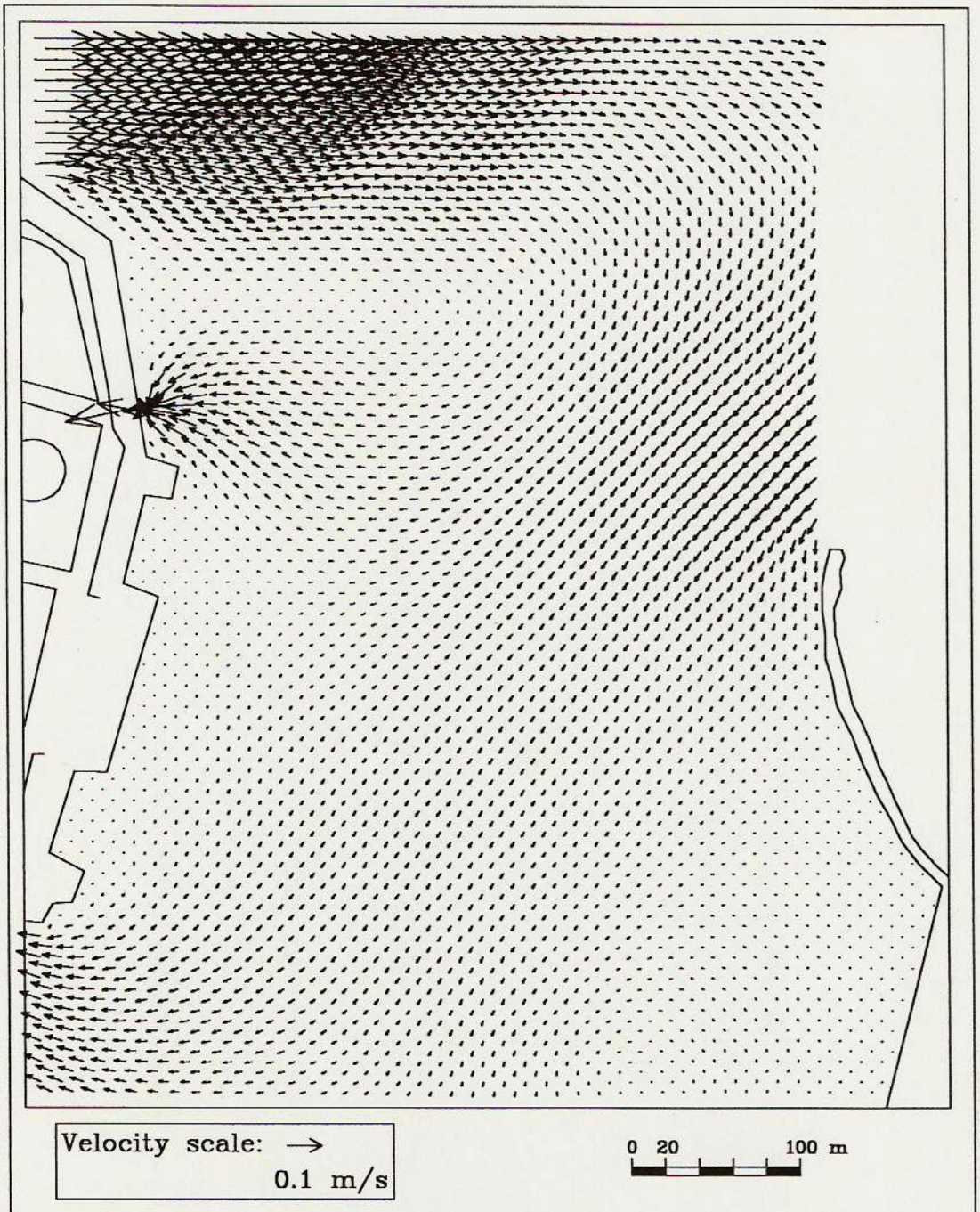

VELOCITY FIELD FOR THE DETAIL MODEL. SCENARIO A. T=1.7 AND T=8.9 HOURS. FUTURE CONDITIONS.

FIGURE 4.9

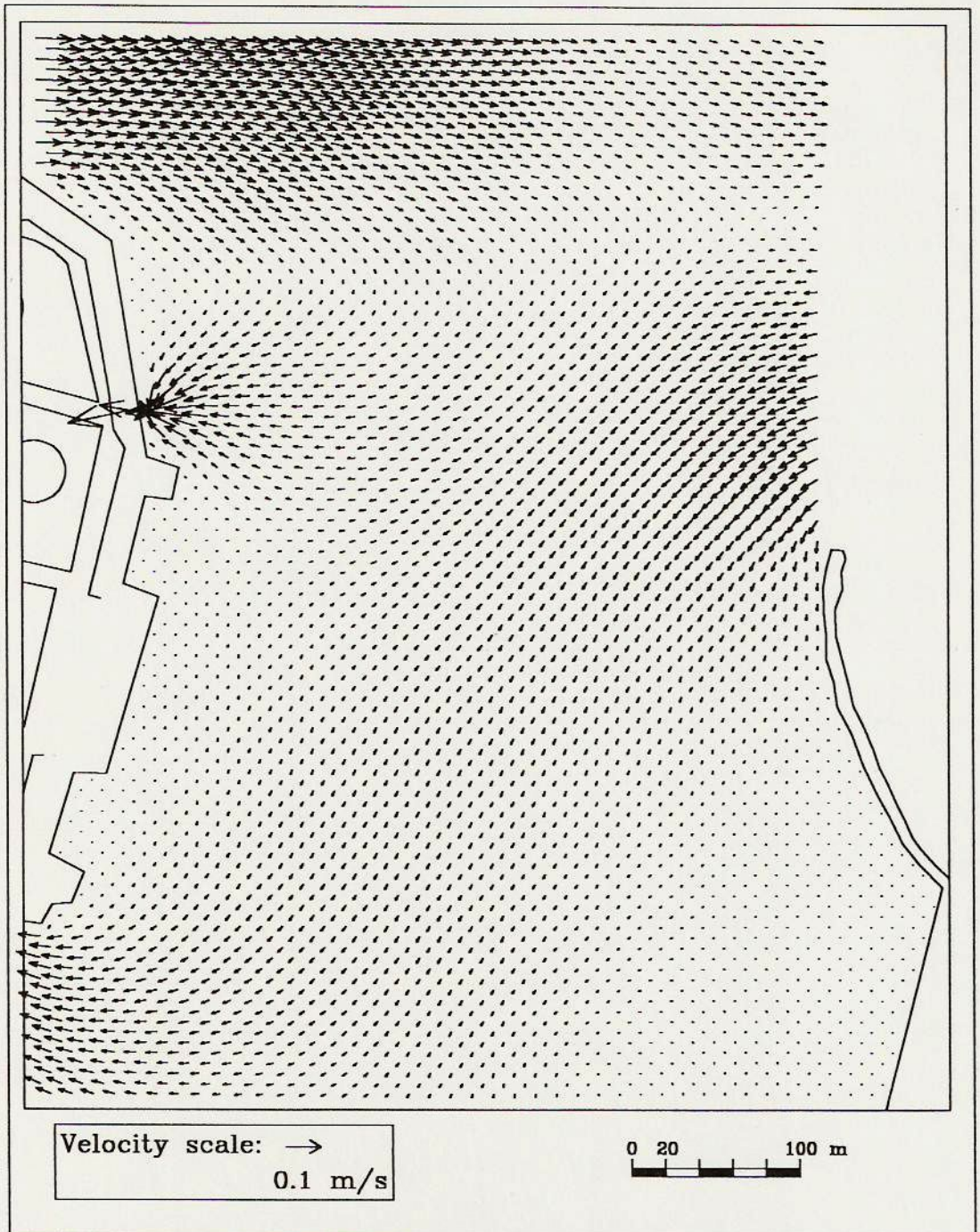

VELOCITY FIELD FOR THE DETAIL MODEL. SCENARIO A. T=2.3 AND T=8.2 HOURS. FUTURE CONDITIONS.

FIGURE 4.10

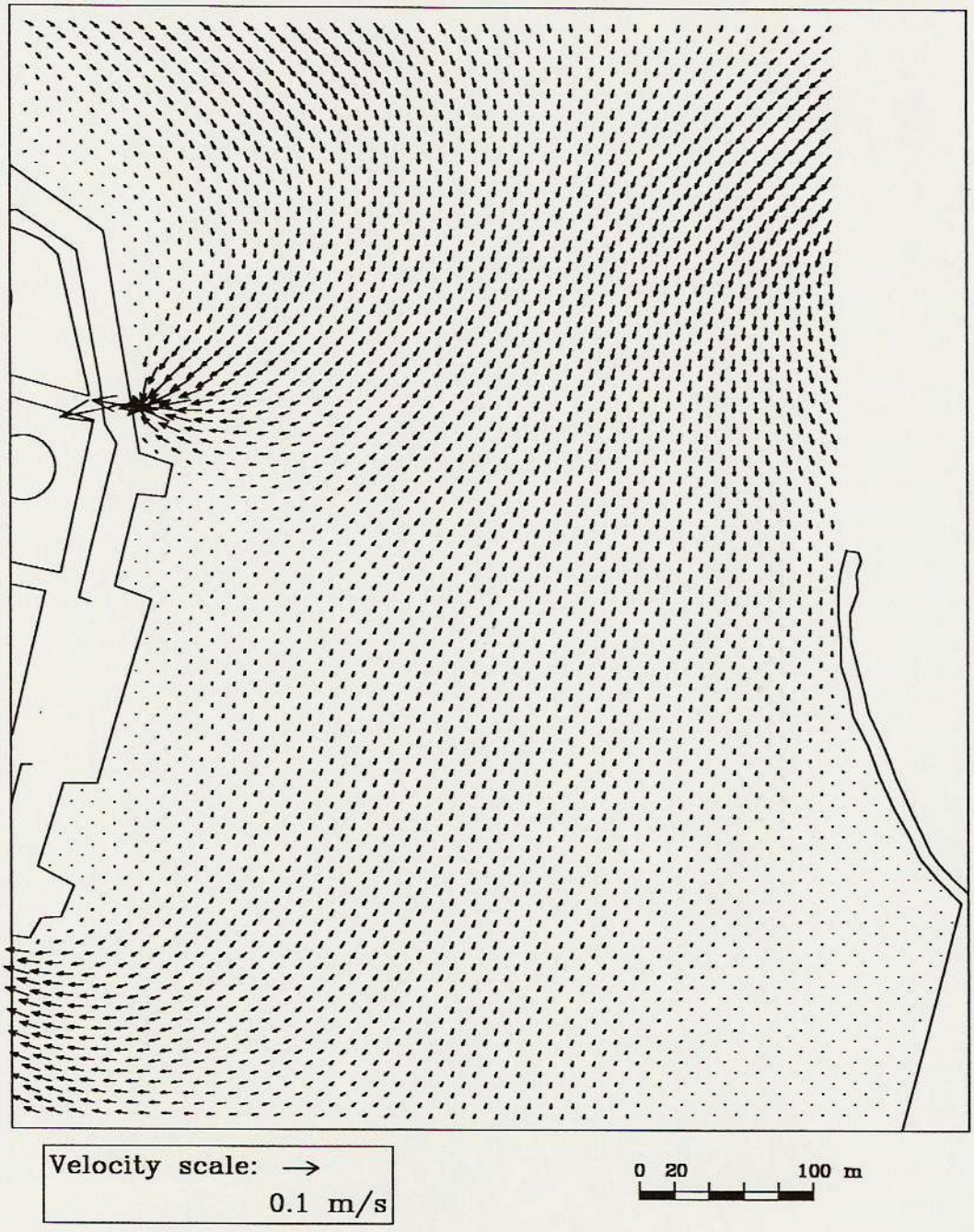

VELOCITY FIELD FOR THE DETAIL MODEL. SCENARIO A. T=2.7 AND T=7.7 HOURS. FUTURE CONDITIONS.

FIGURE 4.11

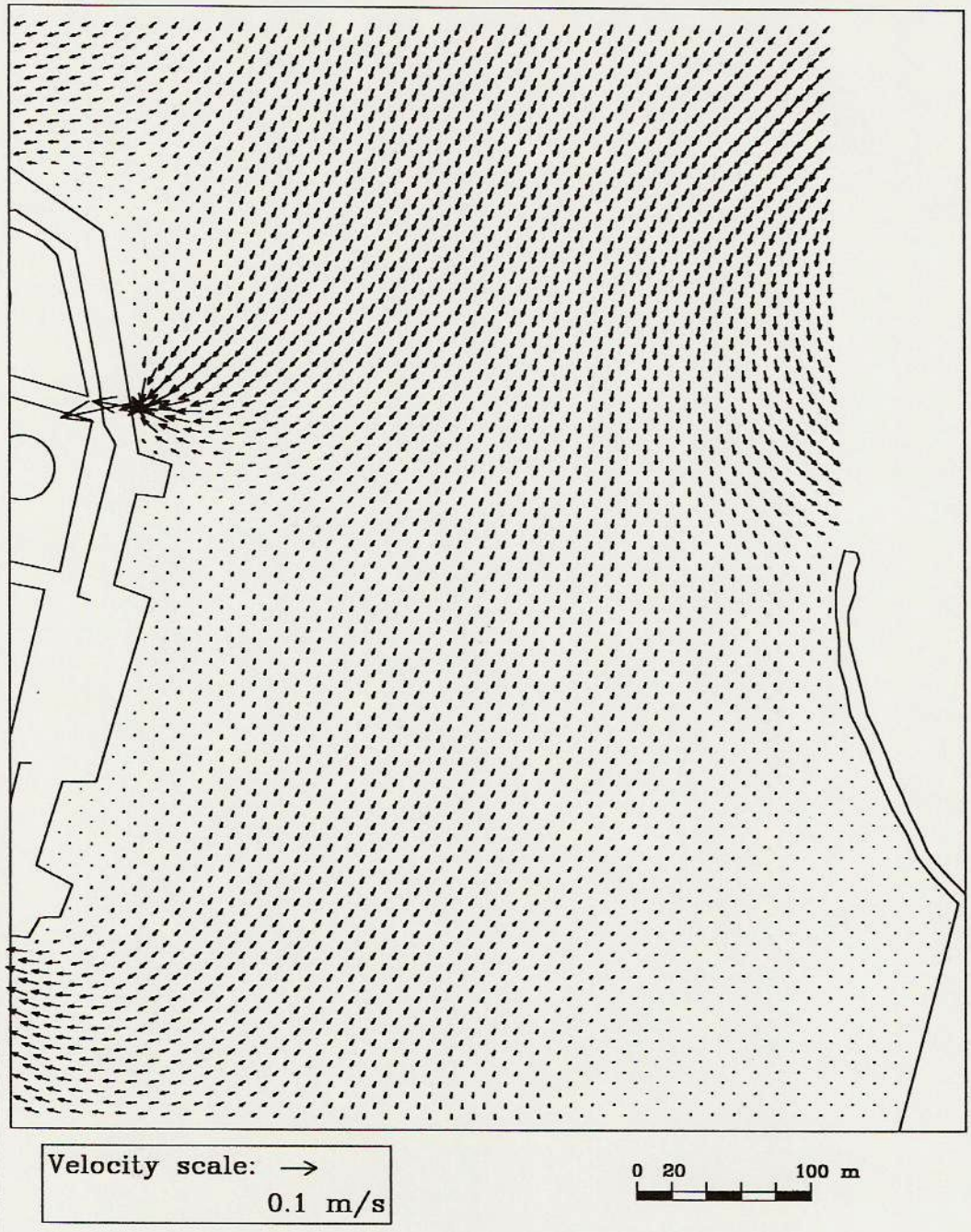

VELOCITY FIELD FOR THE DETAIL MODEL. SCENARIO A. T=3.3 AND T=7 HOURS. FUTURE CONDITIONS.

FIGURE 4.12

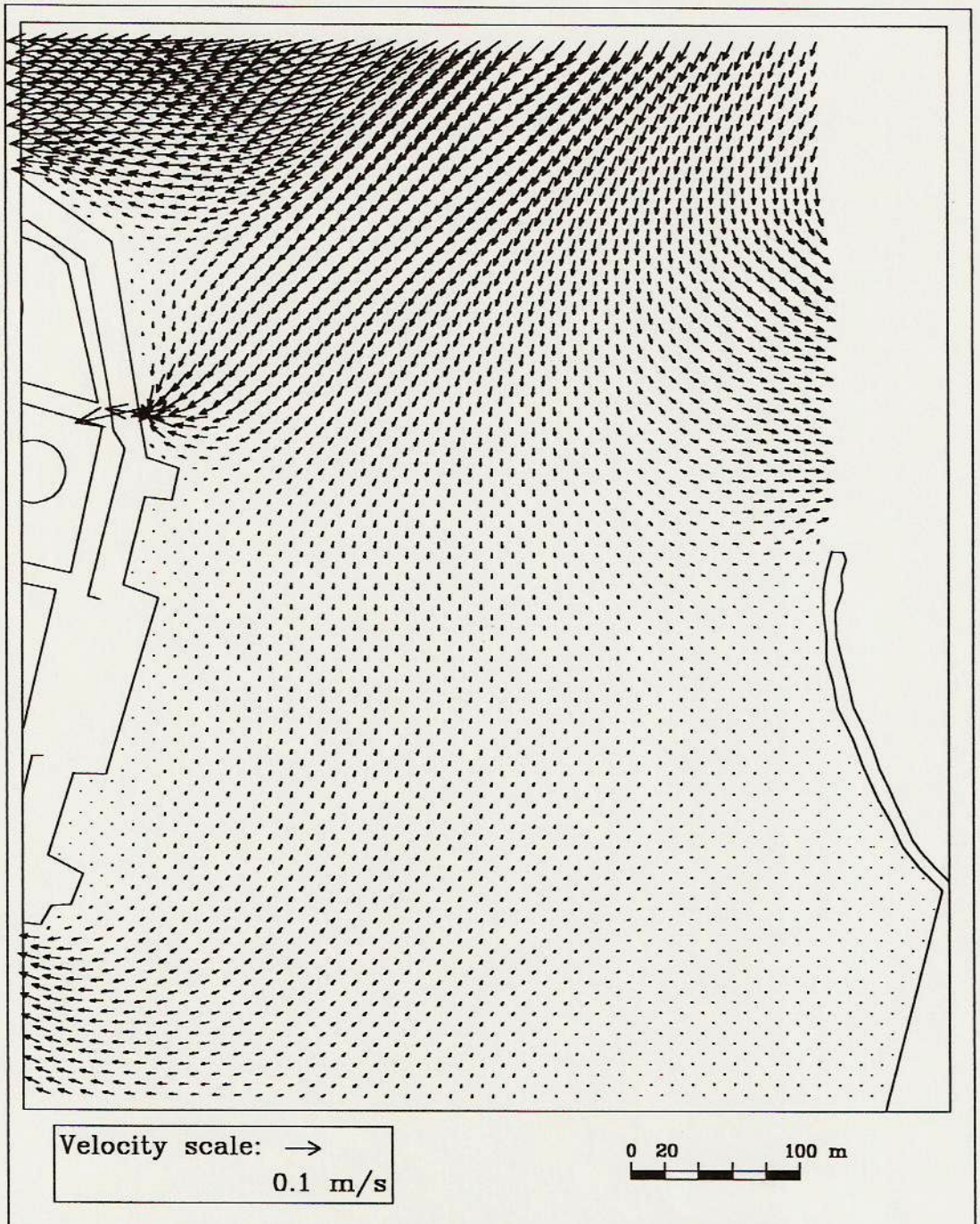

VELOCITY FIELD FOR THE DETAIL MODEL. SCENARIO A. T=5 HOURS. FUTURE CONDITIONS.

FIGURE 4.13

Siltation rate contour lines
Actual conditions

diameter= 15 µm

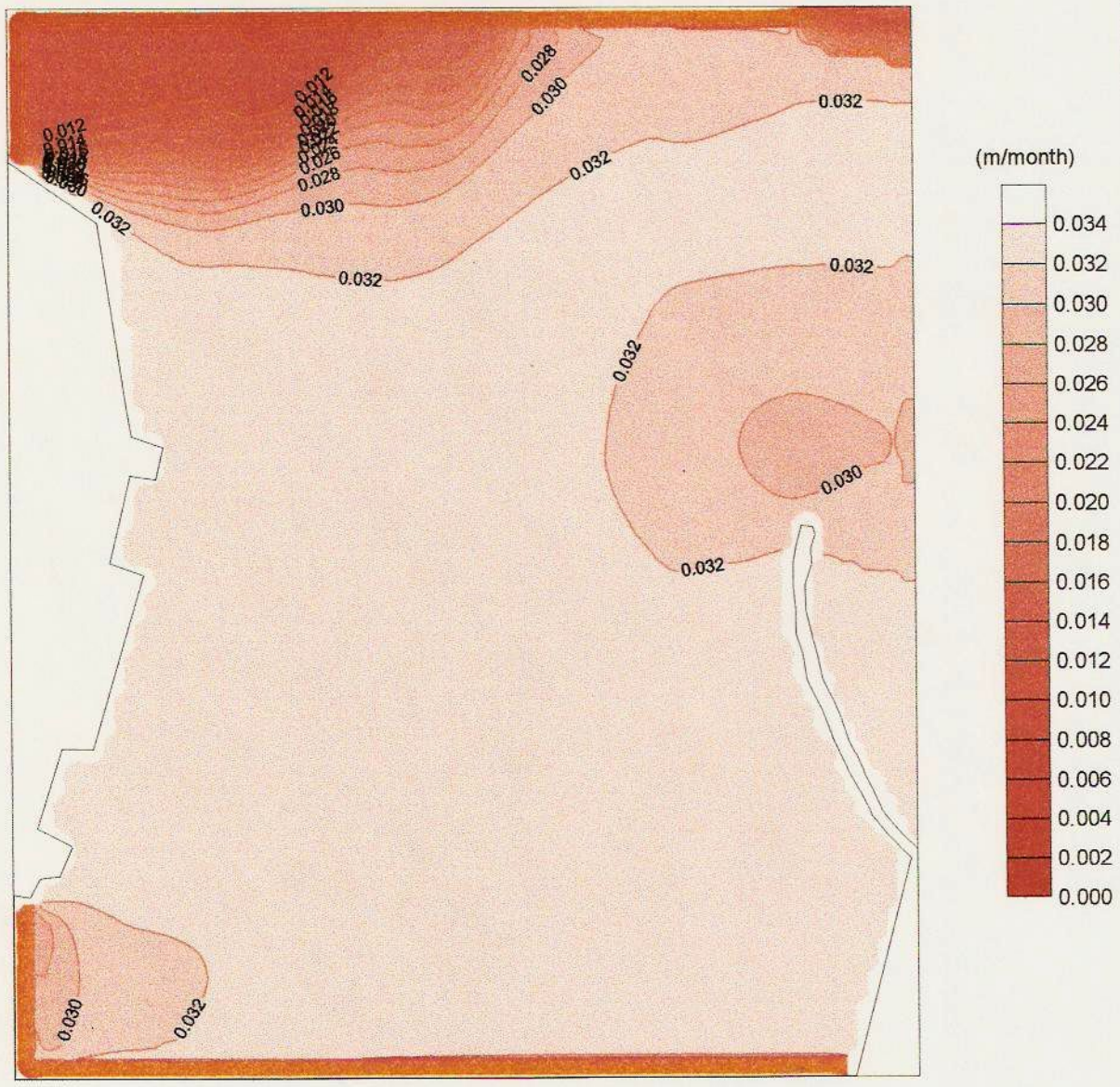

FIGURE 4.14

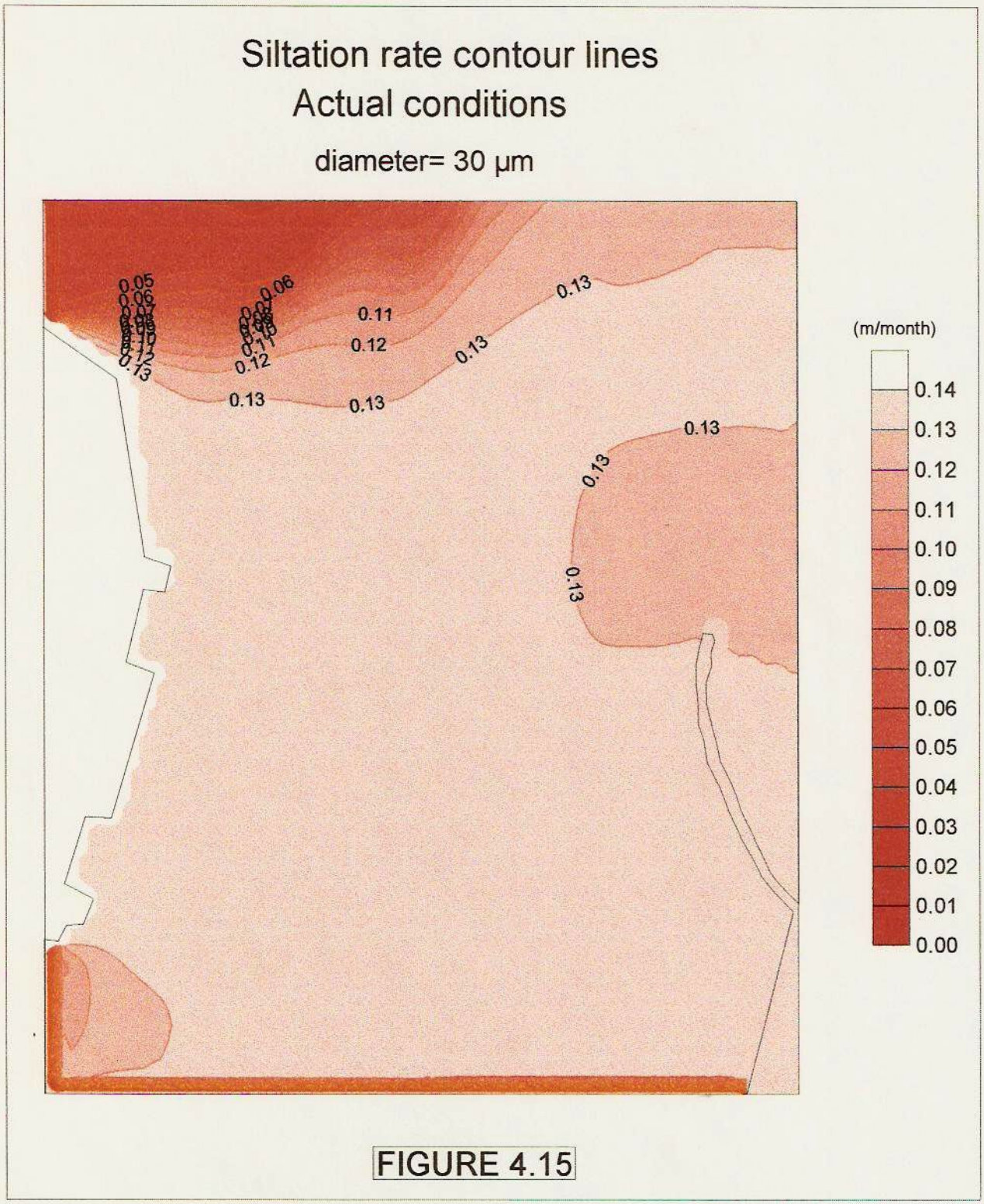
Siltation rate contour lines
Actual conditions
diameter= 30 µm
0.05
0.06
0.11
0.12
0.13
0.14
(m/month)
0.10
0.09
0.08
0.07
0.04
0.03
0.02
0.01
0.00

FIGURE 4.15

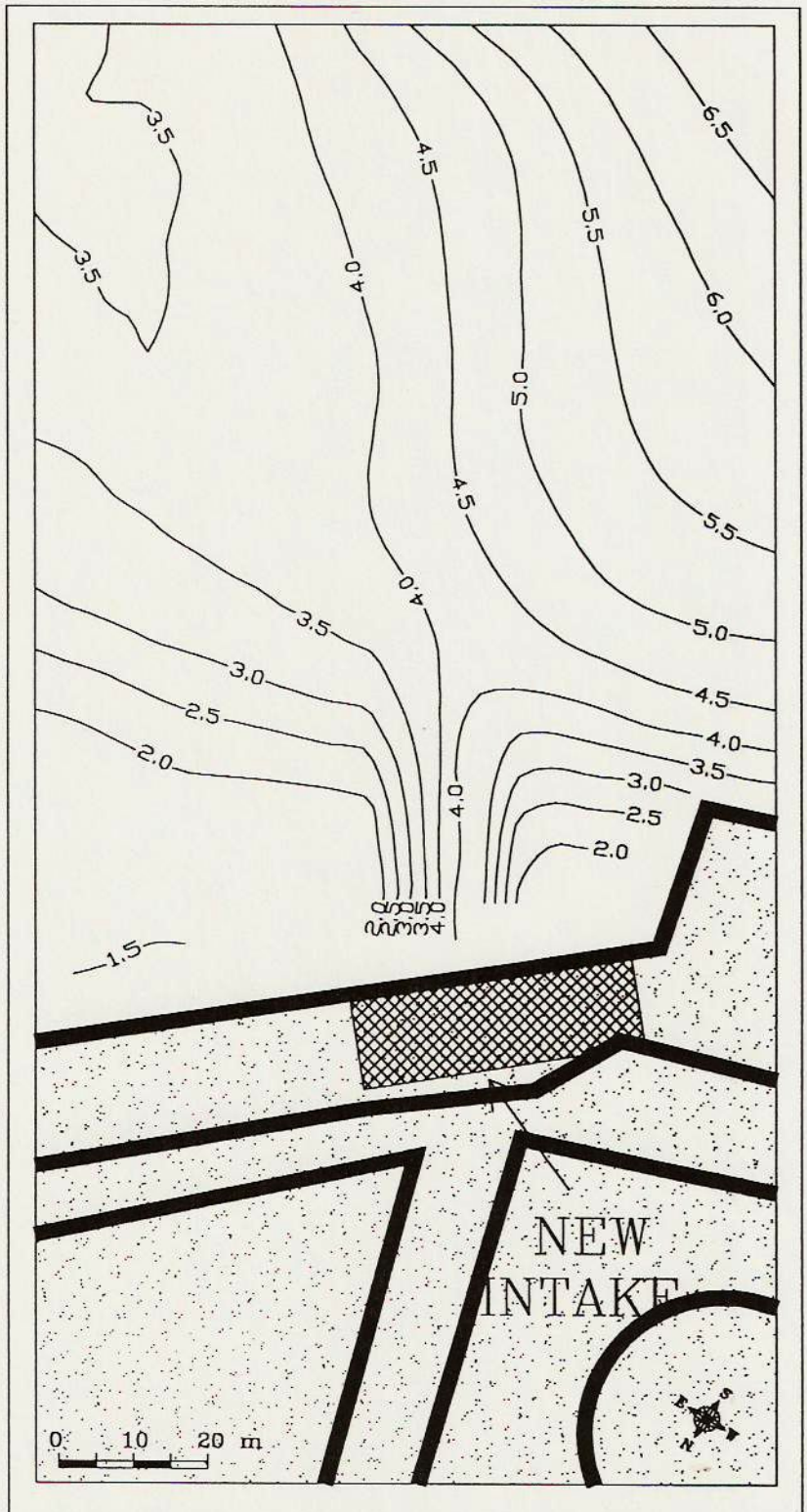

DREDGED ZONE | FIGURE 4.16

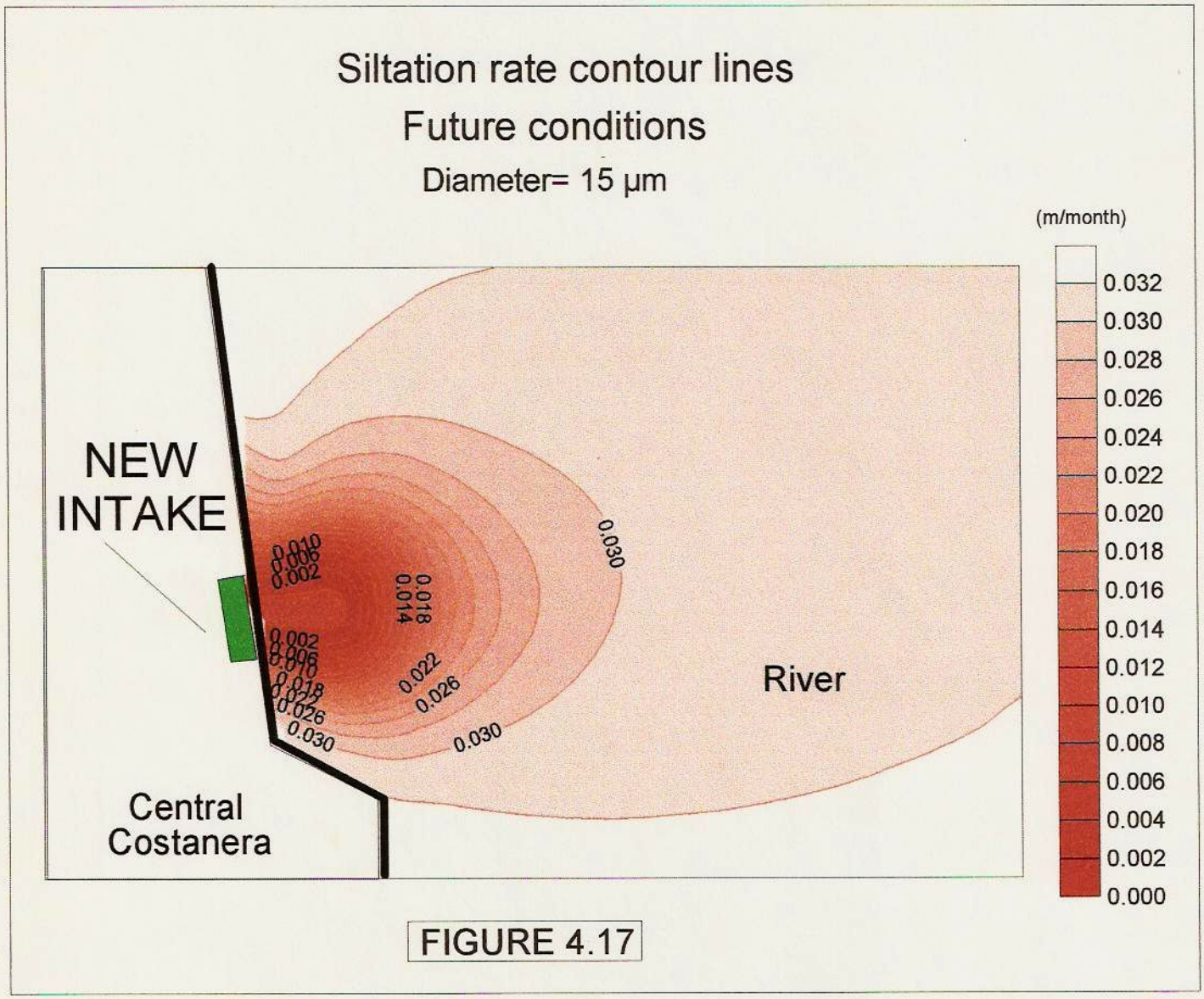
Siltation rate contour lines
Future conditions
Diameter= 15 µm
(m/month)
0.032
0.030
0.028
0.026
0.024
0.022
0.020
0.018
0.016
0.014
0.012
0.010
0.008
0.006
0.004
0.002
0.000
NEW
INTAKE
0.010
0.006
0.002
0.018
0.014
0,030
0.002
0.006
0.010
0.018
0.022
0.026
0.030
0.022
0.026
0.030
River
Central
Costanera

FIGURE 4.17

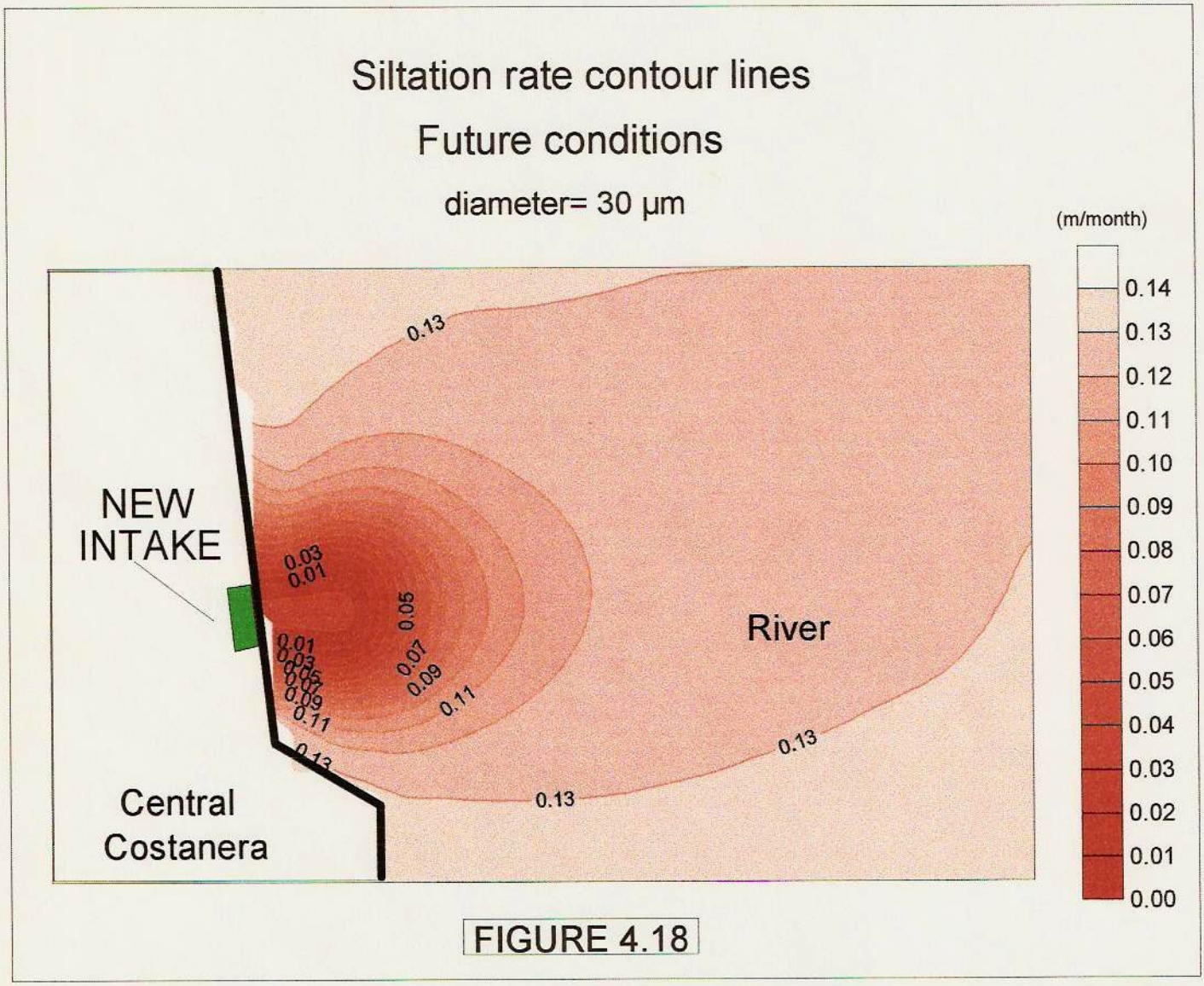
Siltation rate contour lines
Future conditions
diameter= 30 µm
(m/month)
0.14
0.13
0.12
0.11
0.10
0.09
0.08
0.07
0.06
0.05
0.04
0.03
0.02
0.01
0.00
NEW
INTAKE
Central
Costanera
River
0.13
0.13
0.13
0.11
0.09
0.07
0.05
0.03
0.01

FIGURE 4.18

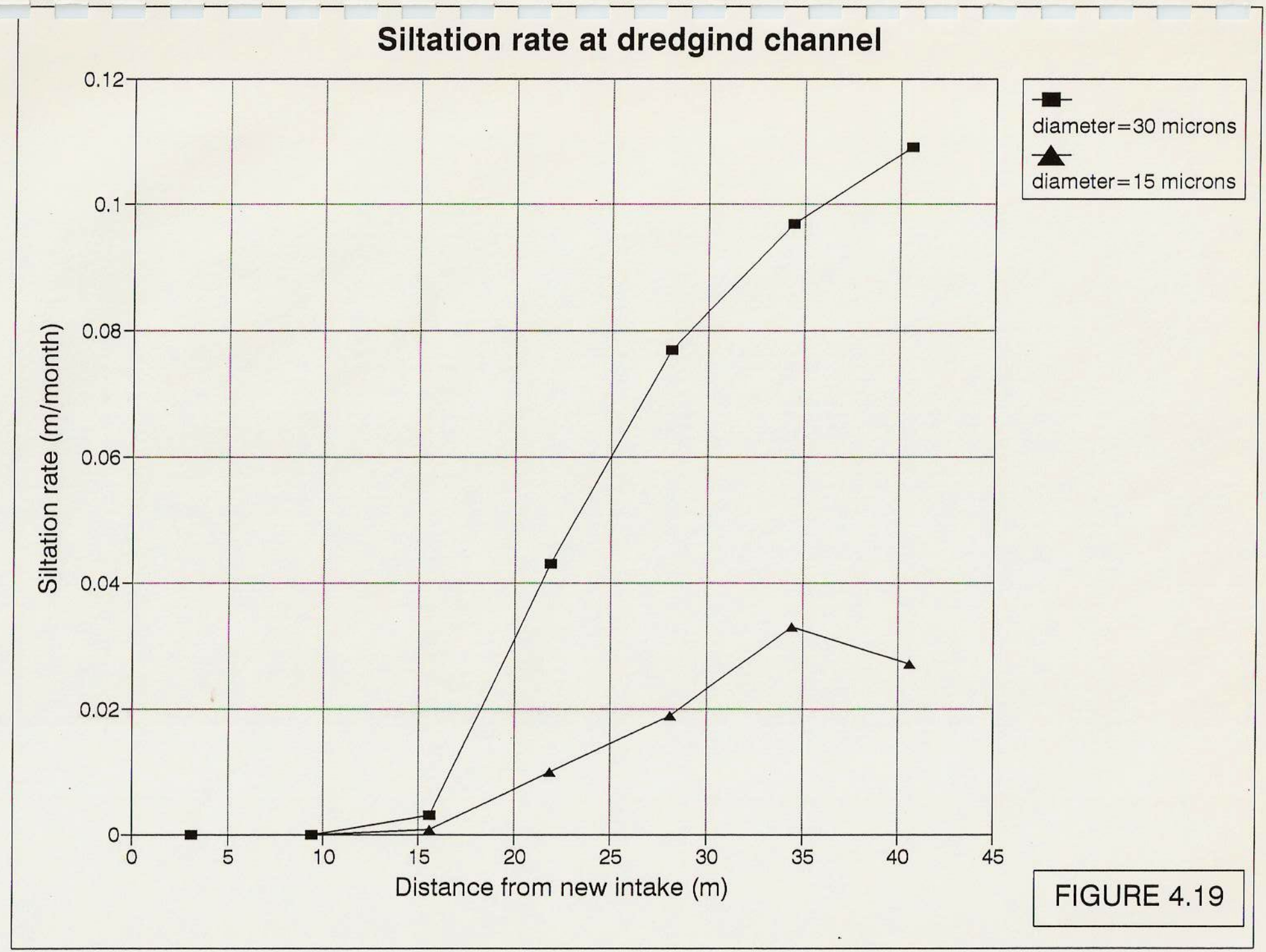
Siltation rate at dredgind channel
0.12
0.1
0.08
0.06
0.04
0.02
0
Siltation rate (m/month)
0
5
10
15
20
25
30
35
40
45
Distance from new intake (m)
diameter=30 microns
diameter=15 microns

FIGURE 4.19